Alkaline fuel cell using direct hydrazine-borane

Anicet Zadick

Communauté
UNIVERSITÉ Grenoble Alpes

THÈSE

Pour obtenir le grade de

DOCTEUR DE LA COMMUNAUTE UNIVERSITE GRENOBLE ALPES

Spécialité : **Matériaux, Mécanique, Génie Civil, Electrochimie**

Arrêté ministériel : 7 août 2006

Présentée par

Anicet ZADICK

Thèse dirigée par **Marian CHATENET** et
codirigée par **Christophe GEANTET**

préparée au sein du **Laboratoire d'Électrochimie et de Physicochimie des Matériaux et des Interfaces (Grenoble-INP)**
dans **l'École Doctorale I-MEP2 (Grenoble)**

Pile à combustible alcaline directe à hydrazine-borane

Thèse soutenue publiquement le **20 Octobre 2016**,
devant le jury composé de :

Monsieur, Gaël, MARANZANA
Professeur, Université de Lorraine, Président
Monsieur, Philippe, MIELE
Professeur, Université Montpellier, Examinateur
Monsieur, Têko, NAPPORN
Chargé de recherche, Université de Poitiers, Rapporteur
Monsieur, Frédéric, JAOUEN
Professeur, Université Montpellier, Rapporteur
Monsieur, Umit, DEMIRCI
Professeur, Université Montpellier, Invité
Monsieur, Marian, CHATENET
Professeur, Université Grenoble Alpes, Encadrant
Monsieur, Christophe, GEANTET
Directeur de recherche au CNRS, IRCELYON (Lyon 1), Co-encadrant

“Nou sé dé jenn ti frè é nou tout’ nou sé sè (fo nou alé douvan)

Nou pani tan a pèd, nou pani tan a pèd (fo nou alé douvan)

Si nou travèsé mizè, si nou travèsé lanmè

Sé pou nou tout là rivé prèmyé douvan”

Erik Pédurand, *Alé douvan*, Chayé kòw.

À mes parents.

ABSTRACT (English version)

The present PhD work focusses on the development of an original and innovative technology of direct liquid alkaline fuel cell (DLAFC) using hydrazine borane as a fuel for the anode. Thermodynamically, a direct hydrazine borane fuel cell (DHBFC) system can have an operating voltage value around 1.6 V when the most commercialized and mature proton membrane exchange fuel cell (PEMFC) technology can only reach 1.23 V (and in practice this value is even lower than 1 V). In principle, a direct alkaline fuel cell technology such as the DHBFC addresses most of the issues encountered in acidic PEMFC systems (such as the cost of the platinum-containing electrodes and their poor durability) and hydrazine borane is a relevant alternative to store chemically the hydrogen in the form of a white powder that is stable in alkaline solutions; this chemical hydrogen storage is easier, safer and more user-friendly than compressed H_2 gas.

This PhD work demonstrates that the HB electrooxidation reaction (HBOR) in alkaline medium is possible and efficient on noble metals such as palladium (cheaper than platinum) and more importantly on noble-free nickel-based materials. For those materials, the HBOR onset potential is measured below 0 *vs.* RHE, which enables to expect promising operating voltage if they are used as anode electrocatalysts in DHBFC systems. This solution allows to diminish the technology's cost (both in terms of fuel storage and electrocatalyst materials) and could enable to rival industrially PEMFC systems, if the anode durability is demonstrated.

On this prospect, whereas non-noble metals (such as nickel) can generally not be used as anode electrocatalysts in acidic PEMFC systems because of their instability, this work demonstrates that they are stable in alkaline environment. Surprisingly, "state-of-the-art" platinum (and palladium) electrocatalysts, generally used in PEMFC, are unstable in alkaline medium: indeed, platinum (and palladium) carbon-supported nanoparticles are highly degraded (and in a lesser extent for palladium) in alkaline solution, after 150 potential cycles in a usual potential window; so, these "state-of-the-art" noble electrocatalysts are not suitable for real DHBFC system applications. Therefore, the nickel-based electrocatalysts (both active and stable) are found to be the most suitable electrocatalyst materials for the DHBFC anode.

Finally, it is also demonstrated that the nature of the borane fuel is critical for utilization in DALFC system; hydrazine borane is found to be the most promising fuel against ammonia borane (AB) or dimethyl amine borane (DMAB). The borane electrooxidation reaction (BH_3OR), carried out on palladium electrocatalysts (despite its relative instability for real systems, palladium is a suitable noble and model electrocatalyst to get a better understanding of the BH_3OR mechanism), using these various fuels sheds light on the detrimental (poisoning) role of the counter-borane fragments of AB and DMAB (ammonia and dimethyl amine, respectively); on the contrary, the counter-borane fragment of HB (hydrazine) is found to have no detrimental effect on the BH_3OR. Interestingly, the hydrazine moiety is

completely electrooxidized on palladium, leading to n_{e^-} = 4 exchanged electrons in addition to the n_{e^-} = 6 exchanged electrons generated by the BH_3OR.

To conclude, this PhD work underlines the interest of hydrazine borane for the DHBFC systems, in particular for nomad applications, where the hydrogen storage can be a problem. HB is a relevant fuel to store chemically the hydrogen and to be valorized on noble-free materials, diminishing the overall system cost while ensuring a sufficient durability for the DHBFC anode.

ABSTRACT (version française)

Ces travaux de doctorat se concentrent sur le développement d'une technologie originale et innovante de pile à combustible alimentée directement à l'anode par une solution alcaline contenant de l'hydrazine borane (HB), celui-ci intervenant comme combustible (technologie notée DHBFC pour direct hydrazine borane fuel cell). Thermodynamiquement, il est possible d'atteindre une tension de pile avoisinant 1.6 V avec une DHBFC alors que la technologie la plus commercialisée et mature, à membrane échangeuse de protons (PEMFC), ne peut offrir au mieux que 1.23 V (en pratique cette valeur est même inférieure à 1 V). En outre, la DHBFC permet de répondre à plusieurs problèmes rencontrés par la PEMFC (tels que le coût des électrodes contenant du platine et leur faible durabilité) et le choix de l'HB comme alternative chimique au stockage de l'hydrogène, sous la forme d'une poudre blanche soluble et stable en milieu alcalin, rendra le stockage plus simple, sûr et commode que celui de l'hydrogène gazeux sous pression.

Ensuite, ces travaux démontrent que la réaction d'électrooxydation de l'HB (HBOR) en milieu alcalin est possible et efficace sur des métaux nobles tels que le palladium (moins cher que le platine) et sur des matériaux non nobles à base de nickel. Pour tous ces matériaux, la HBOR démarre à des potentiels inférieurs à 0 V *vs.* RHE, ce qui permet d'espérer des valeurs élevées de tension de pile pour les DHBFCs. Aussi, cette solution permet-elle de diminuer le cout général de la technologie (en termes de matériaux d'électrode et de stockage de l'hydrogène) pour rivaliser économiquement avec les PEMFCs ; il est important de rappeler que de tels électrocatalyseurs métalliques non nobles (à base de nickel) ne seraient pas stables dans des technologies acides telles que la PEMFC.

Dans ce cadre, ces travaux apportent des résultats surprenants quant à l'instabilité des électrocatalyseurs de platine (et de palladium) largement utilisés dans les PEMFCs. En effet, les nanoparticules de platine (et de palladium) supportées sur carbone sont très significativement dégradées (dans une moindre mesure pour le palladium) après une centaine de cycles dans une fenêtre de potentiel classique dans une solution légèrement alcaline. Il semble donc que les électrocatalyseurs à base de nickel soient des matériaux plus appropriés pour une utilisation industrielle comme anode dans des DHBFCs au vu de leur activité électrocatalytique et de leur grande stabilité.

Enfin, ces travaux soulignent l'importance du choix du combustible sur les performances de tels systèmes alcalins. Parmi les composés de la famille des boranes testés, l'HB présente les performances les plus intéressantes, en comparaison avec l'ammonia borane (AB) ou le dimethylamine borane (DMAB). L'étude du mécanisme de la réaction d'électrooxydation du fragment borane (BH_3OR) est menée sur des électrocatalyseurs de palladium (car bien que ceux-ci subissent une dégradation non négligeable en milieu alcalin, ils restent néanmoins des matériaux nobles et modèles permettant de mieux comprendre le mécanisme de la BH_3OR). Cette étude permet d'observer l'impact négatif de la présence des fragments d'ammoniac et de dimethylamine contenus dans l'AB et le DMAB sur la

BH_3OR. En revanche, le fragment « hydrazine » de l'HB n'empoisonne pas le palladium et peut quant à lui être complétement valorisé en produisant 4 électrons échangés qui s'ajoutent aux 6 électrons échangés issus de la BH_3OR, rendant alors la technologie alcaline DHBFC encore plus attrayante du point de vue de la densité énergétique.

Ainsi, ces travaux soulignent l'intérêt de l'hydrazine borane pour les piles à combustible directes et alcalines, en particulier pour les applications nomades pour lesquelles le stockage d'hydrogène gazeux sous pression est délicat. Enfin, l'anode des DHBFCs pourrait être composée d'électrocatalyseurs métalliques à base de nickel, garantissant une durabilité satisfaisante et diminuant le coût général de la technologie.

Table of Contents

General introduction

I. General introduction

The information contained in this chapter are mostly originating from the six volumes of Handbook of Fuel Cells [1–4]; the aim hereafter is to briefly introduce the main events that took place in the history of the fuel cell development and to present more specifically the direct hydrazine borane fuel cell (DHBFC) systems.

i. Context & contribution of that PhD work

a. Context

The overall population growth and inevitable rise in energy consumption per capita (needed to reach and to maintain a sufficient human development) coupled with the increasing global warming concerns force our societies to look for new technologies in energy production, storage and conversion. In the particular case of the powering of portable electronic device, the most used generators are based on lithium-ion batteries since nearly three decades (for storage and conversion), but these "closed" generators face great difficulties to overcome their intrinsic limitations in energy densities (*ca.* 250 Wh kg^{-1} is a practical upper limit). As materials breakthroughs enabling to double this figure with "beyond Li-ion systems" (*e.g.* lithium-sulfur, lithium-air, sodium-air, redox-flow, *etc.*) [5–7] is unlikely, other technologies must be developed.

In that context, open generators like fuel cells are relevant alternatives, especially for high-energy density systems, easily and directly fed by non-toxic and convenient fuels. Among the possibilities, new fuel cell technologies are emerging such as the direct hydrazine borane fuel cell (DHBFC), that electrooxidizes the hydrazine borane dissolved in an alkaline solution. Hydrazine borane falls within the family of boron based materials (BBM), and is synthesized from sodium borohydride (another BBM) and hydrazine hemisulfate. Generally, BBMs are used as hydrogen carrier (releasing gaseous hydrogen in a catalytic converter, which is further valorized in a proton exchange membrane fuel cell (PEMFC) on demand) and have already allowed, in the case of sodium borohydride, the development of portable electronic devices such as laptop or smartphone (see the example from *Intelligent Energy*, **FIGURE I-1**). This technology is often denoted as "indirect" borohydride fuel cell (IDFC), and suffers from intrinsically-low efficiency; indeed, the H_2-release by hydrolysis and subsequent valorization in a proton exchange membrane fuel cell (PEMFC, see **TABLE I-1**) is in practice difficult to control and losses are common; besides, H_2 is only valorized above E = 0 V *vs*. RHE when sodium borohydride can in principle

be (thermodynamically) directly valorized at E = -0.4 V *vs*. RHE *via* the direct electrooxidation of sodium borohydride.

Figure I-1 Commercialized fuel cell system for portable applications developed by Intelligent Energy. This system uses a PEMFC fed in hydrogen via sodium borohydride hydrolysis.

Table I-1 Data sheet of commercialized fuel cell system developed by Intelligent Energy.

Fuel cell technical data	
Output voltage	11.1 – 24 V (scalable to device)
Rated power	Up to 20 W (dependent on device)
Fuel cell type	PEM (Proton Exchange Membrane)
Fuel cell format	Planar array
Size	< 1 mm thick (area scalable to application)
Weight	< 10 g
Fuel cartridge	
Cartridge capacity	200 Wh. Equivalent to 18 200 mA h
Fuel type	Hydrogen
Storage	Sodium borohydride
Laptop operating time	Up to 13 hours (based on 16 W average power consumption)

Therefore, in a direct borohydride fuel cell (DBFC, or also in a DHBFC), the sodium borohydride (or the hydrazine borane) is used as fuel and not as hydrogen carrier but as an **energy carrier**; in principle, this enables a full valorization of the BBM fuel, *i.e*. at its thermodynamic potential. But, after a decade of intense research, DBFC are still not accomplished enough to compete with PEMFC, the acidic fuel cell technology which remains the most mature and commercialized. In a recent review comparing several fuel cell technologies and published in *Renewable and Sustainable Energy Reviews* [8], Sharaf *et al.* reported the several specific disadvantage of DBFC systems that need to be addressed, as presented in **TABLE I-2**:

Table I-2 Specific advantages and disadvantages of direct borohydride fuel cell system. Extracted from [8].

Specific advantages	Specific disadvantages
• Compact size • High fuel utilization efficiency • High fuel gravimetric hydrogen content • No carbon dioxide (CO_2) • Low toxicity and environmentally-friendly operation	• Fuel crossover • High cost • Low power density • Lack of analytical modeling techniques due to unknown borohydride oxidation reaction mechanisms • Expensive catalyst • Chemical instability of membrane and catalyst • Inefficient cathodic reduction reaction • Inefficient anodic oxidation reaction due to hydrogen evolution from hydrolysis of borohydride and partial release of fuel electrons.

However, according to the work carried out during that PhD and to the results presented in the present manuscript, it is demonstrated that some disadvantages of the DBFC systems can be *easily* solved in DHBFC systems, such as:

- "high cost";
- "expensive catalyst";
- "inefficient anodic oxidation reaction due to hydrogen evolution from hydrolysis of borohydride and partial release of fuel electrons";

To understand how the above assertion can be reached, the present PhD will firstly present the DHBFC systems, then participate to its scientific and technological developments and finally show how this original technology can be a real and a relevant alternative for small portable generators. More generally, this PhD fits into the regain of interest for direct liquid alkaline fuel cells.

b. Contribution of that PhD work

This manuscript is written like a journey in the whole PhD research project, and interlocks each piece of knowledge obtained during three years into a bigger and more complex puzzle. The results and their interpretations are presented to the reader in the most understandable way, which is not necessarily chronological.

The exact topic of that research project is:

"Mechanism and electrocatalysts
for the direct electrooxidation of hydrazine borane in alkaline medium"

That PhD effort to develop an original alkaline fuel cell system working with hydrazine borane as fuel (DHBFC) is supported by the discovery of electroactive and stable materials for hydrazine borane electrooxidation in alkaline electrolyte and by the understanding of the mechanism of the hydrazine borane electrooxidation reaction (HBOR). The common strategy to investigate new electrocatalysts for a given fuel generally consists in a massive screening of different materials (differing by their composition, structure, morphology *etc.*) or in a change of some experimental parameters (such as pH, concentrations, temperatures *etc.*), in order to find the most electroactive materials and then to optimize the process of the fuel electrooxidation reaction happening on their surface (see **FIGURE I-2**). Although such strategy brings a great quantity of data about many types of electrocatalysts, it generally lets unexplored (or unfortunately not explored deep enough) the stability (in the meaning of durability) of the tested materials in real conditions. So, despite their interest, these materials discoveries cannot (always) be transformed into better fuel cell systems (durability is as important as activity for the targeted application).

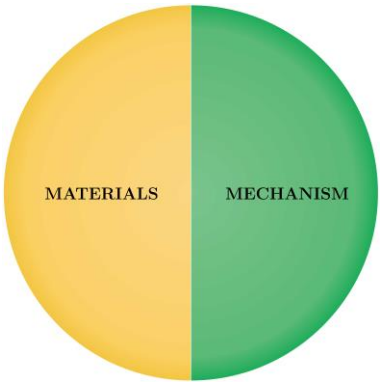

Figure I-2 General philosophy of research efforts

So, to develop DHBFC systems, it was decided to operate counter-stream and to focus on the research of electroactive materials and the understanding of their electroactivity for hydrazine borane electrooxidation reaction, primarily with a vision of stability (see **FIGURE I-3**). This choice, which could appear strange at first sight, was dictated by a rapid observation that "classic" (noble) electrocatalysts are highly instable in alkaline conditions, *a priori* even preventing kinetics/mechanistic measurements at these materials (if done in a "blind" manner). This time-consuming strategy explains why only a limited number of electrocatalysts has been tested during the PhD.

Given the general consensus in the literature on the supposed "softness" of alkaline media on (electro)catalyst materials, the reader may be surprised that stability issues are so much emphasized. In fact, this manuscript attempts to convince the readers that electrocatalyst stability problem can be a real challenge in alkaline systems, and sometimes even harsher than what is observed in acidic conditions, for example in PEMFC systems.

In that context, this work firstly emphasizes stability issues in "alkaline medium", before shedding light on the activity of the tested electrocatalyst materials and on the mechanism of the hydrazine borane electrooxidation reaction. This gives us the opportunity to re-ask ourselves some essential questions such as:

- Why should we move to an alkaline technology?
- What are its advantages?
- How could the scientist trust kinetic studies performed in alkaline medium if the electrocatalysts' stability is not assessed first?

From a pragmatic point of view, this PhD work intents to show the fantastic potential of DHBFC systems; so, by ensuring the stability (durability) of the materials used, one consequently ensures (in principle) the sustainability of this original system.

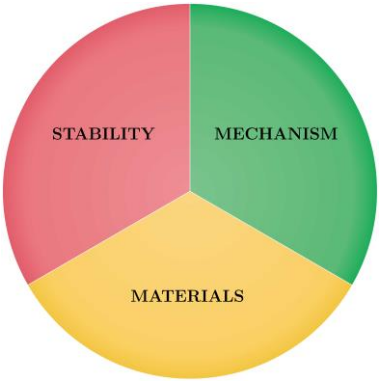

Figure I-3 Philosophy adopted in that PhD research effort

ii. Fuel cells history

To really evaluate the interest of this PhD work, it seems important to introduce alkaline fuel cell systems in the global history of fuel cell developments. This subsection briefly explains the origin of the regain of interest for alkaline systems after decades of research focusing mostly on acidic systems such as PEMFC.

a. Basics about fuel cells

There are several types of fuel cell technologies, and each of them has its own properties, characteristics and most suitable applications. Those characteristics are summarized in **TABLE I-3**.

Table I-3 Different existing fuel cell technologies

Fuel Cell Type	Electrolyte	Operating Temp.	Efficiency %	Common Size	Fuels	Primary Applications	Benefits
Alkaline (AFC)	Aqueous solution of potassium hydroxide soaked in a matrix	90–100ºC	60 %	10 –100 kW	Hydrogen	Controlled aerospace and underwater environments	Small size, high efficiency, water production
Direct Methanol (DEMFC)	Perfluorosulfonic acid	60–130ºC	30–40 %	< 1 – 50 kW	Methanol	Portable power, small vehicles	Ease of fuel transport, energy density
Molten Carbonate (MCFC)	Solution of lithium, sodium, and potassium carbonates	600–700ºC	50 %	300 kW – 3 MW	Reformed Hydrocarbons	Distributed power	High efficiency, fuel flexibility, combined heat and power operation
Phosphoric Acid (PAFC)	Phosphoric acid soaked in a matrix	150–250ºC	40 %	100 – 400 kW	Reformed Hydrocarbons	Distributed power	
Polymer Exchange Membrane (PEMFC)	Perfluorosulfonic acid	80ºC	30–40 %	1 – 100 kW	Reformed Hydrocarbons	Transportation	Low temperature, flexibility, higher power density
Solid Oxide (SOFC)	Yttria stabilized zirconia	700–1000ºC	60 %	1 kW – 10 MW	Reformed Hydrocarbons	Distributed and utility scale power	High efficiency, fuel flexibility, combined heat and power operation, amenable to hybridization

Among all those technologies, one focusses here on two main technologies: the alkaline fuel cell (AFC) has the lead role in that PhD work and the proton exchange membrane fuel cell (PEMFC) is the benchmark, for comparison. In both of those technologies (as in other technologies), the system is composed to two electrodes; the anode and the cathode, separated by an electrolyte. The nature of the anode and cathode are historically different between the AFC and PEMFC; nonetheless, recent AFC systems are using metal-based nanoparticles generally supported on carbon as it is the case in PEMFC. **FIGURE I-4** schematically presents a fuel cell in operation and a micrograph of a typical electrocatalyst material.

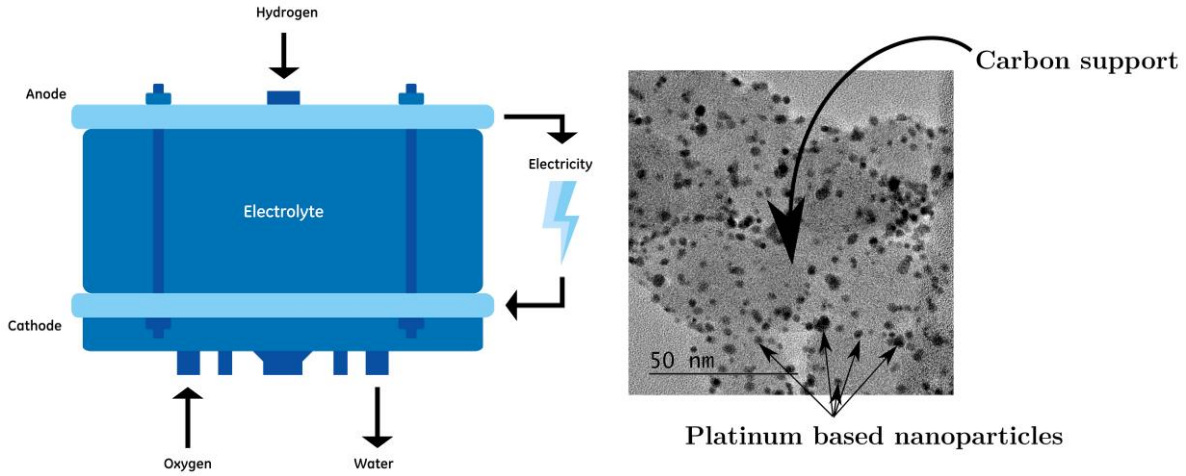

Figure I-4 (a) Usual representation of a fuel cell system. (b) Electrocatalyst composed of the platinum-based carbon-supported nanoparticles.

The nature, the size, the composition of the metal-based nanoparticles and of the support may change depending on the technology (AFC or PEMFC) and depending on their utilization at the anode or at the cathode in the system.

In the usual version of the two technologies (AFC and PEMFC), gaseous hydrogen is electrooxidized on the anode electrocatalyst (*e.g.* Pt/C for PEMFC) and gaseous oxygen is electroreduced on the cathode electrocatalyst (*e.g.* PtCo/C for PEMFC). The process produces electricity and water which make it *ecofriendly* in theory (in reality, the hydrogen production is still based on fossil compounds and generally not ecofriendly at all).

NOTA BENE:

It seems important to keep in mind that:

1. At the anode, a reaction of electrooxidation happens (electrochemistry)

2. At the cathode, a reaction of electroreduction happens (electrochemistry)

The words oxidation and reduction can (and are) nevertheless be abusively used for electrochemical reaction instead of electrooxidation (or electroreduction). When a complex fuel is fed to a direct fuel cell, (*e.g.* hydrazine borane), it can be involved in both chemical and electrochemical processes simultaneously, and so in the whole manuscript, the words oxidation and electrooxidation will be used with respect to their exact meanings (*idem* for reduction and electroreduction).

In a usual alkaline fuel cell (AFC) system, the electrochemical reaction happening at the anode is the hydrogen electrooxidation reaction (HOR):

$$2H_2 + 4OH^- \rightarrow 4H_2O + 4e^-$$

Equation I-1

In the meantime, the produced electrons pass in the external circuit to reach to cathode and react following the oxygen electroreduction reaction (ORR):

$$O_2 + 4e^- + 2H_2O \rightarrow 4OH^-$$

Equation I-2

The global reaction is therefore:

$$2H_2 + O_2 \rightarrow 2H_2O$$

Equation I-3

In a usual AFC, the electrolyte is an alkaline solution of sodium hydroxide (NaOH) or potassium hydroxide (KOH). These compounds are generally used because they are cheap, highly soluble and conductive to ions, but they are non-negligibly corrosive, however. The main advantages of the AFC technology are:

- The overvoltage at the cathode for the oxygen electroreduction reaction (ORR) is generally lower with an alkaline electrolyte than with an acidic electrolyte. This phenomenon is still not clearly understood, but nevertheless allows to reach operating voltages (for the complete system) as high as 0.875 V for a cell (using hydrogen and oxygen), which is higher than for usual PEMFC (using the same reagents).

- Another advantage of great importance is related to the AFC system cost. In addition to the low cost of the electrolyte, the cathode can be made with non-precious metals (such as nickel, cobalt, iron, or carbon nitride-based nanocatalysts).

Historically, AFCs were used in the Apollo missions that took man to the moon and several applications of AFC systems for agricultural tractors, cars, offshore navigation equipment, boats and fork lift trucks have also existed. Nevertheless, despite the fact that they were reasonably working, the AFC technology was facing major difficulties in terms of practical cost, reliability, ease of use, ruggedness and safety, which extinguished the scientific interest until the very beginning of the 21st century. At this latter period, the interest started to resume, owing to the development of alkaline/anionic polymer electrolytes [9] and to the fresh interest for hydrogen fuel alternatives such as BBMs (*e.g.* sodium borohydride and boranes) and alcohols from biomass.

b. How did PEMFC compete AFC?

In PEMFC systems, the same electrochemical reactions than for AFC systems are happening on the electrodes, but in acidic medium. At the anode, the hydrogen electrooxidation reaction (HOR) is rewritten as:

$$2H_2 \rightarrow 4H^+ + 4e^-$$

Equation I-4

At the cathode, the oxygen electroreduction reaction (ORR) is rewritten as:

$$O_2 + 4H^+ + 4e^- \rightarrow 2H_2O$$

Equation I-5

The global reaction remains unchanged:

$$2H_2 + O_2 \rightarrow 2H_2O$$

Equation I-6

The electrolyte is an ion-conducting polymer acting like an acidic electrolyte, in which the mobile ion is the H^+ ion (proton). The standard membrane is made of a perfluorosulfonated polymer, typically Nafion®, a registered trademark of Dupont de Nemours. The electrocatalysts can be directly bonded to both sides of the membrane in order to make an MEA (Membrane Electrode Assembly) in which the polymer acts as electrolyte, binder and also as a separator.

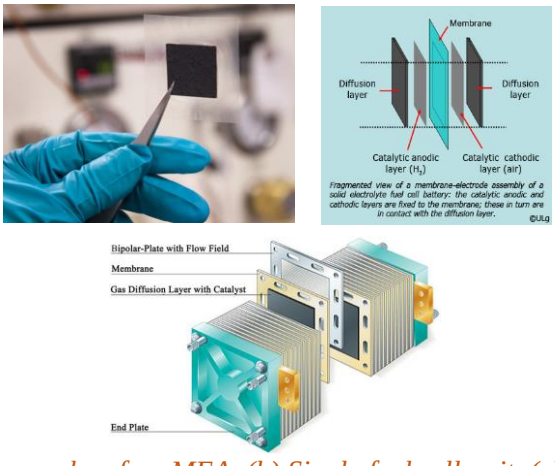

Figure I-5 (a) Photography of an MEA. (b) Single fuel cell unit. (c) A stack composed of several single fuel cell unit.

The advantages of PEMFC systems are linked to the use of the polymer electrolyte membrane:

1. The thinness of the membrane electrode assembly (MEA) allows to design compact fuel cell systems (stacking several MEAs);
2. The fluid produced (water) is not corrosive;
3. The fuel cell systems can operate in any orientation.

For those reasons, PEMFC is *a priori* perfectly suitable for portable applications; nonetheless, the technology cost and the difficulties to manage the water produced *in operando* were the main issues explaining why they went more or less into abeyance until the early 1990s, to the benefits of others fuel cells technologies such as AFCs and phosphoric acid fuel cells [1–4].

Fortunately for PEMFC (and unfortunately for AFC), great improvements have been made for PEMFC efficiency in the beginning of the 1990s. Indeed, the need in electrocatalysts decreased from 28 mg of platinum for each centimeter square of MEA to *ca.* 0.2 mg cm^{-2} or less now [1–4]. Those developments were accompanied by a dramatic increase of the operational current densities (up to around 1 A cm^{-2} or more), leading to huge reductions in cost per kilowatt of power and much improved power density. This strong effort in reduction of platinum became possible by the electrode tailoring, described in the following section **"TAILORING OF ELECTROCATALYST MATERIAL"**.

c. Drawbacks of PEMFC and the rebirth of AFC

Despite its assets and its amazing improvements for last decades, PEMFC still face many technical, industrial and commercial issues related to their cost and safety. Many of those issues can be addressed by AFC and more specifically by the direct hydrazine borane fuel cell (DHBFC), making of it a competing technology for nomad applications:

1. Even if the use of platinum has been reduced and optimized, PEMFC is still using platinum (or platinum-based) nanoparticles on both electrodes (anode and cathode). So, the system remains too expensive for a massive commercial deployment (because the tension on the platinum market will likely not be sustainable).

   On that point, alkaline technology can offer a larger set of non-precious metals that could be both stable and electroactive, reducing dramatically the fuel cell cost in reason of the materials' availability.

2. The durability of the cathode in PEMFC is still a complete challenge. *In operando*, the platinum nanoparticles (supported on carbon) face many degradation phenomena such as agglomeration, dissolution/redeposition or detachment, in particular due to their ability to promote the corrosion of their carbon support.

   On that point, alkaline technology is usually presumed to offer a better stability for the metal-based nanoparticles and for the carbon support. However, dramatic degradation fates can also be observed in alkaline medium for noble electrocatalysts in some cases; this is detailed later, especially in "**DEGRADATION OF NOBLE ELECTROCATALYSTS IN ALKALINE MEDIUM**", and mitigation strategies/materials are proposed.

3. The PEMFC commercial market is intimately linked to the hydrogen market. This is generally the "spooky point" about PEMFC; indeed, the hydrogen market is still at its infancy, and only few regions (or even countries) in the world are equipped with hydrogen infrastructure (hydrogen stations for example).

   Then, from an ecological point of view, it is worth noting that 96% of the hydrogen production is still produced from fossil fuels by steam reforming or partial oxidation of methane and coal gasification. Only a small quantity is produced by other routes such as biomass gasification or water electrolysis.

Finally, for portable applications (phones, computers *etc.*), PEMFC still struggle to provide an efficient and safe hydrogen storage means, which meets the customer expectations.

On those points, AFC offers the possibility to use fuels that are dense in energy and easily produced, stored and transported, in particular for portable applications. The family of boron based materials (BBMs) is a typical example; BBMs store chemically the hydrogen in the form of white powders such as hydrazine borane (easy to store and to transport), which are soluble and stable in alkaline electrolytes, and directly usable on demand (when the electricity is needed).

4. Finally, despite the strong effort of the scientific community, it remains difficult to improve significantly the kinetics of the oxygen electroreduction reaction (ORR) happening at the cathode; in consequence, the operating voltage of a PEMFC stands well below the thermodynamic maximum value of 1.23 V (0.9 V is hardly reached in practice).

   If a DHBFC also suffers this ORR kinetic limitation in alkaline medium, it however presents huge advantages: the ORR is usually faster in alkaline than in acidic medium (even on non-Pt electrocatalysts [1–4]); more importantly, hydrazine borane (and other BBMs) can be electrooxidized in alkaline medium at lower potential value than H_2, leading to higher operating voltage with AFC systems fed with BBMs (for example, a DHBFC can in principle operate at 1.64 V, values above 1 V being achieved in practice); this point will be further described in the following section "**DIRECT HYDRAZINE BORANE FUEL CELL (DHBFC)**".

These arguments show the PEMFC failures in addressing its own limitations; from that point, it is clear that AFC can represent a relevant alternative technology for fuel cell applications, explaining why alkaline systems now experience a regain of interest.

iii. Nanomaterials for fuel cells & Stability

a. Tailoring of electrocatalyst material

As mentioned in the section "**HOW DID PEMFC COMPETE AFC?**" the PEMFC became the most interesting fuel cell technology because of the improvement in the utilization of platinum which reduced the technology cost. This was the results of a massive effort in material tailoring to provide composition-size-shape-controlled and efficient electrocatalysts.

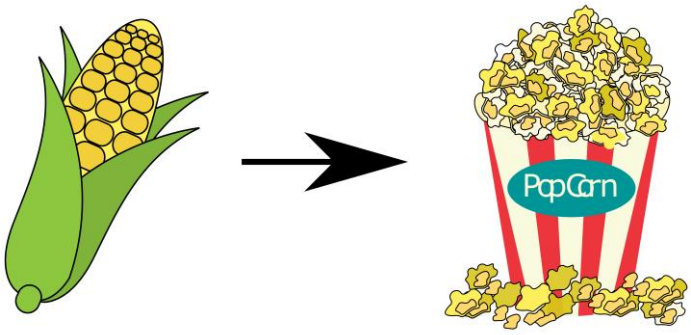

Figure I-6 Poetic illustration of the electrocatalyst tailoring

Electrocatalyst synthesis for fuel cells generally consists in the reduction of a metal salt on a support, which is generally a high-surface area carbon (HSAC) material. Researches in methods, techniques and protocols have permitted to tailor the nanoparticles shape, size, composition and dispersion on the carbon support. Obviously, all those parameters have an impact on the electrochemical performances for a given reaction. In PEMFCs for example, the kinetics of ORR on platinum-based electrocatalysts can be improved by changing the nanoparticle morphology. Hereafter, is an example published by Zhang *et al.* [10] where it was demonstrated that that ORR electroactivity in acidic electrolyte strongly depends on the terminal facets of Pt_3Ni nanocrystals: nanooctahedra with {111}-oriented facets are significantly more electroactive than {100}-bounded nanocubes. This result underlines that controlling the shape of electrocatalysts is an effective way to improve ORR electroactivity and to develop highly active electrocatalysts for PEMFC.

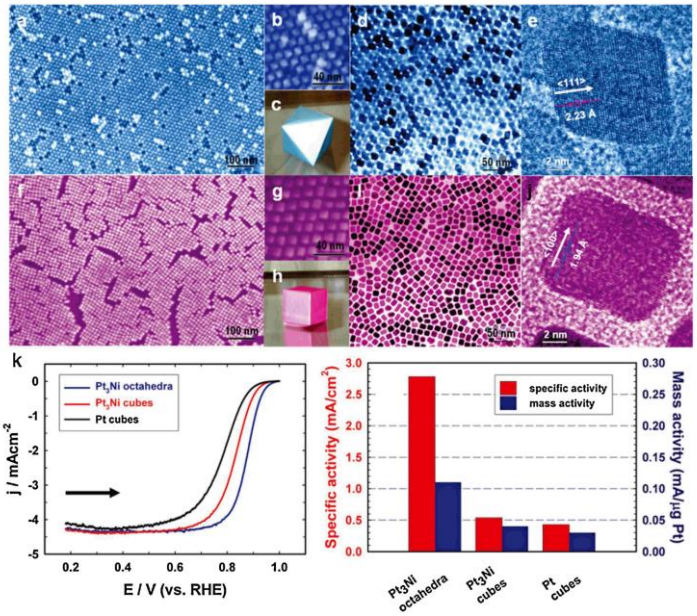

Figure I-7 (a-e) Images for Pt_3Ni nanoctahedra. (f-j) Images for Pt_3Ni nanocubes. (a, f) Field-emission SEM images. (b, g) High-resolution SEM images. (c) 3D image of an octahedron. (d, i) TEM images. (e, j) High-resolution TEM images of single NCs. (h) 3D image of a cube. (k) Polarization curves for ORR on Pt_3Ni nanoctahedra, Pt_3Ni nanocubes, and Pt nanocubes supported on a rotating GC disk electrode in O_2 saturated 0.1 M $HClO_4$ solution and the specific activity and mass activity measured at E = 0.9 V vs. RHE at 295 K. Extracted form Zhang et al. [10]

The increase in electrocatalytic performances of synthesized bimetallic platinum-based electrocatalysts *versus* pure platinum electrocatalysts is also accounted for by the presence of the transition metal within the synthesized bimetallic electrocatalyst, which induces a strain effect that leads to electrocatalytic enhancement. This property is shared by many other bimetallic electrocatalysts; for example, Strasser *et al.* have studied PtCu/C [11] and found that electrochemical dealloying of copper metal from copper-rich Pt bimetallic electrocatalysts significantly alters surface catalytic rates of the resulting Pt shells, creating favorable structural arrangements of Pt atoms at the particle surface, such as more active crystallographic facets or more favorable Pt-Pt interatomic distances for ORR.

The effort in tailoring the electrocatalyst/electrode can also aim to target an improvement of the mass-transport kinetics inside the electrocatalytic layer, optimizing the removal of reaction products and the arrival of fresh reactant/electrolyte in the vicinity of the electrocatalyst surface. Hereafter is an example of this with an electrocatalyst of platinum nanoparticles deposited on vertically aligned carbon nanofilaments; this original support improved the electrocatalyst performances for ORR and enabled to shed light on the mechanisms of reaction [12,13].

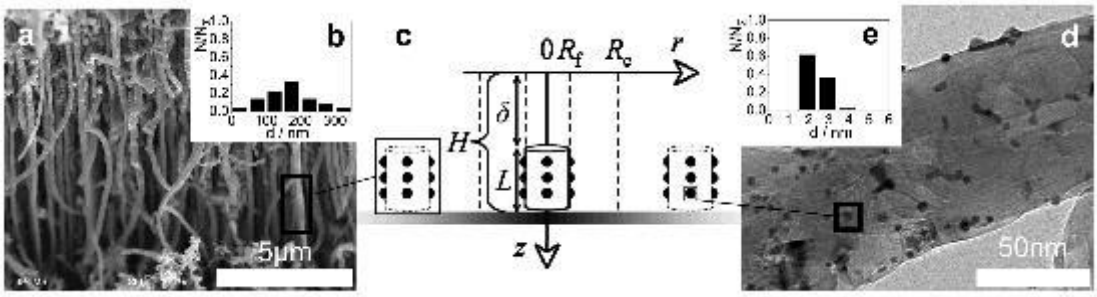

Figure I-8 (a) SEM image of a VACNF layer grown on TiOx/Ti/Si substrate with corresponding TEM-based diameter distribution diagram (b). (d) TEM image of a carbon nanofilament modified with Pt nanoparticles with corresponding Pt nanoparticle size distribution diagram (e). (c) Schematic representing system geometry.

These selected examples, among the abundant literature available on the topic, illustrate the variety of material developed and the knowledge accumulated during the last decades; they also illustrate that PEMFC became the major center of interest since the 1990s. It is relevant at that stage to have a look on the state of development in alkaline fuel cell technology before the decline of interest for these systems. Hereafter is an extract from a review lecture written by Bacon and Fry in 1973 [14] (**FIGURE I-9**)

Review Lecture 433

(*b*) *Choice of materials*

As regards cell temperatures below 100 °C, and especially around room temperature, it can safely be said that platinum, in the form of platinum black with a particle size of the order of 0.01 µm, and to a lesser extent palladium, are more effective than any other catalyst for hydrogen ionization; and in general, the higher the catalyst loading, the better the performance. Nevertheless, cheaper metals, especially nickel, are also quite effective when prepared with a very high surface area. Raney nickel is normally made from a powdered alloy of nickel and aluminium, the aluminium content of which is subsequently leached out by

434 F. T. Bacon and T. M. Fry

treatment in caustic alkali solution, giving surface areas of the order of 100 to 200 m²/g. In recent years, improvement in both catalyst performance and life have been achieved in Germany by alloying the nickel with other transition metals (with electron gaps in the d-band) such as iron, molybdenum and titanium, as well as combinations of such metals. Cell temperature is usually limited to 70 °C, as life suffers above this temperature; and if cells are overloaded, there is always the danger that the nickel will be irreversibly oxidized; the oxidation of nickel starts at +170 mV versus the reversible hydrogen electrode. The new nickel alloys are said to be much better in this respect also.

Figure I-9 Extract from [14] describing the type of electrocatalyst historically used for AFC systems.

When alkaline systems were at the top of their popularity, the materials used were basically platinum black or Raney nickel. Today, the majority of the papers dealing with alkaline fuel cells are based on

the same kind of electrocatalysts used for acidic fuel cell (such as for PEMFC), *i.e.* metal-based nanoparticles generally supported on carbon. Is it really without consequences?

This question is addressed in the present PhD work, different metal-based carbon-supported (or unsupported) electrocatalysts being compared for electrocatalysis in alkaline conditions:

- Several commercial electrocatalysts of platinum and palladium supported on carbon (Vulcan XC-72); these are state-of-the-art electrocatalysts and generally used in PEMFC electrodes and for electrochemical kinetic investigations in acidic (or alkaline) medium.
- One unsupported cubic palladium electrocatalyst, which allows to see if the cubic shape is sustainable (or not) in alkaline media;
- Some homemade nickel-based electrocatalysts supported on carbon (Ni_3Ag/C, Ni_3Pd/C and Ni_3Co/C), which allow to survey non-noble metals to diminish the materials' and system cost.

b. Stability issues and characterization: acidic *vs.* alkaline medium

As mentioned before, the degradation of PEMFC materials (and performances) is still an important issue. After decades of intense research, the mechanisms of degradation are now known and many studies focused on the improvement of material stability in acidic conditions to limit the PEMFC cathode degradation. **FIGURE I-10** gives an example of an aged membrane electrode assembly [15].

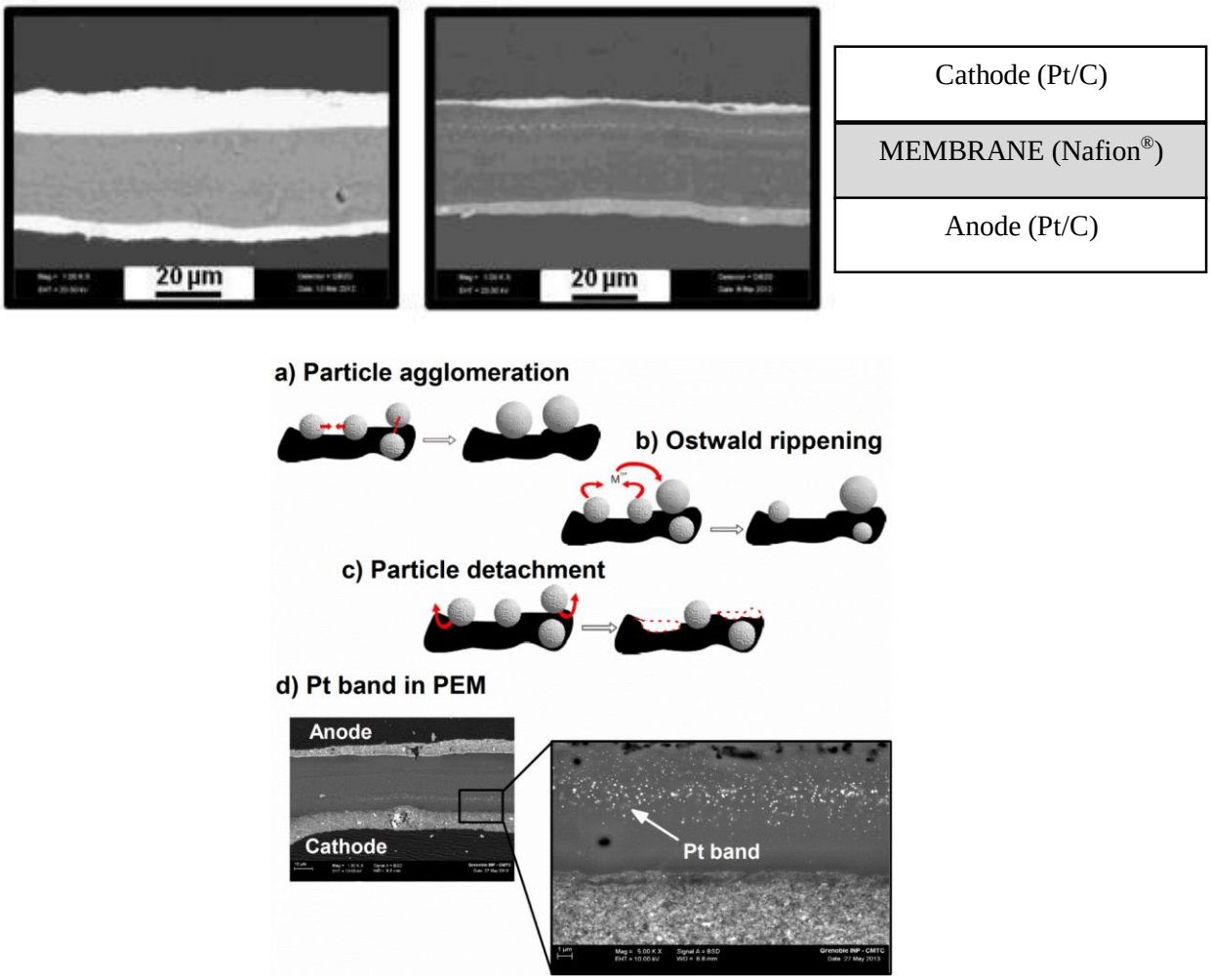

Figure I-10 SEM images of PEMFC cathode degradation and presentation of the different mechanisms of degradation.

The aging of PEMFC cathode is generally occurring from:

1. The 3D Ostwald ripping (dissolution/redeposition);
2. The agglomeration of the platinum nanoparticles;
3. The corrosion of the carbon support (also catalyzed by platinum particles).

Those 3 main modes of degradation could be distinguished in two sections: one dealing with the platinum nanoparticles (#1 and #2) and another one dealing more specifically with the carbon support (#3).

Concerning the platinum nanoparticles stability, it is good to keep in mind that small nanoparticles have the inherent tendency to dissolve at the expense of larger ones into bigger particles in order to reduce the high surface energy (Ostwald ripening). To some extent, the metal cations originating from the dissolution of the nanoparticles, can be transported into the ionomer and membrane, and be reduced there (likely by the fuel that crosses over from the anode) [16] . Besides this growth of existing particles, their agglomeration is possible, usually because of the corrosion of their (carbon) substrate (even if particles migration is often mentioned). Large agglomerates are usually stabilized in "pockets" of the electrode after aging [16–18]. Then, if carbon corrosion is severe, the nanoparticles can also simply fall from the substrate and be disconnected electronically and therefore lost to any electrochemical reaction. One solution to reduce to platinum stability issue is to alloy the platinum with other metals, a solution that also enables to reduce the electrocatalyst cost. It has been demonstrated for example that the dissolution of platinum in PtCo/C is reduced and so increase the durability of this latter bimetallic compared with pure Pt/C electrocatalysts [19]. The "improvement" in stability is however imperfect, since PtCo/C electrocatalysts are subjected to intense Co dissolution [20], which can adversely affect the electrocatalyst (and fuel cell) performances [21,22].

About the carbon support stability also involved in PEMFC cathode degradation, two main strategies have been employed: the graphitization of the carbon support or the replacement of the carbon support by (in principle) corrosion-resistant materials. On the former point, Castanheira *et al.* [23], by studying 3 different platinum based electrocatalysts supported on three different carbon support demonstrated the interest of graphitized carbon support. In this study, it has been demonstrated that the reinforced-graphite (RG) carbon support is more resistant to electrochemical corrosion than structurally disordered carbon supports such as Vulcan and high-surface area carbon (HSAC) as reported in **FIGURE I-11**; despite the fact that a good dispersion of platinum nanoparticle is made difficult with graphitized carbon, graphitized carbon supports appeared to be an interesting compromise between metal dispersion and limited carbon corrosion for PEMFC. Then other types of carbon support such as carbon nanotubes, nanofibers, aerogel and xerogel have demonstrated their potential as electrocatalyst support for PEMFC.

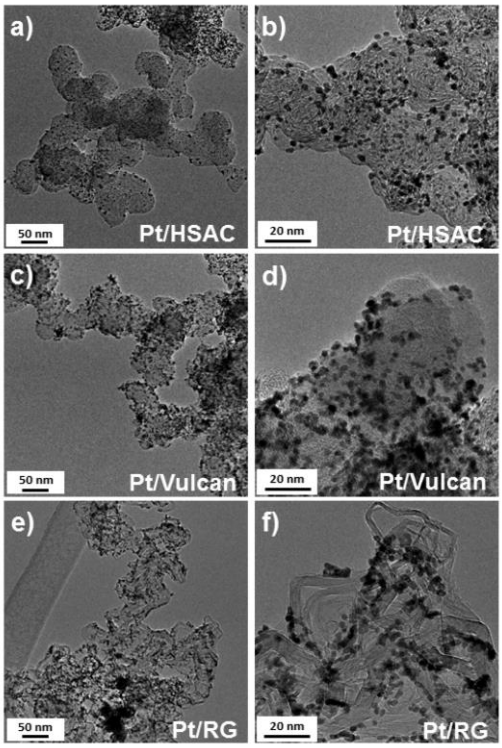

Figure I-11 TEM images of the different Pt/C electrocatalysts: (a,b) Pt/HSAC, (c,d) Pt/Vulcan, (e,f) Pt/RG.

Other studies focused on alternative support materials (instead of carbon), such as titanium oxide, tungsten carbide, tungsten oxide, indium tin oxide. Those materials have a better durability than conventional carbon supports (such as Vulcan XC-72, Ketjen black, *etc.*). However, improvements on synthesis, surface area and dispersion ability, conductivity and interaction with the platinum nanoparticles are still required, to enable the usage of such alternative supports in PEMFC [24–26].

The literature related to PEMFC degradation (in acidic electrolytes) is very abundant, and many strategies of "material tailoring" are including the degradation issue to provide both electroactive and stable electrocatalysts. In alkaline medium, the picture is dramatically different; indeed, almost no literature is dealing with electrocatalysts degradation in alkaline medium. To visualize the research effort concerning the alkaline fuel cell developments, all the papers available on *Web of knowledge*'s database corresponding to the following key words "Alkaline" + "Fuel cell" were gathered, and the results were refined and restricted to the papers that belong to the "electrochemistry" research field. **FIGURE I-12** gives a graphical representation of the research on alkaline fuel cell development, from 1974 to 2015, for the 2315 published papers respecting the mentioned criteria.

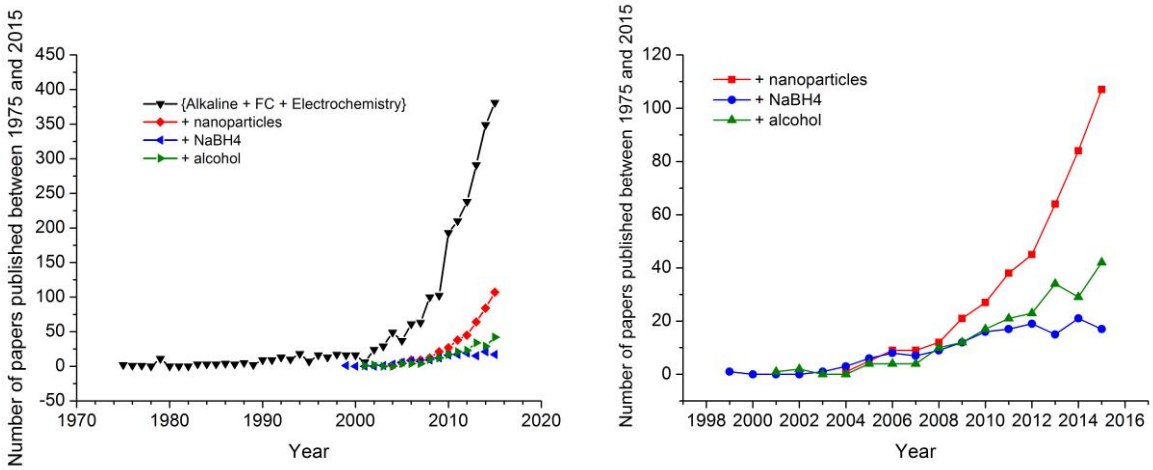

Figure I-12 Number of paper dealing with {Alkaline + Fuel cell + Electrochemistry} published per year between 1974 and 2015

FIGURE I-12 confirms that the research for alkaline systems has regained interest at the very beginning of the 21st century with, among other electrochemical reactions, the electrooxidation of sodium borohydride (which is a BBM as hydrazine borane) and alcohols. In a non-negligible part of those published papers, the experiments are performed on metal-based nanoparticles as remarkable on **FIGURE I-13**.

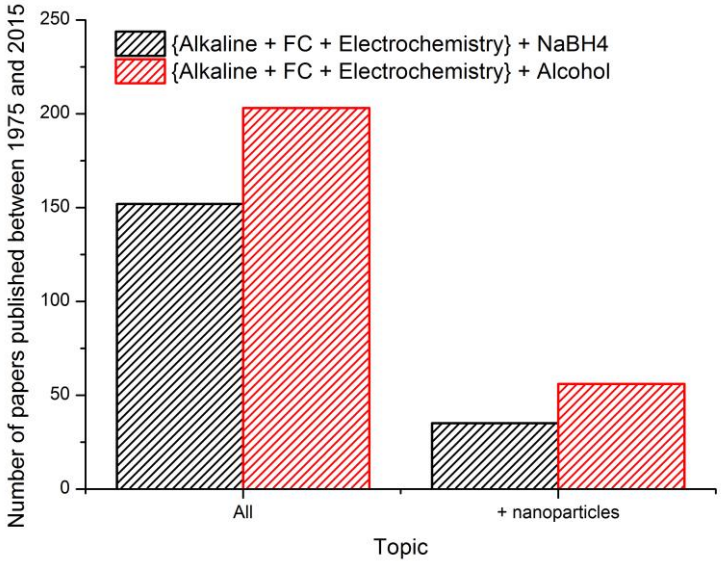

Figure I-13 Number of papers dealing with sodium borohydride or alcohol electrooxidation in general (All) and specifically with nanoparticles (+nanoparticles).

If ~25% of the published papers dealing with sodium borohydride or alcohol electrooxidation is referring to experimentations on metal-based carbon-supported materials, one could be afraid about the very small fraction of the published papers dealing with "durability" or "degradation" issues in alkaline conditions. Indeed, **FIGURE I-14** demonstrates that only a very small fraction of the specific research effort concerning nanoparticles concerns "durability" or "degradation" issues. The fraction of the published papers related to "stability" issues seems important but this value is however unrepresentative; in those papers, the term "stability" refers to electrochemical signals or performance stabilities (usually at time scales that are short – below hours) and does not refer to a specific investigation on the stability of the electrocatalysts used.

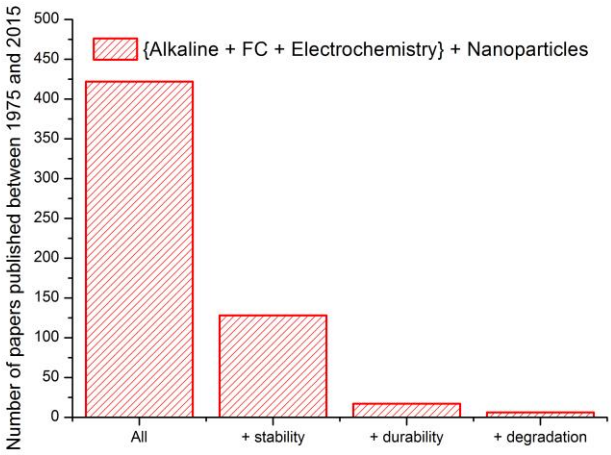

Figure I-14 Number of papers dealing alkaline fuel cell and using nanoparticles (All) and dealing more specifically with stability (+ stability) or durability (+ durability) or degradation (+degradation) behavior.

So, the fate of metal-based carbon-supported electrocatalyst in AFC (and so in DHBFC) is essentially unknown. In this thesis, the reader will be presented the first steps made in the world of degradation in alkaline medium. As detailed above, the success of PEMFC largely results from the innovations made in diminishing and optimizing the quantity of platinum metal used in those systems. Those improvements have been made possible notably by the use of efficient means of characterization to probe the nanoscale, such as high-resolution scanning transmission electron microscopes (HRSTEM, in particular equipped for chemical analyses: energy-dispersive spectrometry (EDS) or electron energy loss (EELS), corrected from chromatic aberrations and baring advanced detectors: *e.g.* high-angle annular dark field), spectroscopic techniques (Fourier Transform infra-red: FTIR, Raman, X-Ray photoelectron: XPS and absorption: XAS) to guide the research effort. Now, with the rebirth of the alkaline technology, all those techniques, protocols and characterization tools can be reemployed for original investigations of degradation in alkaline conditions and the obtained results can be compared with the data available for acidic conditions.

iv. Direct hydrazine borane fuel cell (DHBFC)

AFC systems using BBMs are viewed as an alternative for PEMFCs. The family of BBMs is very large and among its most interesting members one can identify the hydrazine borane (HB) (which is in the center of that PhD work), the dimethyl amine borane (DMAB), the ammonia borane (AB) or the most studied sodium borohydride ($NaBH_4$). All those BBMs can be valorized in fuel cell systems, either in an *indirect* or in a *direct* manner; the next sections will go further in the explanation, taking the $NaBH_4$ as an example, since this BBMs has been paid the most attention until now; nevertheless, the following discussion is transposable in the case of hydrazine borane.

a. The indirect and direct ways to use BBMs.

In the indirect approach, BBMs are just used as hydrogen carriers. As an example, the sodium borohydride ($NaBH_4$) can release hydrogen when dissolved in aqueous solutions, according to the homogeneous hydrolysis reaction:

$$NaBH_4 + 2H_2O \rightarrow 4H_2 + NaBO_2$$

Equation I-7

$NaBH_4$ (such as most of BBMs) is quite stable in water and its solubility is of 550 g in 1 L of water at *T* = 25°C. Alkaline solutions are stable for longer periods (though hydrogen evolution occurs slowly) and the "half-life" of these solutions has empirically been shown to follow the equation as stated by Amendola *et al.* [27].

$$\log_{10}\left(t_{\frac{1}{2}}\right) = pH - (0.034 * T - 1.92)$$

Equation I-8

With T in Kelvin and $t_{1/2}$ in minutes.

For a pH value of 13 and a solution thermostated at T = 25°C, the half-time can be estimated at about 43 days, even though this formula can normally not be applied at such high pH.

It is also possible to accelerate this chemical reaction by catalysis, using metals (metal salts reduced by the $NaBH_4$) such as platinum, ruthenium, cobalt or others [28–31]. Obviously, removing the catalyst stops the hydrolysis reaction. The reaction is exothermic and generates water vapor when the system is getting warm, in addition to hydrogen gas; this combination of hydrogen proprieties (high purity, warmth and

humidity) is perfect for an injection in a PEMFC system, as represented hereafter (see **FIGURE I-15**). However, in that case, the fuel is (indirectly) valorized at the hydrogen potential (at best) and not at its thermodynamic potential. In the particular case of $NaBH_4$, the loss is cell voltage is as high as 0.4 V (*ca.* 30% in terms of energy).

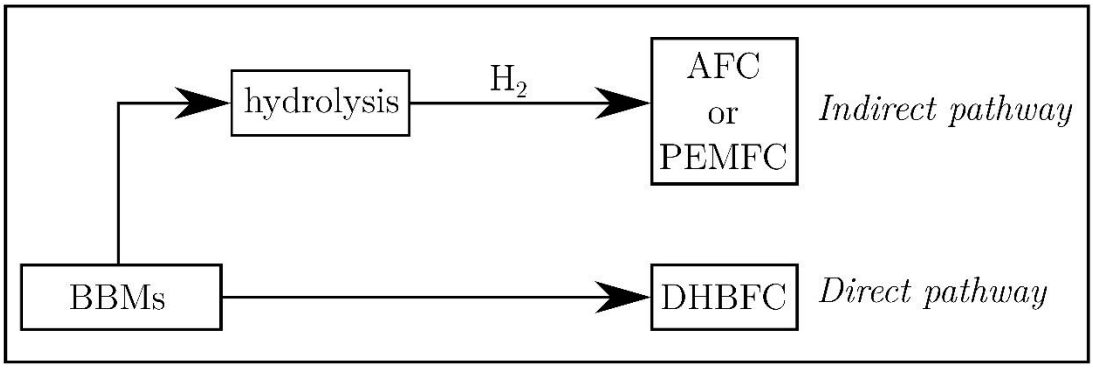

Figure I-15 Indirect vs. direct pathways to use BBMs for fuel cell systems.

Another way to use BBMs is to "directly" electrooxidize them on appropriate electrocatalysts. In that strategy, one does not expect the BBMs to release any hydrogen but in contrary to take benefit of their ability to be electrooxidized below the hydrogen potential (lower than E = 0 V *vs.* RHE, **FIGURE I-16**). Overall, such strategy shall increase the operating voltage of the fuel cell and therefore improve the electrical performances of the DAFC system by up to 30% versus an indirect PEMFC.

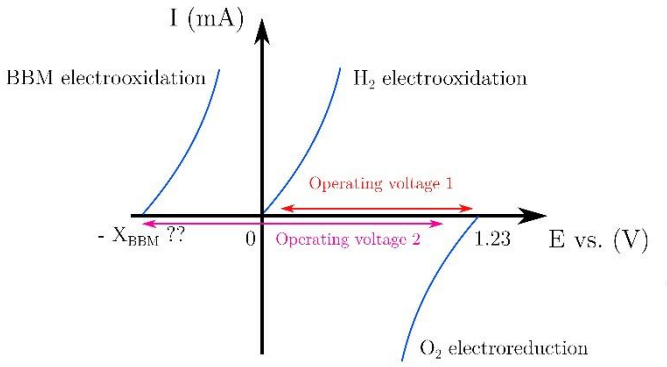

Figure I-16 Fuel cell operating gain using BBM instead of hydrogen.

In a recent work published by Olu *et al.*, ammonia borane electrooxidation was studied on palladium and platinum electrocatalysts [32]. Borane electrooxidation reaction (BH_3OR), using ammonia borane, was detected at potential value as low as E = -300 mV *vs.* RHE on palladium, which is 300 mV lower than the hydrogen electrooxidation reaction. However, with sodium borohydride or on platinum based

electrocatalysts the reaction begins at E = 0 *vs*. RHE (the potential where the HOR can also begin), which underlines the importance in the choice of both the BBM and the electrocatalyst, thereby illustrating the complexity of the DAFC systems fed with BBM fuels.

As a further complexity, most of the active electrocatalysts for direct BBM electrooxidation are unfortunately also good catalysts for their hydrolysis into hydrogen gas [33]. A natural goal of this PhD is therefore to investigate the best compromise between direct BBM electrooxidation and BBM hydrolysis, in order to improve the performance for the direct liquid alkaline fuel cell (DLAFC) system. In that regards, four kind of (electro)catalysts can be distinguished (**FIGURE I-17**):

1. The catalysts only very good for BBM hydrolysis;
2. The electrocatalysts only very good for BBM direct electrooxidation reaction;
3. The (electro)catalysts good for both BBM direct electrooxidation reaction and BBM hydrolysis, **BUT** not efficient for hydrogen electrooxidation reaction;
4. The (electro)catalysts good for both BBM direct electrooxidation reaction and BBM hydrolysis, **AND** also efficient for hydrogen electrooxidation reaction.

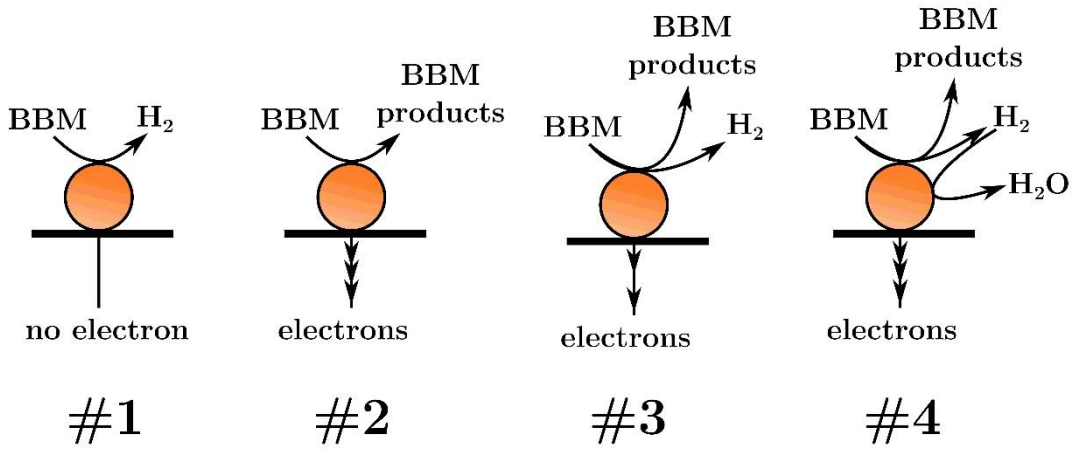

Figure I-17 Several kind of (electro)catalysts for BBM electrooxidation.

The electrocatalysts #2 and #4 are *a priori* the best ones to extract the maximum of the electrons inside the BBMs. In particular, the ability of electrocatalysts #4 to electrooxidize hydrogen enables to extract electrons lost in the form of gaseous H_2, and therefore in principle to completely valorize the BBM fuel in terms of faradaic efficiency (if no fuel is lost, of course). On the contrary, for the electrocatalysts #3 the hydrogen produced and released by BBM hydrolysis will not be electrooxidized in order to generate current and therefore will be lost, overall yielding lower faradaic efficiency (the extreme case being 0 if 100% of the BBM is converted into H_2 and 0% H_2 is electrooxidized, corresponding to the electrocatalysts #1).

In addition, the electrocatalysts #2 and #3 are *a priori* the best ones to reach a high operating voltage for the fuel cell. Because of their inability to hydrolyze the BBMs or to electrooxidize hydrogen, the anodic current will be entirely related to the direct electrooxidation of the BBM and can proceed at very low potential values, thereby ensuring high operating voltage for the DLAFC using the BBM as fuel (such as DHBFC using hydrazine borane). All those considerations are detailed after, especially in the chapters "**NICKEL-BASED ELECTROCATALYSTS FOR DIRECT BBM FUEL CELL**" and "**EFFECT OF THE NATURE OF THE BORANE FUEL ON THE ELECTROCATALYTIC ACTIVITY**".

b. The choice of hydrazine borane as a fuel

The choice of hydrazine borane as a fuel for liquid alkaline fuel cell is the result of decades in research on other BBMs (sodium borohydride, ammonia borane, dimethyl amine borane, *etc.*). The relatively intense research effort for sodium borohydride has led to great discoveries and the investigations of the borohydride electrooxidation reaction (BOR) have brought further knowledge of its mechanism, which is practically much more complex than the overall BOR (Equation I-9) suggests.

$$BH_4^- + 8OH^- \rightarrow BO_2^- + 6H_2O + 8e^- \quad with\ E° = -0.41\ \text{V}\ vs.\ \text{RHE}\ (at\ pH = 13)$$

Equation I-9

Indeed, Equation I-9 is only a theoretical construction and in practice, the electrooxidation of BH_4^- proceeds *via* a combination of multiple chemical and electrochemical elementary steps as anticipated half a century ago [34] and lately calculated [35] and then modeled [36] for platinum surfaces. One major discovery of the last decade is that the BOR generates poisoning intermediate species such as $BH_{x,ads}$, the value of *x* being still subjected to debate and depending on the electrocatalyst material used [36–39]. Those adsorbates are produced by the dissociative adsorption of BH_4^- onto the electrocatalyst surface, as reported for platinum electrocatalysts [36], and by the reaction mechanism itself. It is demonstrated that $BH_{x,ads}$ no longer poisons the surface at high potential values [40], when hydroxyls adsorb (OH^-) quantitatively on the surface [36,41]. This poisoning explains why it is difficult to electrooxidize efficiently BH_4^- at lower potential despite a thermodynamical reaction onset value of $E = -0.41$ V *vs.* RHE. Besides, the electrooxidation of BH_4^- is often accompanied by severe H_2 generation (due to the borohydride heterogeneous hydrolysis) on most electrocatalysts surfaces, even though Pt and Pd are able to electrooxidize most of this H_2 (but only above $E = 0$ V *vs.* RHE, which is not interesting from an energy density view point) [32,42].

Otherwise, the interest of using a borane based compound instead of sodium borohydride was clear since the work of Okinaka and co-workers [43] in 1973. In this study, the BOR is investigated on gold electrode in a 0.2 M KOH solution and as presented in **FIGURE I-18**, an anodic current is obtained at 500 mV lower potential when the concentration in KBH_4 goes from 0.32 to 100 mM.

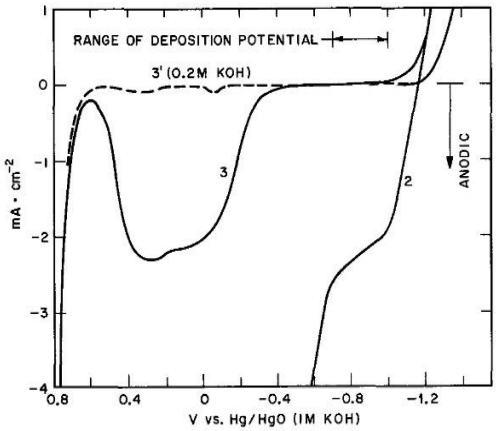

Figure I-18 Voltammogram for borohydride electrooxidation at gold electrode at T = 75°C in (3') 0.2 M KOH supporting electrolyte (3) addition of 0.2 mM KBH_4 and (2) addition of 0.1 M KBH_4.

The authors' explanation was that for higher concentration in KBH_4, a higher production of BH_3OH^- is expected, due to the KBH_4 hydrolysis and this shift in anodic current was assigned to the borane electrooxidation reaction (BH_3OR). However, this shift magnitude depends on the temperature, the concentration (in supporting electrolyte and fuel) and the nature of the electrode material. For example, in a very recent study carried out by Olu *et al.* [32], the shift between the BOR and BH_3OR is also pronounced on a palladium electrode, but remains very slight on a platinum electrode, as presented in **FIGURE I-19**.

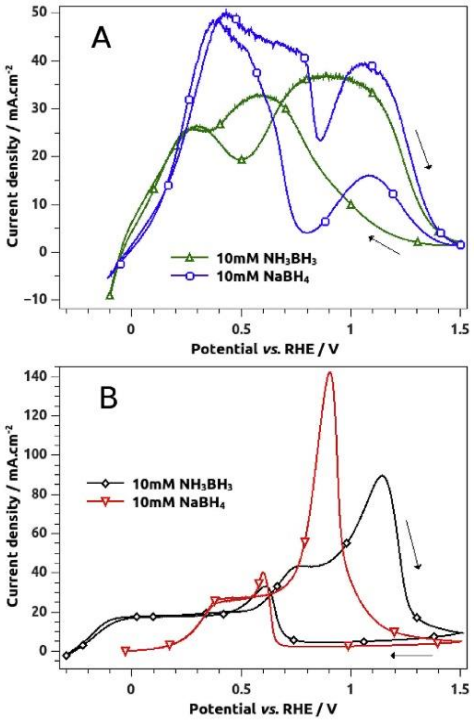

Figure I-19 Platinum (a) and palladium (b) RDE voltammograms of either 10 mM $NaBH_4$ or 10 mM AB in 1 M NaOH. Scan rate of 25 mV s^{-1} and revolution rate of ω = 1000 rpm.

Among the literature available on the borane electrooxidation reaction (BH_3OR, see **TABLE I-4**), all the investigations have been carried out using ammonia borane (AB) and dimethyl amine borane (DMAB); so, the results presented in that PhD thesis are the very first ones using hydrazine borane (HB) in alkaline medium. Unfortunately, the research effort devoted to BH_3OR is still poor and mainly restricted to studies on noble metals (such as platinum, gold and more recently palladium), and the electrochemical performances reached were not spectacular (except for palladium), notably in terms of reaction onset potential [44–53].

Actually, the first papers dealing with the BH_3OR were not targeting a fuel cell application. This initial research effort to understand the BH_3OR, more specifically *via* amine boranes (such as AB and DMAB) in aqueous solutions, has mainly focused on the optimization of the deposition of materials such as metals, semiconductors, and insulators through electroless processing for microtechnology applications using boranes compounds. Indeed, boranes present an advantage over the most widely used alternative reducing agent, hypophosphite: it is catalytically oxidized at technologically-significant substrates, which could reduce the number of processing steps and aid selectivity. For those reasons, BH_3OR has been studied mainly on gold by Burke *et al.* [54] Nagle *et al.* [45], Plana *et al.* [51,55] and Sadik *et al.* [56,57].

Around 2006, the idea of using the borane BBMs as fuels for direct liquid AFC systems emerged; naturally gold bulk electrodes [44,45] were studied first (owing to the knowledge obtained from the studies of electroless plating with this metal) and then a variety of new electrocatalysts such as nanoporous-gold-based [44,50], platinum-based [32,48], titane-carbide-based [49] or palladium-based electrocatalysts [32]. Unfortunately, the literature available is very hard to summarize, owing to the significant differences in the experimental parameters chosen by the authors, which prevents any straightforward comparison.

- The first important difference is the nature of the borane fuel. Indeed, studies generally mention the BH_3OR as if it is independent with the borane fuel. For example, Finkelstein *et al.* [40] consider that the DMAB is chemically dissociated in an alkaline solution into DMA + $BH_3^{\bullet}$, the latter which then reacts with OH^- to form BH_3OH^-. Then it is supposedly the BH_3OH^- anion that is electrooxidized on the electrode surface. However, the BH_3OR mechanism is not exactly the same when AB or DMAB (or other borane fuel) is used; this is further explored in chapter **"EFFECT OF THE NATURE OF THE BORANE FUEL ON THE ELECTROCATALYTIC ACTIVITY OF PALLADIUM"**.

- The second important difference is the nature of the electrolyte. In many studies dealing with electroless deposition, the electrolytes are containing a buffer solution [54,58,59], different borane fuels, different Borane:OH^- ratios, different temperatures, different electrocatalysts and different electrode materials and structures. On the latter point, it is worth noting that the first results obtained with a RDE (Rotating Disk Electrode) have been brought by Sadik *et al.* [57] in 2005 for DMAB electrooxidation on gold; before that very moment, results were only obtained in static conditions,

which were more realistic for an electroless application but rendered difficult any understanding since mass-transport was not well-defined and quasi-steady-state conditions not reached. Then, Nagle *et al.*, using gold micro-electrode in 2005 [60] for the same reaction, also obtained quasi-steady-state results. It is important to keep in mind that because BBMs lead to hydrogen release and because their electrooxidation involve many intermediates, it is impossible to reach a perfect steady-state electrochemical regime on static electrodes (even when micro-electrodes are used, as demonstrated by Chatenet *et al.* – see **FIGURE 7** in [61]). The diversity in experimental conditions makes the results more complicated to reproduce in other laboratories and to compare from one study to another, which calls for benchmarks and methods. Olu *et al.* recently proposed some for the electrooxidation of sodium borohydride$^-$ and AB [32].

- Finally, the nature of the electrode (its composition and morphology) can have a huge impact on the BH_3OR. For instance, Nagle *et al.* [44,50] have investigated the DMAB electrooxidation on nanopourous gold synthesized by the selective dealloying of silver from $Au_{0.18}Ag_{0.82}$ materials. The onset of BH_3OR is clearly impacted by the porosity of the material. In **FIGURE I-20**, one can observe a difference of 300 mV between the lowest and the highest onset potential value, which underline the surface sensitivity of the BH_3OR.

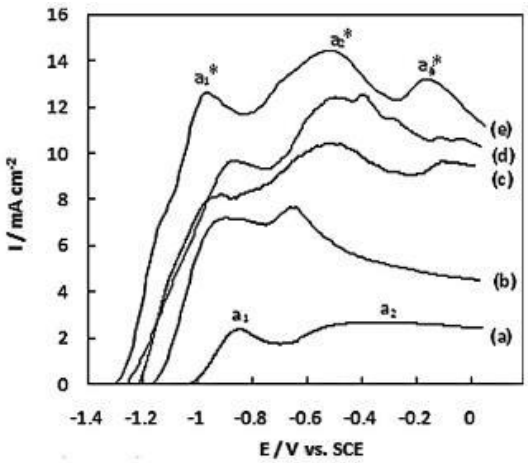

Figure I-20 Linear scan voltammogram recorded at v = 10 mV s^{-1} for (a) Au disc (b) Au wire array (c) NPG-coated Au wire array (d) NPG-Au segmented wire array and (e) NPG wire array. All performed in 1 M NaOH containing 20 mM AB. Extracted from Nagle et al.[44]

On that point, it is worth noting that the PhD work targets a real application; so, metal-based carbon-supported electrocatalysts are generally used. However, in the recent studies of the BOR performed with nanoscale materials, the surface sensitivity is also at stake. For example, in [41] Olu *et al.* underlined the effect of the surface morphology of platinum-based carbon-supported nanoparticles for the BOR. **FIGURE I-21** shows that the electrocatalyst loading has a great

influence on the BOR performance. At lower Pt/GC loadings, both the current in the kinetic/mixed region (E < 0.4 V *vs*. RHE) and in the mass-transport-limited region (E > 0.5 V *vs*. RHE) decrease when the Pt nanoparticles loading decreases. This trend depends on the morphology of the Pt/GC nanoparticles, *i.e.*, by the (combined or not) effects of the (1) Pt nanoparticles size, (2) roughness factor, and/or (3) inter-particles distance.

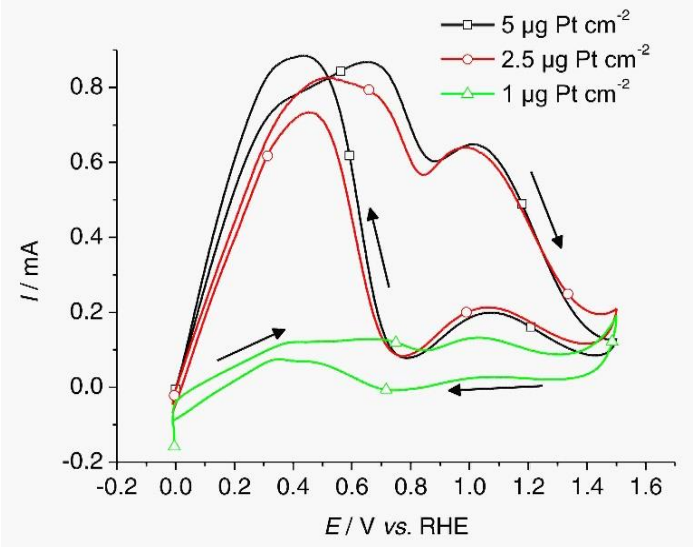

Figure I-21 Quasi-steady-state $NaBH_4$ electrooxidation voltammogram measured at v = 20 mV s^{-1} and ω = 2500 rpm (revolution per minute) on Pt/GC nanoparticles with various Pt loadings in 1 M NaOH + 1 mM $NaBH_4$. Extracted from Olu et al. [41].

Since, BOR and BH_3OR are two very complex (and in appearance rather similar) reactions, one can assume such surface sensitivity for the BH_3OR also. Thus, this calls for a real understanding of the electrode material composition and texture/morphology, to understand the BH_3OR.

To reach such understanding of the BH_3OR mechanism, it is crucial to work in half-cell system to study the electrocatalytic performance of different electrocatalysts; this shall then enable to rank them for a future utilization in DLAFC. Indeed, working directly with a DLAFC adds a lot of variables such as the membrane, the cathode, the fluidics and load cycle, *etc.*, that bring a higher level of complexity and makes difficult any straightforward comparison of the anode electrocatalysts [32,41]. This is why, this manuscript will only present results obtained in half-cell, in the goal to provide a better understanding of the BH_3OR mechanism, kinetics and the electrocatalyst stability/durability for a utilization as DLAFC anode. Then, because the quasi-steady-state conditions are required to provide reproducible and comparable data, the electrolytes do not contain any buffer or additional species, and the experiments are performed in the rotating disk electrode (RDE) setup, to control the mass-transport process (arrival of fuel and removal of the by-products, the products and the hydrogen released by hydrogen hydrolysis).

Table I-4 Major published papers on the borane electrooxidation reaction

Authors Targeted application	Year Ref	Electrolyte & Fuel	Electrocatalyst nature	Experimental conditions Mass-Transport conditions	Onset for the borane electrooxidation (I = 0 mA)
L. D. Burke *et al.* Electroless plating baths	1991 58	1 M NaOH 0.05 → 0.1 mM DMAB Buffer solutions	Cobalt and iron wire	25 → 60 °C Static	*E* = - 0.26 V *vs.* RHE when pH = 13.6 *E* = - 0.42 V *vs.* RHE when pH = 9 (for the first cycle)
L. D. Burke *et al.* Electroless plating baths	1992 54	1 M NaOH 0.05 mM DMAB & TBAB & PB Buffer solutions	Gold wire	25°C Static or stirred	For DMAB & TBAB > *E* = 0 V *vs.* RHE for pH > 13
A. Sargent *et al.* Electroless plating baths	2001 56	40 g/L KOH 2 g/L DMAB	Gold film	Room Temp Static	*E* ≈ -0.9 *vs.* Ag/AgCl
L. Nagle *et al.* Electroless plating baths	2005 60	1 M NaOH 1 → 160 mM DMAB	Gold microdisk	Unknown microdisk	*E* ≈ -0.8 *vs.* Ag/AgCl
O. Sadik *et al.* Electroless plating baths	2005 57	1.8 → 13.2 mM KOH 10 mM DMAB	Gold bulk	Unknown static & rotation	*E* ≈ -0.8 V *vs.* Ag/AgCl In the best cases (Oxygen pollution in the electrolyte…)

L. Nagle *et al.*	2006	1 M NaOH 1 → 70 mM DMAB & AB	Gold microdisk	20°C	*E* ≈ -0.95 V *vs.* Ag/AgCl for AB & DMAB In the best cases
Electroless plating baths First thoughts for AFC	[45]			Static	
X. Zhang *et al.*	2007	2M NaOH 20 mM AB	Gold disk Pt/C	Room Temp	*E* ≈ -0.95 V *vs.* SCE In the best cases
Fuel cell	[62]			Static & pumped in DABFC	
J. Martins *et al.*	2008	3 M NaOH ≈ 0.01 M DMAB	platinum rod	25°C	*E* ≈ -1.1 V *vs.* Ag/AgCl
Fuel Cell	[48]			Static	
X. Zhang *et al.*	2008	2 M NaOH 10 → 500 mM AB	Pt/C	25, 35, & 45°C	No three-electrode electrochemical experiment
Fuel cell	[53]			pumped in DABFC	
D. Plana *et al.*	2009	0.7 M KOH 3 → 10 mM DMAB	gold disk	Irrelevant experiments for our discussion	
Electroless plating baths	[55]				
X. Zhang *et al.*	2009	2 M NaOH 10 → 100 mM AB	Gold disk	Room Temp	*E* ≈ -1.1 V *vs.* Ag/AgCl
Fuel cell	[46]			Static	
L. Nagle *et al.*	2010	1 mM NaOH 20 mM AB	Gold disk & microdisk & nanoporous	Unknown	From *E* ≈ -1.1 to -1.3 V *vs.* SCE depending on the electrode used.
Fuel cell	[50]			Static & microdisk	
K. Freitas *et al.*	2011	0.1 M NaOH 1mM AB	Platinum disk	25°C	*E* ≈ -0.95 V *vs.* Hg/HgO
Fuel cell	[63]			rotating disk	

V. Kiran *et al.*	2011	1 M NaOH 50 mM AB	Titanium carbide	25, 60, 80°C	Irrelevant experiments for our discussion
Fuel cell	[49]			Static & pumping for DABFC & DBFC	
L. Nagle *et al.*	2011	1 M NaOH 20 mM AB	Nanoporous gold	Room Temp	E = -1.3 V *vs.* SCE depending on the electrode used
Fuel cell	[44]			Sattic & rotating electrode	
D. Plana *et al.*	2011	KOH (pH 13.6) ≈ 1 → 2 mM DMAB	Pt & Au disks Au microelectrode	Unknown	E = -0.8 V *vs.* Ag/AgCl (Au) E ≈ -0.9 V *vs.* Ag/AgCl (Pt)
Electroless plating baths	[51]			Static experiments on Pt & Au disks Gold microelectrode	
D. Plana *et al.*	2011	0.1 KOH 2 mM DMAB	Au single crystals	Unknown	E > 0.1 V *vs.* RHE
Fuel cell	[52]			rotating electrode	
N. Kulyk *et al.*	2012	Complex electrolytes with DMAB, buffer solution (pH<9)	Cu wire	Irrelevant experiments for our discussion	
Electroless plating baths	[64]				
D. Finkelstein *et al.*	2013	1 M NaOH 5 mM DMAB	Pt & Au disk	Room temperature	E ≈ -0.9 vs. Ag/AgCl (Au) E ≈ -0.6 vs. Ag/AgCl (Pt)
Fuel Cell	[40]			Rotating Electrode	
B. Concha *et al.*	2013	1M NaOH 1 → 10 mM AB	Au disk	25°C	E > 0 V *vs.* RHE
Fuel cell	[47]			Rotating Electrode	
P. Olu *et al.*	2015	Fuel Cell 5 M NaOH + 1 M AB Half Cell 1 M NaOH + 10 mM AB	Pt/C & Pt disk Pd/C & Pd disk	Room temperature	E ≈ -0.3 V *vs.* RHE (Pd disk) E ≈ -0.05 V *vs.* RHE (Pt disk)
Fuel Cell	[32]			Rotating Electrode	

Otherwise, it is important to mention that liquid AFC systems are not utopic and have demonstrated their feasibility in the case of DBFC (direct borohydride fuel cell) and in a lesser extent DABFC (Direct Ammonia Borane Fuel Cell, see **TABLE I-5**). Zhang and coworkers [53,62] have brought results for a practical DABFC system. They obtained power density value about 14 and 110 mW cm^{-2} using platinum-based carbon-supported electrocatalysts in 2 M NaOH + {10 mM → 0.5 M} AB solutions using Nafion® or anionic membranes. The same authors found in [53] a positive effect of an increase in temperature from T = 25 to 45°C, which they assigned to "the improved catalytic activities of the anode and cathode at elevated temperatures". This latter quote underlined the fact that the authors were not working in anode-limited conditions which could have permitted to better understand what was going on for the BH_3OR at the anode increasing the temperature. Recently, Olu *et al.* have operated a lab-scale DABFC [32], which reached 181 mW cm^{-2} on Pt/C and Pd/C electrocatalysts in 5 M NaOH + 1 M AB solutions. The particularity of that work is that the DABFC performances were deliberately limited by the anode; the cathode was indeed carefully designed with a higher quantity of Pt/C electrocatalysts and fed with pure oxygen at large stoichiometry. So, the study allowed to underlines the dual effect of temperature on the DABFC performances; with Pd/C, the performances were better at T = 60°C than at 25°C but worse than at T = 80°C due to increased ammonia borane hydrolysis at elevated temperature, leading to H_2 generation (and partial electrooxidation) and a loss of performance. More interestingly, the impact of the anode texture has been underlined and better performances were obtained with a cracked catalytic layer than with a smooth and homogeneous one: a cracked catalytic layer facilitates the anolyte circulation and the removal of hydrogen bubbles generated by the hydrolysis. That complexity is also observed in half-cell experiments and is further discussed in chapters **"NICKEL-BASED ELECTROCATALYSTS FOR DIRECT BBM FUEL CELL"** and **"EFFECT OF THE NATURE OF THE BORANE FUEL ON THE ELECTROCATALYTIC ACTIVITY OF PALLADIUM"**. Finally, Yao *et al.* [65] operated a DABFC with static anolyte, in which they underlined the good activity of MnO_2-based electrocatalyst for ORR in alkaline medium even when it is in contact with AB, a result that can be ascribed to the tolerance of MnOx/C materials to fuels [66–68].

Table I-5 Data available on direct borane fuel cell systems

Authors & Year & Ref	Anode Nature Loading (mg cm^{-2})	Anolyte Nature Flow ($mL.min^{-1}$)	Separator	Cathode Flow ($mL.min^{-1}$)	Catholyte Loading (mg cm^{-2})	T	S (cm^2)	P (mW cm^{-2})	Operating voltage (Volt)
Zhang *et al.* 2007 [62]	Pt/C 0.15	2 M NaOH 10 mM AB *Unknown*	Nafion® 117	Oxygen *Unknown*	Pt/C 0.15	Room Temp	25	14	≈ 0.9
Zhang *et al.* 2008 [53]	Pt/C 0.76	2 M NaOH 0.1 → 0.5 M AB 50	Anion membrane	Oxygen 120	Pt/C 0.93	25, 35, 45°C	*Unknown*	110	$0.8 \leq x \leq 0.9$
Yao *et al.* 2007 [65]	Ag/C Unknown	6 M KOH 0.5 M AB *No flow*	No separator	Air cathode *No flow*	MnO_2/C	Room Temp	1	*Unknown*	1.15
Olu *et al.* 2015 [32]	Pt/C or Pd/C 0.5	5 M NaOH 1 M AB 7.5	Nafion® NRE-212	Pure oxygen 300	Pt/C 2	25, 60, 80°C	25	181 (at 25°C)	1.05

To the authors' knowledge, no study concerning the performances of DLAFC systems using DMAB (DDMABFC) have been carried out. In addition, despite the theoretical promises, none of the studies dealing with DABFC systems have reported operating voltage value higher than 1 V [32,65], although up to 1.61 V could be expected for borane fuels. This explains why BH_3OR still has to be investigated, in particular to understand what prevents to reach the optimal operating voltage value. Only a better understanding of the BH_3OR (and BOR) can allow to improve the performances in real liquid AFC systems. If possible improvements in electrocatalysis for AB and DMAB electrooxidation reactions (DABOR and DDMABOR) are possible, there is no doubt that both ammonia (NH_3) and dimethylamine (DMA) are useless "fuel-wise" and can even be detrimental to the environment or to an industrial application; besides, they have deleterious properties for a use as fuel for DLAFC: DMA and NH_3 are strongly adsorbing on most catalysts surfaces, which induces poisoning issues, are corrosive (in the case of NH_3) and toxic. In that perspective, hydrazine borane (HB) combines the intrinsic advantages of its two moieties (hydrazine and borane), both of them being interesting fuels for a DLAFC. Indeed, the hydrazine fragment is also stable and electrooxidizable in alkaline medium, and the reaction only releases nitrogen (without any ammoniac production) on suitable electrocatalysts [69–72]. Moreover, in term of gravimetric hydrogen storage capacity, denoted GHSC, hydrazine borane ($N_2H_4BH_3$) can experimentally store 6 wt% of H_2, versus *ca.* 6-7 wt% for sodium borohydride ($NaBH_4$) and 7 wt% for ammonia borane NH_3BH_3 (AB, this figure excluding the valorization of NH_3, which is not practical in a DABFC). So, HB is a clear competitor to sodium borohydride and AB in terms of energy density, and is in principle less affected by any electrocatalyst poisoning phenomena and management difficulties (*e.g.* with $BH_{x,ads}$ intermediate form during the BOR, and with ammonia pollution during the BH_3OR using AB), making of HB an interesting alternative BBM to feed a DLAFC.

Otherwise, in DHBFC systems fed with an alkaline solution containing hydrazine borane, it is important to mention that the two fragments of HB will be present at the anode, the borane fragment (BH_3) and the hydrazine fragment (N_2H_4). So in addition to the BH_3OR, the hydrazine electrooxidation reaction (noted HHOR) is also expected to (simultaneously) happen at the anode. Interestingly, the hydrazine fragment is thermodynamically electrooxidized at a potential lower than the hydrogen potential which is another clear interest in terms of energy density for the DHBFC systems. To sum up, the electrochemical reactions at stake in a DHBFC are:

- The borane electrooxidation reaction (BH_3OR) at the anode, in principle occurring at $E°$ = -1.21 V *vs*. SHE (pH = 14)

$$BH_3OH^- + 6OH^- \rightarrow BO_2^- + 5H_2O + 6e^-$$

Equation I-10

- The hydrazine electrooxidation reaction (noted HHOR) at the anode, in principle occurring at $E°$ = -1.16 V *vs*. SHE

$$N_2H_4 + 4OH^- \rightarrow N_2 + 4H_2O + 4e^-$$

Equation I-11

- The oxygen electroreduction reaction (ORR) at the cathode, in principle occurring at $E°$ = 0.39 *vs*. SHE (pH = 14),

$$O_2 + 4e^- + 2H_2O \rightarrow 4OH^-$$

Equation I-12

To ease the discussion at that stage (complexity will come soon enough), one can imagine that a single electrocatalyst may be used at the anode to perform both the BH_3OR and the HHOR simultaneously; in that case, the theoretical operating voltage of the DHBFC would reach *ca.* 1.6 V, and a total of n_{e^-} = 10 electrons would be generated per HB species. It is worth noting that this voltage value is significantly higher than the 1.23 V expected by electrooxidizing gaseous hydrogen at the anode instead of HB, which justifies the present attempts to find the best electrocatalysts for HB electrooxidation. Of course, in practice, some piece of complexity must be introduced to fulfill the HB electrooxidation reaction at the lowest possible anode potential; those elements represent the main challenges faced in that PhD thesis:

1. What if the anode electrocatalysts cannot succeed in electrooxidizing both the borane and hydrazine fragments at low potential values?

2. Are the hydrazine and/or the borane fragment(s) subjected to hydrolysis on a given electrocatalyst? If yes, is the hydrogen electrooxidation reaction (HOR) happening? If not, can the system be considered efficient?
3. What if the choice of hydrazine fragment (instead of ammonia or DMA) also has an impact (positive or not) on the electrooxidation of the borane fragment?

These questions are the essence of this PhD work…

c. Hydrazine borane synthesis, catalysts degradation & cost aspects

Before diving into fundamental issues, it seems relevant to briefly mention some economic thoughts about hydrazine borane. The hydrazine borane used in that manuscript has been synthesized at the Institut Européen des Membranes (IEM) laboratory, in the group of Umit DEMIRCI [73]. The main steps of synthesis to produce highly pure HB chemical are as follows [73]:

1. In a glove box, 21.59 g of hydrazine hemisulfate and 10.12 g of sodium borohydride are separately and finely ground in agate mortars;
2. Those latter chemicals are then transferred into a 500 mL three-necked round-bottom flask. This flask is put in the argon-vacuum line and in an oil batch thermostated at T = 30°C;
3. Then, 150 mL of dioxane are added under vigorous stirring. The reaction of HB generation starts immediately and H_2 also evolves;
4. The mixture is kept under stirring for 48 hours at T = 30°C;
5. It is then filtrated and the by-products are washed with 50 mL of dioxane;
6. The solvent (dioxane) is slowly removed and the filtrate is dried under vacuum and under room conditions overnight;
7. Finally, 9.8 g of a white solid I obtained (yield: 80.3 %), with a purity of 99.6%.

To the author's knowledge, there is no industrial production of hydrazine borane today. So, it would be difficult to estimate the cost of a practical DHBFC system since even the fuel used is not industrialized. It seems however difficult to claim that HB is a cheap fuel, because even if an industrialization of the synthesis could diminish its cost and optimize the synthesis (especially in terms of time and yield), the HB will remain more expensive than sodium borohydride and hydrogen alone, following the utilization of hydrazine hemisulfate and sodium borohydride as reactants, and because the synthesis also proceeds *via* steps under vacuum, controlled temperature and lasts about 3 days. Disregarding this aspect, the present thesis firstly aims to demonstrate the interest of HB as a fuel for a portable DLAFC; more specifically, it will stick to research aspects related to the anode reaction and electrocatalysts of this system. In particular, like direct borohydride fuel cell (DBFC), DHBFC shall find applications in the field of portable generators, where hydrogen storage, transportation, safety and management remain delicate topics. It can even be anticipated that DHBFC will outperform DBFC, because of the better kinetic of BBM electrooxidation in alkaline medium, lower electrooxidation reaction onset values (and related larger operating voltage of the system), resulting in principle in larger practical energy and power densities. Of course, fundamental research is mandatory to reach these ambitious goals and enable DHBFC (and in general direct liquid alkaline fuel cell systems) to further challenge PEMFC for portable power systems.

v. Thesis decoupage

In **CHAPTER II**, the general conditions of experimentation are given. The electrochemical set-up, the preparation protocols and the characterization techniques are described.

In **CHAPTER III**, the investigations focus on the stability in alkaline medium of platinum and palladium-based carbon-supported electrocatalysts, and, on the stability/durability of one cubic palladium-based unsupported electrocatalyst.

CHAPTER IV focusses on the electrochemical performances of nickel-based carbon-supported electrocatalysts for the electrooxidation of ammonia borane and hydrazine borane in alkaline medium; their stability/durability is simultaneously investigated.

CHAPTER V further investigates the impact of the nature of the borane fuel (ammonia borane, dimethylamine borane, hydrazine borane and hydrazine bis-borane) on its electrooxidation reaction kinetics on a palladium-based carbon-supported electrocatalyst (and also on a platinum-based carbon-supported electrocatalyst for sake of comparison). Those investigations integrate the results concerning palladium (and platinum) material stability (presented in **CHAPTER III**) to provide relevant data.

General experimental section

II. General experimental section

i. Common experimental conditions

a. Electrochemical Set-up

The electrochemical set-up used for the experimentations is mostly the same in the whole PhD work. It consists in a three-electrode cell where:

1. The working electrode (WE) is a thin deposit of the electrocatalysts ink on a 5 mm diameter glassy-carbon electrode. Then, the WE electrode is integrated in a rotating disk electrode (RDE) system that enables to control the rotation speed of the WE electrode within the electrolyte. The rotation speed is given in revolution per minute (rpm);
2. The counter-electrode (CE) is generally a carbon plate (the reader will be informed otherwise), to avoid any possible pollution of the electrolyte and of the WE by the corrosion/degradation of the CE material (more likely if it is metal-based);
3. The reference electrode (RE) can be, depending on the electrolyte nature, a reversible hydrogen electrode (RHE), a mercury/mercury oxides electrode (Hg/HgO) or a mercury sulfate electrode (MSE) (**TABLE II-1**).

Table II-1 Characteristics of the various reference electrodes used in the PhD thesis

Electrolyte type	Reference Electrode type	Conversion to RHE
In alkaline medium	RHE	E = 0 V *vs.* RHE
	Hg/HgO filled with 0.1 M NaOH	E = 0 V *vs.* RHE (in 0.1 M NaOH) → E = -0.935 V *vs.* Hg/HgO
In acidic medium	MSE filled with a saturated K_2SO_4 solution	E = 0 V *vs.* RHE (in 0.1 M H_2SO_4) → E = -0.732 V *vs.* MSE

The electrochemical cell is made with PYREX glass, a material however prone to (slow) dissolution at high pH [74,75]; this is why the concentration of NaOH solution was kept at 0.1 M NaOH. Another reason is that at low supporting electrolyte and fuel concentrations – the conditions used in the present thesis – the understanding of the WE processes is more straightforward, a prerequisite for the elucidation of a

complex reaction like the hydrazine borane electrooxidation reaction. The labware used to prepare and to handle the electrolytes (beakers, flasks, clamps, *etc.*) is PTFE-based.

To ensure the required cleanness in the experimentations, all the electrochemical set-up and the labware are immerged in a concentrated solution of **Caro's acid** (1-1 vol.% H_2O_2 (30%)-H_2SO_4 (> 95%)) during the night preceding the experiment, which enables to oxidize any organics and to dissolve most of the metal impurities. Then all the set-up and labware is abundantly rinsed with both room temperature and boiled MQ-grade water (18.2 MΩ cm, < 3 ppb total organic carbon, Elix + Milli-Q Gradient, Millipore).

b. Electrolytes and electrocatalyst ink

The electrolytes are always prepared with MQ-grade water and pure reagents (H_2SO_4, $HClO_4$ or NaOH) were provided by Merck (suprapur quality). The concentration in H_2SO_4, $HClO_4$ or NaOH is fixed at 0.1 M in every experiment, and electrolytes are always deaerated with Argon (N45 purity, at least).

Concerning the borane fuels used in that PhD work:

- Hydrazine borane (HB) and hydrazine bis-borane fuels (HBB) were provided by the group of Demirci at University of Montpellier.
- Dimethylamine borane (DMAB) and ammonia borane fuels (AB) fuels were provided by Sigma Aldrich.

The electrocatalyst inks are composed with a suspension of carbon-supported (or unsupported) metallic-based nanoparticle powder in a solution containing a certain quantity of ultrapure water, isopropanol and Nafion®. The specific ink composition is adapted for each study and is described in the beginning of the different chapters.

The electrocatalyst inks are then used to prepare the thin-film working electrodes (see **FIGURE II-1**). A typical WE is a thin-deposit formed by the deposition of a 10 or 20 µL-calibrated drop on the surface of a glassy-carbon electrode. This drop is then dried with a hairdryer while the electrode is rotated in the same time. The methodology allows to get an essential uniformity of the thin-deposit for the electrochemical kinetic characterizations as reported previously by Garsany *et al.* [76].

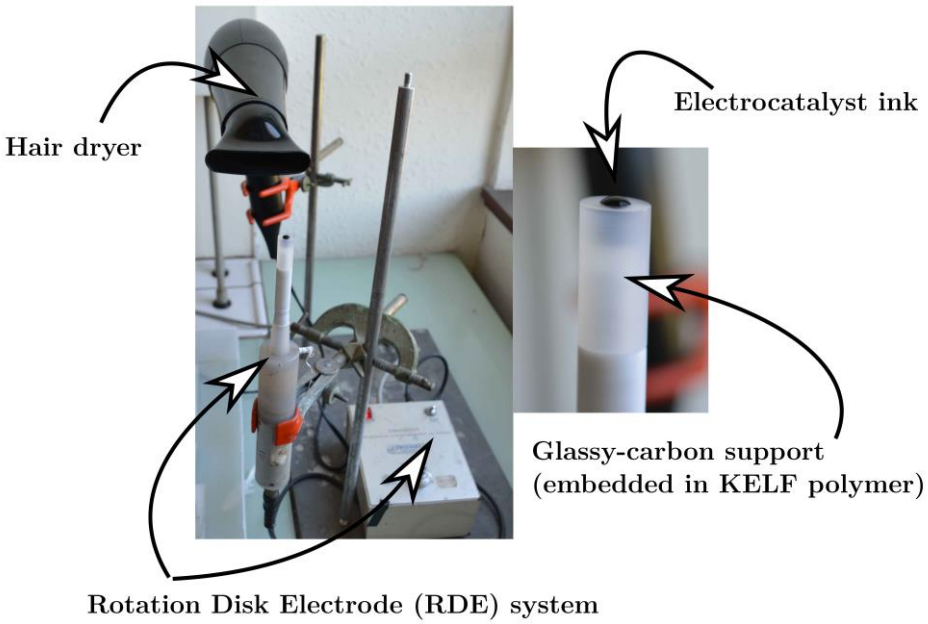

Figure II-1 Working electrode preparation set-up.

ii. Physical & Chemical Characterizations

a. Transmission Electron Microscopy (TEM)

The morphology of the electrocatalyst nanoparticles is investigated using a transmission electron microscope (TEM). The TEM uses highly energetic electrons as a probe and their much lower wavelength than photons of the visible light makes possible to visualize objects at a scale down to the nm. For the electron beam to penetrate the sample, it is required that the thickness of the sample is in the order of a few hundred nanometers or less, which is the case with small aggregates of metal-based carbon-supported electrocatalysts.

The "source of electrons" (filament or gun) emits some electrons that are accelerated at high voltage, travel through vacuum in the column of the microscope and are focused into a very thin beam thank to electromagnetic lenses. Then, the electron beam crosses the studied sample; depending on the density of the material present, some of the electrons are scattered. At the bottom of the microscope, the unscattered (transmitted) electrons hit a fluorescent screen (or a CCD camera), which gives rise to a "shadow image".

In this PhD work, TEM micrographs were obtained on a JEOL 2010 TEM apparatus equipped with a LaB_6 filament operating at 200 kV (point-to-point resolution = 0.19 Å).

TEM is particularly interesting in (electro)catalysis because it allows to image nanoparticles (and their carbon support, when applicable). From TEM images, one can evaluate the particles shape, size (and to draw particle size distribution histograms, PSD) and extent of agglomeration. This information is useful to establish structure/electroactivity relationship, and to follow the possible change of morphology upon electrochemical aging tests.

For PSDs, different averaged mean particle sizes are calculated:

$$\text{the number} - \text{averaged mean particle size} : \overline{d_N} = \frac{\sum_{i=1}^{n} n_i \, d_i}{\sum_{i=1}^{n} n_i}$$

$$\text{the surface} - \text{averaged mean particle size} : \overline{d_S} = \frac{\sum_{i=1}^{n} n_i d_i^3}{\sum_{i=1}^{n} n_i d_i^2}$$

$$\text{the volume} - \text{averaged mean particle size} : \overline{d_V} = \frac{\sum_{i=1}^{n} n_i d_i^4}{\sum_{i=1}^{n} n_i d_i^3}$$

The value of $\overline{d_S}$ enables comparison with the "electrochemical diameter" (originating from electrochemical surface area measurements, ECSA), while that of $\overline{d_V}$ can be compared with the crystallite size measured in X-Ray diffraction.

In this PhD work, TEM analyses are used to access the morphological/chemical properties of the initial electrocatalysts, but also the evolution of these parameters upon electrochemical aging tests. In addition, identical-location TEM (ILTEM) is used as a near *in situ* characterization tool (see specific section below). In any case, the powder of the characterized M/C electrocatalyst is immobilized at a gold + lacey carbon TEM grid, by drop casting from the electrocatalyst ink. Those experiments have been carried out at the CMTC research platform (Materials Characterization Center of Grenoble-INP).

b. Raman spectroscopy

In complement to (IL)TEM characterizations of the metal nanoparticles, their carbon substrate (when applicable) was studied by Raman spectroscopy. Raman spectroscopy is a technique based on the inelastic scattering of a monochromatic light, usually from a LASER source. Inelastic scattering means that the frequency of photons in the monochromatic light changes upon interaction with a sample. In practice, photons from the LASER source are absorbed by the sample and then reemitted at a frequency that can be either lifted up or down in comparison with the original monochromatic frequency: this is the Raman Effect. This shift provides information about vibrational, rotational and other low-frequency transitions in the material composing the sample. Raman spectroscopy is particularly sensitive to the structure/chemistry of high-surface area carbons [23,77–79]. As such, it is particularly used to examine the structure of the fresh and aged carbon supports of the carbon-supported electrocatalysts. Table II-2 presents the vibration modes observable on high surface area carbon supports with Raman spectroscopy.

Table II-2 vibration modes observable on high surface area carbon supports with Raman spectroscopy

Band	Raman Shift	Vibration Mode
G	*ca.* 1585 cm^{-1}	Ideal graphitic lattice
D1	*ca.* 1350 cm^{-1}	Disordered graphitic lattice-graphene layer edge
D2	*ca.* 1610 cm^{-1}	Disordered graphitic lattice – surface graphene layer
D3	*ca.* 1495 cm^{-1}	Amorphous carbon
D4	*ca.* 1190 cm^{-1}	Polyenes, ionic impurities

In this PhD work, Raman spectra were recorded *ex situ* using a Renishaw InVia spectrometer, with the near-IR line of LASER diode (785 nm). The Raman photons were collected on a Peltier-cooled CCD detector, and the spectral resolution was ~1 cm^{-1}. The measurements were performed with a ×50 LF objective, and the LASER power was ~0.2 mW on the sample. For the sake of comparison, the Raman spectra were normalized to the intensity of the peak at ~1350 cm^{-1}, which corresponds to the band of the disordered graphitic lattice-surface layer edge. For Raman spectroscopy measurements, 40 µL of catalyst ink was deposited on the glassy carbon support to avoid (or limit as much as possible) a support (glassy-carbon) contribution, according to the procedure detailed in ref [80]. Those experiments have been carried out at LEPMI laboratory (Grenoble-INP).

c. X-ray photoelectron spectroscopy

The measurements were complemented by X-ray Photoelectron Spectroscopy (XPS), a surface-sensitive spectroscopic technique measuring the elemental composition of a material. In this technique, the material is irradiated with a beam of X-rays while measuring at the same time the kinetic energy and the number of electrons that escape from the top surface of the material analyzed (between 0 and 10 nm below the top-surface). Ultra-high vacuum (UHV, $P < 10^{-9}$ mbar) conditions are required for the XPS analyses of the surface chemistry of the carbon support of the electrocatalysts.

In this PhD work, X-ray photoelectron spectroscopy was performed:

- For the results presented in chapter "**DEGRADATION OF NOBLE ELECTROCATALYSTS IN ALKALINE MEDIUM**" on a XR3E2 spectrometer (Vacuum Generator) having a Mg Kα (1253.6 eV) X-ray source powered at 300 W (15 kV, 20 mA). The kinetic energy of the photoelectrons is measured using a hemispherical electron analyzer working in the constant-pass energy mode (30.0 eV). The analysis chamber is kept below 10^{-9}–10^{-10} mbar background pressure during the data acquisition, which is performed for 0.1 eV increments, at 50 ms dwelling times. The analyses are performed at an angle of 90° between the electrocatalyst sample surface and the analyzer. The charging effect is corrected by referring all the binding energies to the graphene component of the carbon C1s peak at 284.3 eV. Those experiments have been carried out at SIMAP laboratory (Grenoble-INP).

- For the results presented in chapter "**NICKEL-BASED ELECTROCATALYSTS FOR DIRECT BBM FUEL CELL**" on a Kratos Axis Ultra X-ray photoelectric spectrometer with an Al Kα X-ray source operating at 225 W. High-resolution spectra (O1s, C1s, Ni2p, Ag3d, Co2p, Pd3d) were collected at 20 eV pass-energy. Those experiments have been carried out at the University of New Mexico (USA).

d. X-ray Diffraction

X-ray diffraction (XRD) is a nondestructive technique to characterize crystalline materials. X-ray diffraction patterns are obtained by constructive interference of a monochromatic beam of X-rays scattered at specific angles from each set of lattice planes in the sample. The XRD pattern provides information on structures, phases, preferred crystal orientations, and other structural parameters, such as average crystal size, crystallinity, strain, and crystal defects.

In this PhD work, XRD is used to fully characterize some homemade electrocatalysts presented in the chapter **"NICKEL-BASED ELECTROCATALYSTS FOR DIRECT BBM FUEL CELL"**, since the electrochemical kinetic measurements are highly impacted by the material nature and composition. X-ray diffraction patterns are obtained using a Rigaku Smartlab diffractometer with a Cu anode X-ray source operating at 40 kV and 40 mA. A graphite monochromator is used to remove CuK-β radiation. The crystallite size and relative phase composition are determined through Whole Pattern Fitting (WPF) in MDI JADE 2010TM software. Those experiments have been carried out at the University of New Mexico (USA).

e. Brunauer-Emmet-Teller sorptometry

The Brunauer-Emmet-Teller (BET) calculation of the specific surface area of a material is based on the adsorption of gas molecules (such as nitrogen, argon, carbon dioxide, *etc.*) on a solid surface. This technique is especially relevant to investigate the porosity and texture of high-surface area carbon supports for electrocatalytic applications.

In this PhD work, Brunauer-Emmet-Teller surface areas are calculated from a four-point measurement using a Gemini 2360 surface area analyzer. All metal-based carbon-supported nanoparticle electrocatalysts were outgassed with N_2 at T = 120°C for at least 8 hours prior the measurements. Those experiments have been carried out at the University of New Mexico (USA).

iii. Electrochemical techniques

a. Carbon monoxide stripping voltammetry (CO-stripping)

The CO-stripping voltammetry/coulometry is a widely-used method to measure with accuracy the electrochemical surface area (ECSA) value of platinum-based electrocatalysts. This methods, generally applied in acidic electrolytes, consists in firstly saturating (blocking) the surface of the Pt electrocatalyst by bubbling CO for 6 min in the electrolyte (previously deaerated), while holding the electrode potential at E = 0.15 V *vs*. RHE. Then, the excess (non-adsorbed) CO is eliminated from the electrolyte by a 45 min-long argon purge, while keeping the electrode potential at E = 0.15 V *vs*. RHE. The value of the chosen potential has to be sufficiently low to allow the adsorption of CO molecules on the Pt surface, and significantly below the onset potential of carbon monoxide oxidation. Finally, the CO-stripping procedure consists of performing three cyclic voltammograms at v = 20 mV s^{-1} between E = 0.1 and 1.23 V *vs*. RHE. The first cycle (the actual CO-stripping voltammogram) displays a marked peak associated with the oxidation of the adsorbed CO, and the two following cycles serve as baseline for integration of the main stripping peak and to confirm that the electrolyte has been correctly purged from the excess of CO.

In the present work, the procedure is applied to carbon-supported Pt nanoparticles. Assuming that all platinum-based nanoparticles are covered with adsorbed CO molecules in a-top configuration, the oxidation charge is proportional to the number of platinum surface atoms. For the calculation of the ECSA, the third cycle is subtracted to the first one (which enables to remove the double-layer capacitance effect) and it is assumed that the electrooxidation of an adsorbed CO monolayer requires a charge density of 420 µC per cm^2 of Pt, resulting in:

$$ECSA = \frac{Q_{CO}}{420}$$

This electrochemical carbon monoxide electrooxidation on platinum is highly sensitive to the structure of the electrocatalyst surface. Previous studies have underlined the dependence of the main electrooxidation peak on the size distribution (position and shape of the main CO stripping peak) and the degree of agglomeration (presence of a CO pre-electrooxidation peak) of the Pt nanoparticles. These fingerprints were also used to gain some insights into the Pt/C degradation mechanisms [81–85].

If the CO-stripping technique is commonly used for platinum-based electrocatalyst, there are less evidences of its utilization for palladium-based material. Several papers have however shown that CO-stripping can also be used for palladium materials [86–93] and the ESCA calculation theory from CO

electrooxidation coulometry is the same as for platinum materials [94]. Even if no investigation of possible difference between CO-stripping on platinum and palladium materials have been carried out during that PhD work, it is important to mention that this technique has mostly been used to estimate the relative losses ECSA between a fresh electrode of palladium-based electrocatalyst and an aged one. Obviously, the ECSA can also be estimated in acidic media for example by investigations on the hydrogen under potential deposition (H_{UPD}) or the reduction of PdO monolayer, as previously reported in [86,94–96].

Nonetheless, these methods are deliberately not used in that PhD work for several reasons:

1. The first reason is that absolute ECSA estimation is not the main purpose of this study. Using CO-stripping is a relevant, accurate and reproducible technique to evaluate and to compare the ECSA values obtained for the different palladium-based electrocatalysts presented in the manuscript before/after aging tests, at least in a relative manner.

2. The second reason is that **H_{UPD}** and PdO reduction in acid are two methods which require a very meticulous analysis, especially in acidic media.

   For the **H_{UPD}** method, the lower potential value has to be carefully determined to ensure that the Pd surface is totally covered by adsorbed hydrogen. In addition, it is worth noting that Pd materials are also impacted by hydrogen absorption, which really complicates the **H_{UPD}** determination. Specifically, in the case of Pd, the adsorption and absorption of H occur concurrently and in the same potential range, as reported by Jerkiewicz *et al.* [97,98] ; so, it is almost impossible to differentiate between **H_{UPD}** and **H_{ABS}** or to determine the corresponding charge density values by analyzing CV profiles (or other simple electrochemical measurements). The example of **FIGURE II-2** extracted from [96] illustrates this bias.

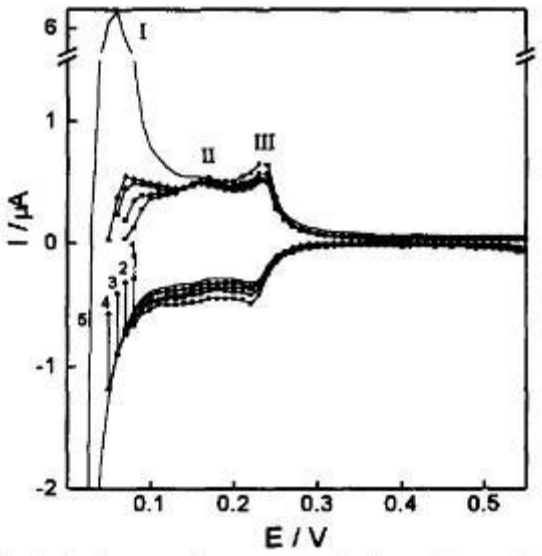

Figure II-2 Steady-state voltammograms for the upd-H potential region on a Pd-Si electrode in 0.5 M H_2SO_4 at different initial potentials E =: (I) 0.07, (2) 0.06, (3) 0.05, (4) 0.04 and (5) 0.01 V vs. RHE. Scan rate v = 0.05 V s^{-1}. Extracted from Correia et al. [96]

- For the PdO reduction in acid, the highest potential value has to be adapted to the total coverage by a PdO monolayer. Unfortunately, smaller Pd (and Pt) nanoparticles being more oxophilic than larger ones, this potential value must differ for the different palladium-based electrocacatlysts used, and for a given new and aged Pd/C electrocatalyst. **FIGURE II-3** illustrates the potential dependence of the PdO-reduction peak [86] as a function of the "amount of Pd oxides present" (PdO-reduction coulometry).

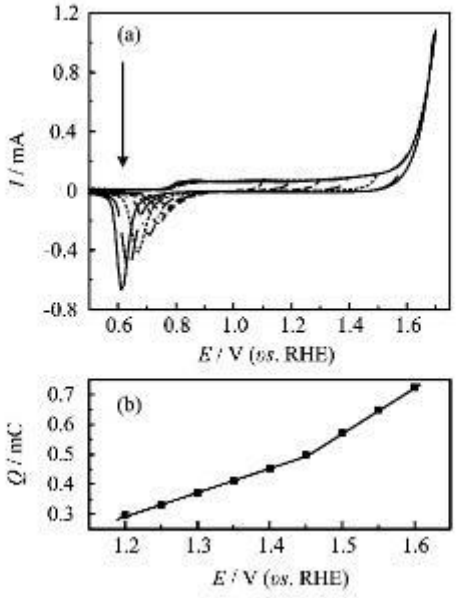

Figure II-3 (a) Series of cyclic voltammograms of Pd electrode in 0.5 M H_2SO_4 with different higher potential limit E_b = 1.1, 1.2, 1.3, 1.4, 1.5, 1.6 and 1.7 V vs. RHE (arrow direction), scan rate: v = 50 mV s^{-1}. (b) The integrated charge for the reduction of oxygen-covered Pd electrode (after double layer correction) as a function of the upper potential limit. Extracted from Fang et al. [86]

So, for each palladium-based electrocatalyst and each state of aging, it requires to target the inflexion point in the curve representing the charge as a function of the highest potential value (see **FIGURE II-3**) in order to determine the exact potential value for which the palladium surface is totally covered by a PdO monolayer.

As a result, both the $\mathbf{H_{UPD}}$ and PdO-reduction methods in acidic electrolyte would have required time-consuming analyses for every one of the different palladium-based electrocatalysts presented in that manuscript, which is absolutely not the purpose of that PhD work and was therefore not attempted.

Moreover, recent studies have brought evidences of the poor stability of Pd materials (in particular for palladium nanoparticles) in acidic medium [88,99–102], and it could be questioned whether the $\mathbf{H_{UPD}}$ and PdO-reduction methods in acid for ECSA estimation are altering (or not) the carbon-supported palladium nanoparticles (particle detachment, dissolution, *etc.*), thereby decreasing the accuracy of those methods.

For all those reasons it was chosen to perform only CO-stripping in acidic medium; this is an accurate technique for which the same protocol can be used for the different electrocatalysts (platinum or palladium based) and no "calibration" of the technique is necessary. Finally, CO-stripping in acidic medium requires only a few number of CV cycles to be performed, which is *a priori* relevant knowing the instability of palladium nanoparticles in acidic conditions.

b. Identical Location Transmission Electron Microscopy (ILTEM)

In 2008, Mayrhofer *et al.* introduced in [103] a novel and non-destructive transmission electron microscopy technique that allows to observe identical locations of an electrocatalyst before or after a given electrochemical treatment. To do so, the electrocatalyst is immobilized on a gold-made TEM grid used as working electrode in the electrolyte. The TEM grid is held in the electrolyte between carbon plates that ensure electronic conduction and avoid any contamination (**FIGURE II-4**). The electrocatalyst loading has to be small enough to ease the selection of studied regions and enable 100% utilization of any M/C nanoparticle; between 3 to 5 regions of the gold TEM grid are randomly selected and imaged at low and high magnification. After a given electrochemical treatment, the TEM grid is abundantly rinsed and dried in air before the TEM images are acquired in exactly the same position (identical-location TEM). Comparing the particle size distribution (PSD) and the carbon support shape, before and after a given electrochemical test, enables to understand and evaluate how the electrocatalyst has been degraded by this electrochemical test.

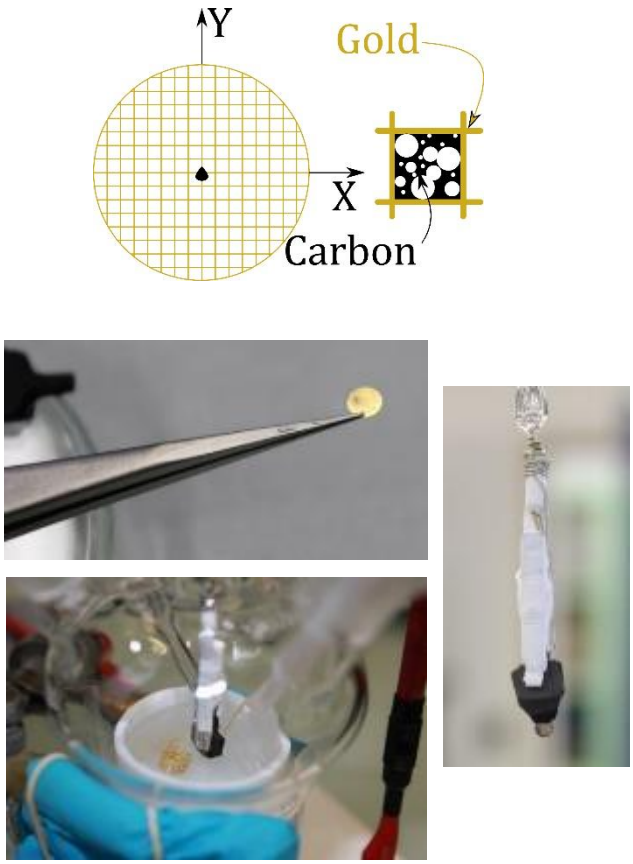

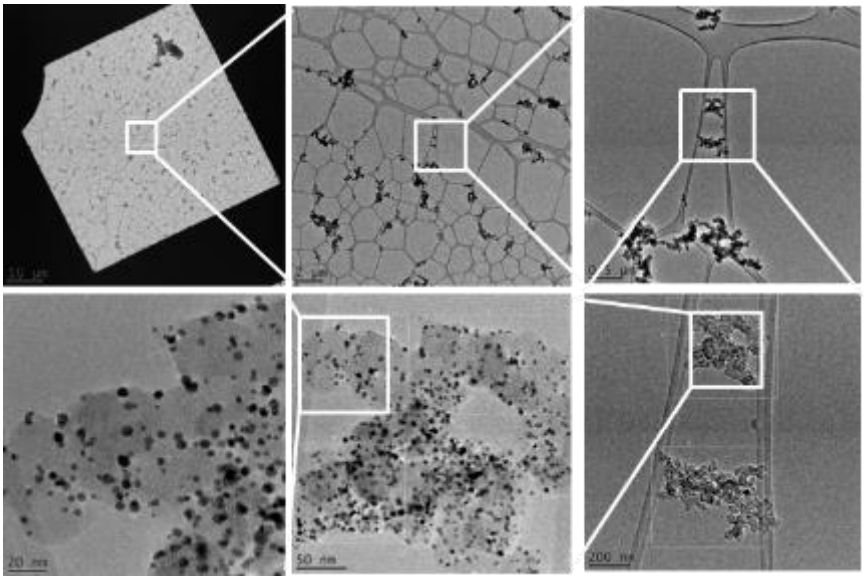

Figure II-4 ILTEM electrochemical set-up and some representative images aquired at increasing magnification from ×250 to ×200,000.

c. Differential Electrochemical Mass Spectrometry (DEMS)

The differential electrochemical mass-spectrometry (DEMS) set-up is assembled by direct connection of the electrochemical cell with the mass-spectrometer system *via* a hydrophobic electrode supported on a stainless-steel frit and gas-inlet system (see **FIGURE II-5**). Volatile product species formed at the electrode are sucked into the mass-spectrometer because of the differential pressure drop held in the vacuum compartments in the gas chambers, and detected shortly after their formation. Electrochemical cyclic voltammograms (CVs) and mass-spectrometric CVs (MSCVs) were obtained with a potentiostat (VSP, Bio-Logic) and a PRISMA PLUS QMG 220 M1 quadrupole mass-spectrometer (Pfeiffer Vacuum) piloted with the Quadera software.

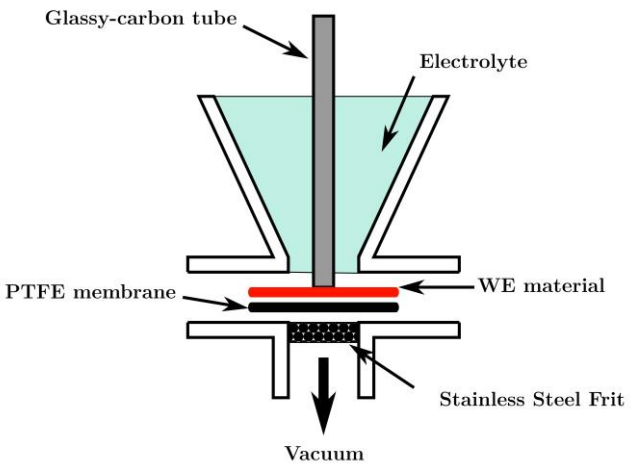

Figure II-5 Electrochemical set-up for DEMS experiments.

In that PhD work, the WE material for the DEMS experiments was a carbon cloth soaked with the ink of the studied electrocatalyst. The electrical contact between the WE and the potentiostat was ensured by the glassy-carbon rod in “soft” contact with the carbon cloth.

Degradation of noble electrocatalysts in alkaline medium

III. Degradation of noble electrocatalysts in alkaline medium

i. Goals of the investigation

a. For platinum and palladium carbon-supported electrocatalysts

The stability of some platinum and palladium based carbon-supported electrocatalysts is investigated in alkaline medium. The choice of those materials has been made because:

1. Platinum is one of the best electrocatalysts in alkaline medium for the hydrogen electrooxidation reaction (HOR) [87,104–107];
2. Palladium is a promising electrocatalyst for the borane electrooxidation reaction (BH_3OR) and a good one for the HOR, in alkaline media [32,108–111];
3. Platinum is still one of the most active electrocatalyst for the oxygen electroreduction reaction (ORR) in alkaline media, even if some platinum-free electrocatalysts have demonstrated interesting performances [112–115];
4. Palladium is also an interesting electrocatalyst for the ORR in alkaline media [114,116–118].

It has been decided to select a specific potential window to study their instability, more precisely $0.1 < E < 1.23$ V *vs.* RHE.

- The lowest potential value, $E = 0.1$ V *vs.* RHE, is realistic for the utilization of Pd/C and Pt/C in the anode of alkaline fuel cell systems and is high enough to limit the production of hydrogen *via* the hydrogen evolution reaction (HER) on the electrocatalysts, which would add other parameters (reducing environment, concerns with gas bubbles, etc.).
  Nonetheless, it is worth noting that the impact of a reducing environment is also investigated in that PhD on palladium-based carbon-supported electrocatalysts (and is presented hereafter).
  The highest potential value, $E = 1.23$ V *vs.* RHE, is realistic for the utilization of Pd/C and Pt/C at the cathode (even if it is not the main topic of this PhD work, it enables others research groups to re-use the results presented here). Finally, the value $E = 1.23$ *vs.* RHE (or even up to $E = 1.5$ V *vs.* RHE [32,36,40,119,120]) is a common choice to investigate any fuel electrooxidation in alkaline medium on a given surface such as alcohols [121–123] or BBMs [47,63,124,125]. So, it appears mandatory to explore whether the metal-based carbon-supported anode electrocatalysts could sustain (or not) such potential variations.

The combination of these two "extreme" potential values makes of the treatment an accelerated stress test (AST) procedure (different organizations such as the American Department of Energy {DoE} and

the Fuel Cell Commercialization Conference of Japan {FCCJ} have their own AST protocols [126,127]), desired to investigate the durability of the catalysts in a reasonable period of time. Besides, it seems important to keep in mind that, in liquid alkaline fuel cells, the anolyte is a solution (of NaOH or KOH) in which Pd/C and Pt/C electrocatalysts take spontaneously an open circuit potential (OCP) around E = 0.9 V *vs.* RHE (or higher if there is some oxygen pollution in the anolyte). It is only when the fuel (such as hydrazine, hydrazine borane or ammonia borane, *etc.*) is introduced that the OCP drops for low potential value (this value depends on the chosen fuel and electrocatalyst material, but can be as low as below E = 0 V *vs.* RHE). So, if one focusses on the utilization of Pd/C and Pt/C electrocatalysts as anode in liquid alkaline fuel cell systems, the succession of presence and absence of fuel in the anolyte can induce a change in potential of the materials between high and low potential values, which legitimates to work within such a large potential window.

Therefore, the stability of those electrocatalysts is investigated in supporting electrolytes (0.1 M of H_2SO_4, $HClO_4$ or NaOH) at T = 25°C by performing potential cycling between E = 0.1 and 1.23 V *vs.* RHE at a potential sweep rate of v = 100 mV s^{-1}.

When this PhD work has been initiated, very little knowledge was available in the literature on the alkaline durability of Pt/C and Pd/C, and this PhD attempts to fill that gap. Also, in order to compare the fate of the platinum and palladium-based electrocatalysts, it was very important to use the same conditions and protocols for their aging and characterizations. To that goal, the common technique to estimate electrochemically the degradation of both Pd/C and Pt/C electrocatalysts is the CO-stripping technique, used to measure the electrochemical surface areas, as described above.

The choice of platinum was a good start to put a first step in the world of alkaline medium degradations. Indeed, this choice was foremost motivated by the huge literature available for Pt/C degradation in acidic media. Platinum (and platinum alloy) nanoparticles supported on high-surface-area carbon (an inexpensive, easily structured, and conductive support material) are the state-of-the-art electrocatalysts for acidic fuel cell systems (such as PEMFC). In addition, it is no secret that these materials undergo severe degradation at the cathode of proton exchange membrane fuel cells as mentioned in the general introduction part.

Pt/C degradations have been massively investigated and especially at high potential values (above E = 0.6 V *vs.* RHE) in acidic media. The research in stability was combined with a research of activity for the oxygen electroreduction reaction (ORR) occurring in the PEMFC cathode. The degradation of platinum (and platinum alloy) carbon-supported nanoparticles is the result of three main mechanisms.

1. 3D-Ostwald ripening (or dissolution/redeposition);
2. Migration and agglomeration of the nanoparticles;
3. Corrosion of the support (generally carbon made) leading to the nanoparticle detachment from to the support.

The ability to determine which degradation phenomenon one electrocatalyst is experiencing for given experimental conditions is a fruit of decades in research and in characterization techniques combining different physicochemical analyses such as Transmission Electron Microscopy, Raman spectroscopy and X-ray diffraction and X-ray photo-electron spectroscopy.

Unfortunately, almost no studies have been conducted for an application in (direct) alkaline fuel cells (*i.e.*, in alkaline media). Very few investigations on bulk platinum (and bulk gold) surfaces have been carried out, to date [128]; yet, most of the groups working on electrocatalysis worldwide are performing electrochemical experiments on carbon-supported nanoparticles in alkaline medium. The stability issues is hardly questioned because of a general consensus on the supposedly higher material stability in alkaline media; this PhD work was an opportunity to compare the stability behavior of platinum and palladium-based electrocatalysts, and it relies on all the characterization tools used to investigate cathode degradations in used PEMFC systems [15,16,18,21,129–133].

Hereafter, the stability of a state-of-the-art Pt/C electrocatalyst is compared in alkaline and acidic media. Concerning the palladium material, two different (in terms of metal loading and particle size distribution) commercial Pd/C electrocatalysts are also investigated and the results are compared with those obtained for the Pt/C electrocatalyst. For each studied electrocatalyst, the electrochemical experiments are correlated to identical-location transmission electron microscopy (ILTEM) imaging, and often, to physicochemical analyses (Raman spectroscopy and by X-ray photoelectron spectroscopy, XPS).

b. For the cubic palladium unsupported electrocatalyst

Many groups are improving the synthesis techniques to tune the electrocatalyst morphology in order to improve the kinetic performances (in alkaline or in acidic conditions) for a given electrochemical reaction; among them, some of those studies focus on providing shape-controlled metal-based nanoparticles, *e.g.* cubes exhibiting {100}-oriented facets (when the metal is a cubic face centered material) [117,134–137]. On that point, it was believed that the specific cubic shape was a good object to confirm (or prove wrong) the sustainability of such shape-controlled materials. Indeed, the cubic shape is perfectly distinguished on TEM images, which makes its degradation easier to monitor; if degradation is observed, the results will be very hard to refute.

Concerning the choice of palladium, it is justified by its promising electrocatalytic performances for borane electrooxidation reaction in alkaline medium [32]. Therefore, that chapter opens the investigation of durability with a case study on cubic palladium nanoparticles. Obviously, the results presented hereafter are not directly transposable to other materials; each tuned electrocatalyst would deserved its own study but it is far beyond the aim of that present PhD work to generalize the results to every sort of shape-controlled electrocatalysts. Nonetheless, the present attempt remains quite original and is another invitation to carry out stability studies in alkaline medium for real application; one can indeed wonder if it is useful to tune a given electrocatalyst to enhance its electroactivity for a given electrochemical reaction when that material is not sustainable for the targeted application…

ii. Specific experimental section

a. For platinum and palladium carbon-supported electrocatalysts

In addition to the information given in "**GENERAL EXPERIMENTAL SECTION**", the results presented in the next sections "**STABILITY OF PLATINUM A STATE-OF-THE-ART ELECTROCATALYST IN ALKALINE MEDIUM**" and "**STABILITY OF COMMERCIAL PALLADIUM ELECTROCATALYSTS IN ALKALINE MEDIUM**" have been obtained with the following specific experimental conditions and protocols.

- The Pt/C state-of-the art catalyst was provided from E-Tek (20% weight fraction, Vulcan XC72 carbon black substrate);
- Two Pd/C electrocatalysts were also provided from E-Tek (Vulcan XC-72 carbon black substrate). The first one (noted Pd/C#1, with large nanoparticles) and the second one (noted Pd/C#2, with small nanoparticles); they have a weight fraction in palladium of 20% and 10% respectively.

Electrocatalyst inks were prepared by mixing 10 mg of catalyst powder, 7.74 mL of MQ-grade water (18.2 MΩ cm, < 3 ppb total organic carbon, Elix + Milli-Q Gradient, Millipore), 18.3 µL of 5 wt% Nafion® solution (Electrochem. Inc.), and 33.9 µL of isopropyl alcohol.

After 30 min of ultrasonic stirring before each experiment, a given volume of ink was deposited on a 5 mm-diameter glassy-carbon electrode:

1. 10 µL for Pt/C and Pd/C#1 electrocatalyst inks;
2. 20 µL for the Pd/C#2 electrocatalyst ink.

Therefore, for every electrocatalysts, the loading in metal on the working electrode surface is similar and about 13.07 $\mu g_{Pt\ or\ Pd}\ cm^{-2}$.

To evaluate the stability of those electrocatalysts, some accelerated stress tests (ASTs) are performed. An AST consists in n = 150 cycles between E = 0.1 and 1.23 V *vs.* RHE at ν = 100 mV s^{-1} in a given electrolyte solution (0.1 M of H_2SO_4, $HClO_4$, or NaOH).

Each AST precedes and is preceded by two measurements performed in 0.1 M H_2SO_4:

- A characterization test consisting in n = 15 cycles at ν = 50 mV s^{-1}, between E = 0.1 and 1.33 V *vs.* RHE;
- Then, a CO-stripping test consisting in 6 minutes of CO adsorption, followed by 39 min of argon purge, at E = 0.15 V *vs.* RHE, and finally, followed by n = 3 cycles in 0.1 M H_2SO_4, at ν = 20 mV s^{-1}, between E = 0.1 and 1.33 V *vs.* RHE.

The CO-stripping voltammograms are used to measure the electrochemical surface area (ECSA) of the Pt/C (and Pd/C) electrocatalysts prior to and after each AST, and the corresponding values enable the calculation of the relative ECSA losses upon each AST.

Basically, each experiment requires two different cells (**FIGURE III-1**):

- Cell#1 with a 0.1 M H_2SO_4 solution thermostated at T = 25°C, in which the characterization test and the CO-stripping test are performed;
- Cell#2 in which the accelerated stress test (AST) is performed, containing a solution of 0.1 M of H_2SO_4, $HClO_4$ or NaOH.

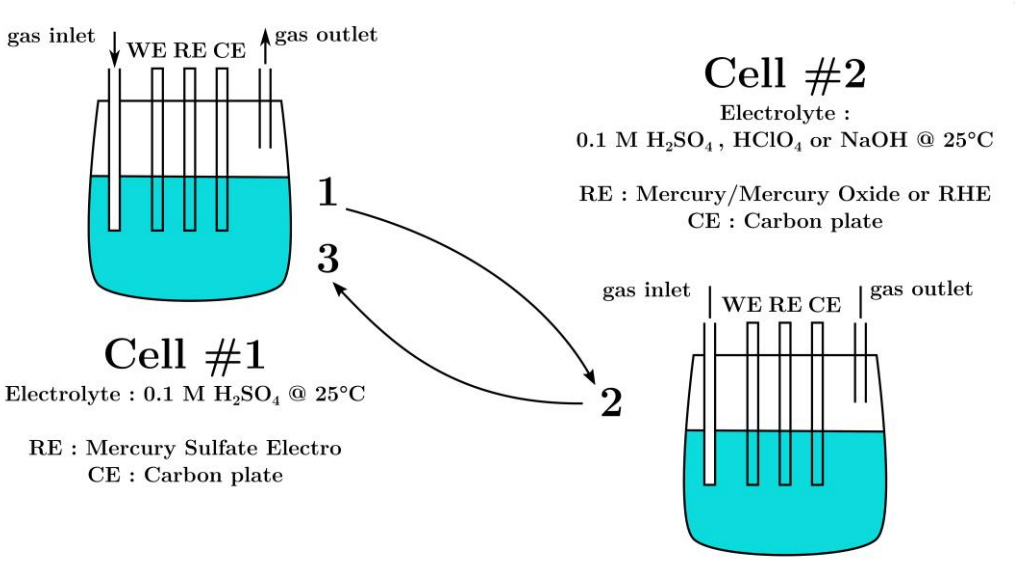

Figure III-1 Steps 1 and 3 = Characterization steps (characterization test + the CO-stripping test). Step 2 = Accelerated Stress Test

Cell#1 is used to probe the electrocatalysts (step 1 and step 3) before and after an AST (step 2 in Cell#2) in a given solution, in order to determine how the material has been degraded by the AST.

b. For the cubic palladium unsupported electrocatalyst

For the results presented in the section "**STABILITY OF CUBIC PALLADIUM NANOPARTICLES IN ALKALINE MEDIUM**", all experiments are performed at room temperature and pressure (*ca.* T = 20°C, P = 1 atm) under argon atmosphere in a PTFE-made three-electrode cell. The counter-electrode is a gold plate and the reference electrode is a freshly-prepared reversible hydrogen electrode (RHE). A new RHE is prepared every 2 hours of experiments, to avoid any bias in the reference potential value.

The cubic palladium nanoparticles were synthesized by Zalineeva *et al.* in Poitiers University (France) using a colloidal method described largely in [135]. It is worth noting that the cubic palladium nanoparticles are unsupported and are directly deposited on the glassy carbon electrodes.

The electrochemical degradation protocol consists of successive chronoamperometries (CA) and cyclic voltammetries (CV), as detailed below:

1. CA at E_{low} for 15 minutes;
2. CV from E_{low} to E_{high}, at ν = 100 mV s^{-1}, for n = 25 cycles;
3. CA at E_{low} for 15 minutes;
4. CV from E_{low} to E_{high}, at ν = 100 mV s^{-1}, for n = 100 cycles;
5. CA at E_{low} for 15 minutes;
6. CV from E_{low} to E_{high}, at ν = 100 mV s^{-1}, for n = 25 cycles.

With E_{low} and E_{high} the lowest and the highest potential values of the chosen potential range of study, respectively.

This degradation protocol is not the same than for the sections "**STABILITY OF COMMERCIAL PALLADIUM ELECTROCATALYSTS IN ALKALINE MEDIUM**" and "**STABILITY OF PLATINUM A STATE-OF-THE-ART ELECTROCATALYST IN ALKALINE MEDIUM**". Actually, the results presented for this cubic palladium electrocatalyst were the first obtained during this PhD work and have been published in [100]. At that moment, we had a very limited knowledge about degradation in alkaline media.

For example, the electrochemical set-up is PTFE-made based and not made of Pyrex glass because of the risk in electrolyte contamination coming from the glass degradation even at pH 13 (0.1 M NaOH); then, studies performed by Oliveira *et al.* [138,139] in the present conditions (in LEPMI laboratory and for platinum single crystal electrodes) have shown no significant glass degradation pollution for that NaOH concentration. Another, important element is the counter-electrode material (a gold plate); indeed, in the study of the Pd nanocubes, a gold electrode was used as CE and it must be stated that the aggressiveness

of alkaline medium on noble metal (even for a bulk Au electrode) was probably underestimated. It is possible that the corresponding results were impacted by the dissolution of the gold CE metal and its re-deposition at the working electrode. However, no Au redeposition was witnessed during the ILTEM experiments (on the TEM images), and one can reasonably assume that the possible pollution from the CE metal only happened in a negligible manner (if any).

iii. Stability of Platinum a state-of-the-art electrocatalyst in alkaline medium

a. Results & Discussions

Characterization and CO-stripping tests performed before and after each AST are shown in **FIGURE III-2**; the comparison of the ECSA losses is given in **FIGURE III-2-H** for the three different media, 0.1 M of NaOH, $HClO_4$, or H_2SO_4 solution. The results show a loss of active surface-area for both acidic and alkaline media, with an average value of 57.4, 17.3, and 22.4% of ECSA loss, respectively for the NaOH, $HClO_4$ and H_2SO_4 solutions.

The utilization of $HClO_4$ and H_2SO_4 solutions enables the observation of a possible effect of the anion-adsorption strength at the Pt sites (larger for sulfate than for perchlorate anions): only a slight difference can be observed between the results obtained in $HClO_4$ and H_2SO_4. This anion adsorption strength explains the potential shift of Pt oxide formation visible between **FIGURE III-2-C** and **FIGURE III-2-E**, as previously reported in ref [83]. As obtained here, H_2SO_4 seems slightly more aggressive than $HClO_4$, which is in agreement with previous results. [140,141]

Strikingly, the degradation (ECSA loss) in alkaline medium is about 3 times worse than for acidic media. The modification of the CO-stripping voltammogram after the AST in 0.1 M NaOH clearly gives additional information. Indeed, the development of a pre-peak at E = 0.7 V *vs.* RHE upon AST in alkaline medium, associated with a shift of the main peak toward a lower potential, is related to the agglomeration and apparent growth (*via* a platinum dissolution/redeposition mechanism, or 3D Ostwald ripening, or even because only the largest Pt nanoparticles remain isolated after the AST) of the Pt nanoparticles on the carbon support (**FIGURE III-2-B** and **FIGURE III-3,A–D**).[81,82]

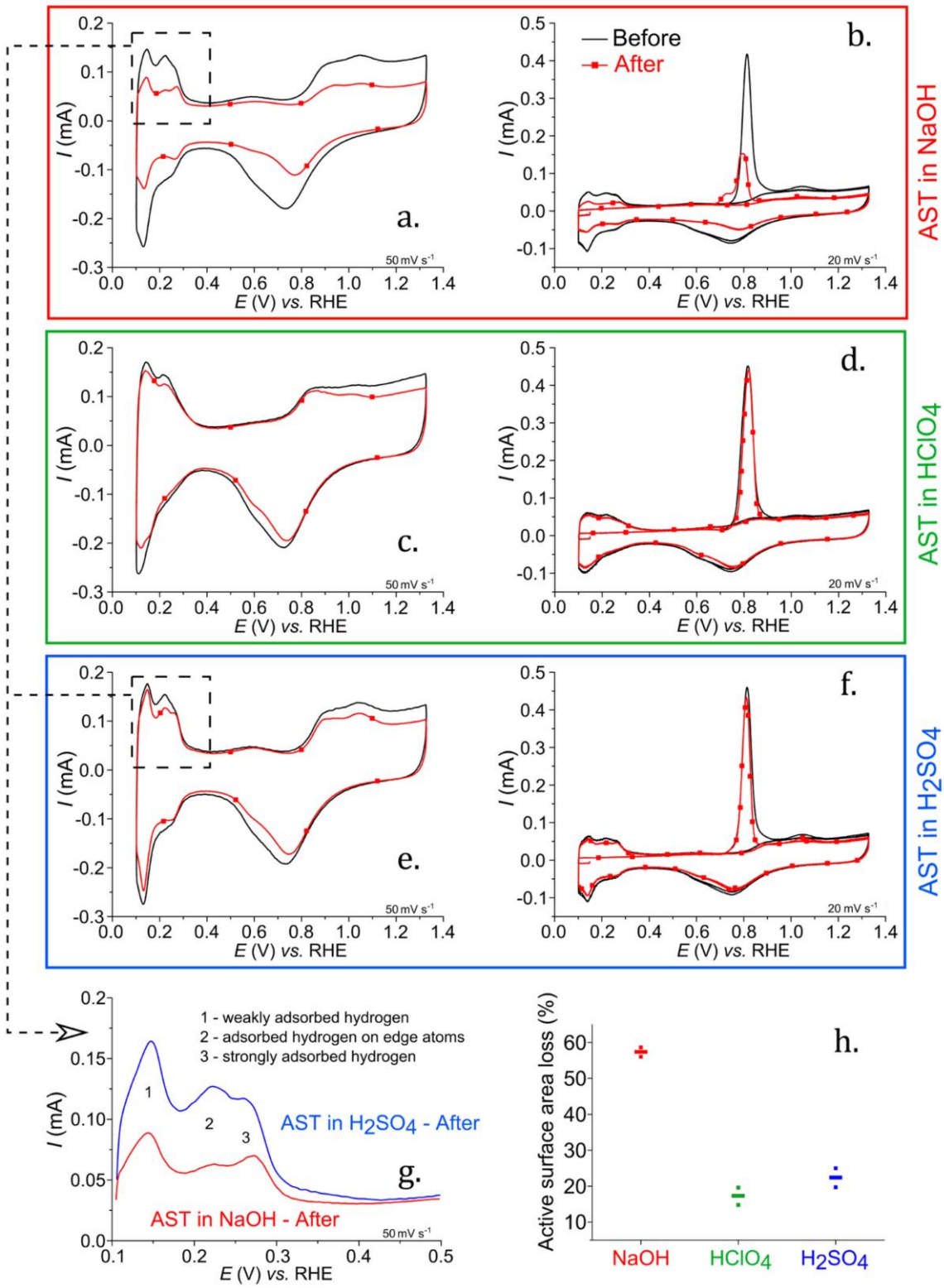

Figure III-2 Characterization and CO-stripping voltammograms carried out in 0.1 M H_2SO_4 solution at T = 25°C before and after AST performed in (a, b) NaOH, (c, d) $HClO_4$, or (e, f) H_2SO_4. (g) Comparison of characterization voltammograms performed after an AST in NaOH and in H_2SO_4 solutions. (h) Corresponding relative active surface-area losses for each electrolyte medium.

Interestingly, the intensity of peak 2 (in **FIGURE III-2-G**), corresponding to the hydrogen adsorption on edge atoms of platinum particles, has significantly decreased (relatively to peak 3) after the AST in NaOH in comparison with the results obtained for the H_2SO_4 solution; this indicates a smaller number of edge atom sites and is another evidence of the agglomeration process [142].

None of these features are visible in **FIGURE III-2-D&F**, where the CO-stripping voltammograms before and after the AST in the acidic media (H_2SO_4 or $HClO_4$) are nearly unchanged. This very high extent of ECSA loss in alkaline medium (60% *vs.* ~20% in acidic media) only happens for much harsher or longer degradation protocols and at higher temperatures in acidic media [20,77]. This extreme degradation for a somewhat mild AST (T = 25°C, n = 150 cycles between E = 0.1 and 1.23 V *vs.* RHE), reveals the aggressiveness of the alkaline medium toward the carbon-supported platinum nanoparticles. This result echoes the recent findings of Cherevko *et al.* [143]; the "transient" corrosion (*i.e.*, that which proceeds when cycling the potential in a CV) of smooth Pt surfaces in alkaline medium starts at lower potential (by ~ 50 −100 mV) and is about twice as harsh as than in acidic medium. In acidic media, such an extent of agglomeration monitored on the CO-stripping CV is observed only in the presence of a reducing agent such as a CO atmosphere in acidic environment.[77,144]

To visualize this degradation and to describe it properly, ILTEM imaging was performed to shed light on the morphological changes of the Pt/C electrocatalyst and to understand the origin of the differences in ECSA loss. **FIGURE III-3** shows the micrographs obtained before and after the AST in 0.1 M solutions of NaOH, $HClO_4$, and H_2SO_4 and the associated particle size distribution histograms.

A slight increase in the Pt nanoparticles' sizes is observed in acidic media (**FIGURE III-3-F&H**) as a result of the Pt dissolution/ redeposition mechanism, which is expected for such high/low vertex potential used in the AST.[20,77] It corresponds to a tailing of the PSD toward large nanoparticle sizes at the expense of the smaller nanoparticle sizes, which can indicate non-negligible dissolution/redeposition (3D Ostwald ripening) processes.[16,21,145]

In alkaline medium, **FIGURE III-3-E** also indicates a slight increase in the nanoparticles' size, but in this case, the PSD histogram essentially flattens. The amount of both very small nanoparticles (between 1 and 2 nm) and of larger nanoparticles slightly increased, too. One must however note that the former could be a "false positive", and result from the better contrast of the micrographs after aging in NaOH (the smaller nanoparticles are better visualized then, owing to the sharp decrease in the density of the nanoparticles over the carbon support (see below)). So, in alkaline medium, the non-negligible agglomeration of the Pt particles evidenced by ILTEM (**FIGURE III-3-A-D**), confirms the shape of the CO-stripping features previously presented, with a large CO-electrooxidation pre-peak at E = 0.7 V *vs.* RHE (attributed to the nanoparticles agglomeration [82]).

Whatever the media, particle detachment is evidenced (white markers ease the observation in **FIGURE III-3-D&G&J**; obviously these markers are by no means quantitative). The absolute number of Pt

nanoparticles counted on the ILTEM images before and after the "acidic" AST, however, demonstrates that the loss of spherical-shape (isolated) nanoparticles after the AST (10 and 15% for an AST in H_2SO_4 and $HClO_4$, respectively) is not enough to account for all the ECSA loss (22 and 17% for an AST in H_2SO_4 and $HClO_4$, respectively). This again shows that the nanoparticle size increase (by Pt dissolution/redeposition) non-negligibly accounts for the active surface area loss electrochemically measured upon acidic AST (see **FIGURE III-3** and **FIGURE III-3-F-K**). On the contrary, the AST in alkaline medium yields a very large extent of Pt nanoparticle loss (63%), and is sufficient to account for the ECSA loss (57%). This shows that most of the surface area loss after the "alkaline" AST is due to the simple loss of Pt nanoparticles, not from quantitative dissolution/redeposition.

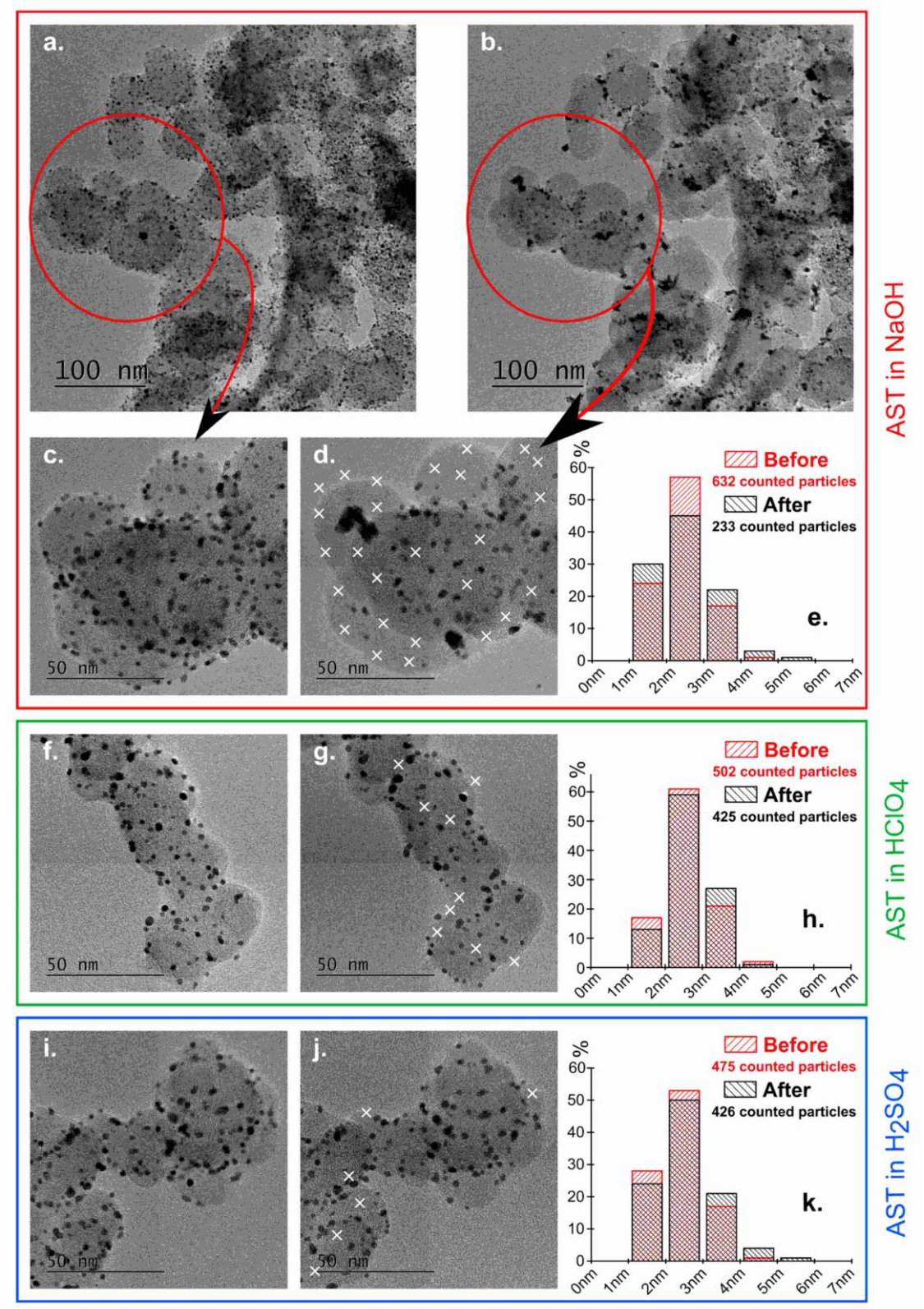

Figure III-3 ILTEM micrographs pre- and post-AST at T = 25°C in NaOH (a−d), $HClO_4$ (f, g) and H_2SO_4 (i, j). The white crosses (x) highlight the nanoparticles' loss (in a non-comprehensive manner). Corresponding nanoparticle size distribution histograms in (e) NaOH, (h) $HClO_4$, and (k) H_2SO_4. The numbers of particles counted on the ILTEM images before and after the AST demonstrate the much larger loss of nanoparticles in alkaline medium than in acidic ones.

Finally, it was attempted to determine which degradation mechanism was taking place for ASTs in alkaline media.

According to the CO-stripping and ILTEM results, it can be affirmed that:

- There is no doubt that "migration and agglomeration" processes do happen in alkaline medium;

- The existence of "3D-Ostwald ripening", consisting in particle dissolution into ions followed by some ion reposition on the carbon support, seems questionable since no apparition of new particles has been noticed; in particular, the apparent growth of isolated nanoparticles diameter noted in CO-stripping CV is probably due to the fact that the large nanoparticles are more resistant to migration and agglomeration than the small ones, thereby resulting in increased fraction of large *vs*. small isolated nanoparticles after AST (small ones tend to agglomerate);

- Intense carbon corrosion seems not to be the reason of the degradation since ILTEM images suggest no change of the shape of the carbon support.

Raman spectroscopy measurements, performed on the pristine electrode and after four successive degradation tests (n = 250 cycles in 0.1 M NaOH between E = 0.1 and 1.23 V *vs.* RHE at ν = 100 mV s^{-1} and T = 25°C) confirm that such a huge degradation in alkaline medium cannot be related to severe carbon corrosion (**FIGURE III-4**), which is however a major issue, leading to the cathode degradation, in the acidic environment of a PEMFC, especially for long-term operation [145].

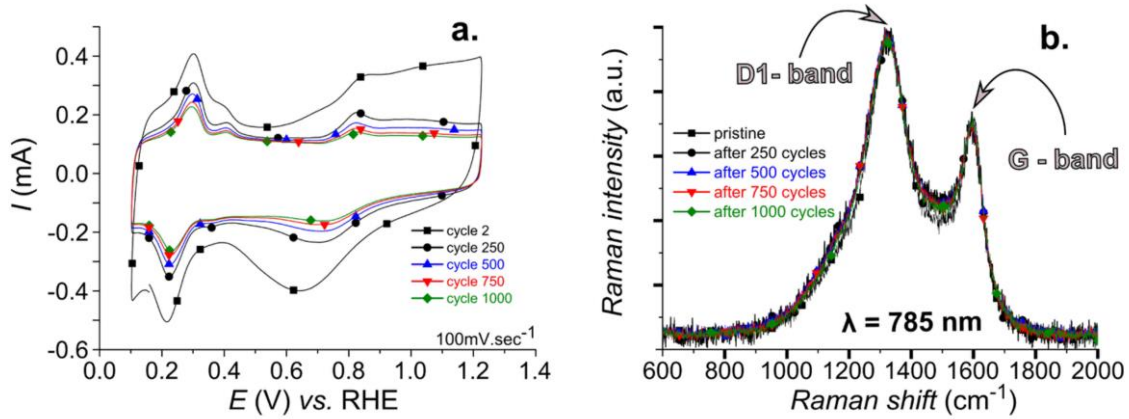

Figure III-4 (a) Successive AST performed in 0.1 M NaOH at T = 25°C and (b) Raman spectroscopy results (normalized) obtained after each AST.

Whereas **FIGURE III-4-A** clearly illustrates the loss of active surface area in the H_{UPD} and platinum oxides regions (the degradation being more intense during the first part of the degradation protocol, suggesting that the first cycles are the most detrimental), the Raman spectra (**FIGURE III-4-B**) show no modification of the intensity of the G-band (1585 cm^{-1}, ideal graphitic lattice) and D1-band (1350 cm^{-1}, disordered graphitic lattice-graphene layer edge) vibrational modes. This indicates that no significant carbon corrosion processes happen until n = 1000 cycles under these conditions, which obviously rules out any carbon corrosion processes after only n = 150 cycles in the AST results previously reported in **FIGURE III-2** and **FIGURE III-3**.

Also, particle detachment can be linked both to a modification of the surface chemistry of the carbon support, which could change the interaction between the Pt particles and the support by modifying their anchoring sites on the support, and to consequent carbon corrosion in the vicinity of the nanoparticles [20,145–147]. This hypothesis could also explain the "migration and the agglomeration" of Pt nanoparticles.

The XPS patterns of the C1s contribution (**FIGURE III-5**) show nonetheless no sign of severe carbon corrosion after the AST, should it be in alkaline or acidic medium. Therefore, a "general" modification of the surface carbon chemistry is not the explanation for the degradation observed in alkaline medium.

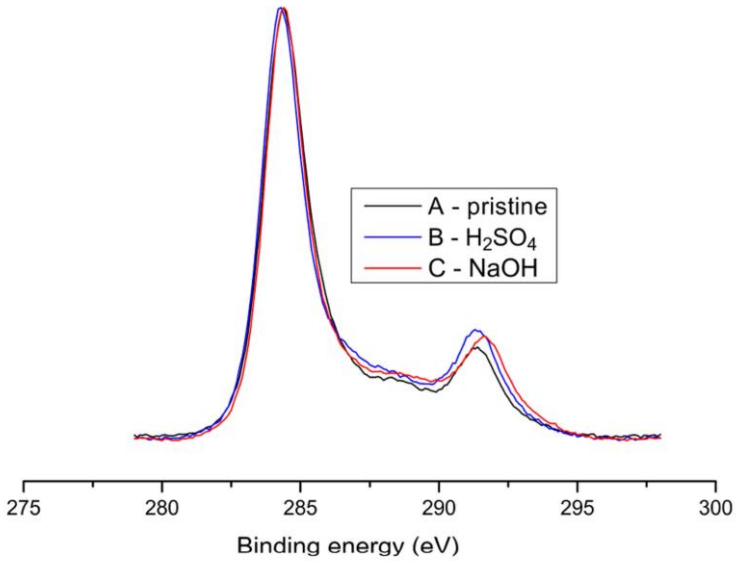

Figure III-5 XPS data for the Pt/C electrocatalysts in (a) its pristine state and after the AST in (b) 0.1 M H_2SO_4 and in (c) 0.1 M NaOH.

Nonetheless, a modification of the "local" carbon chemistry in the immediate "vicinity" of the nanoparticles is still possible but the demonstration of such hypothesis would need other characterization tools that could not have been performed in the timeframe of the PhD.

b. Intermediate milestone

This PhD work clearly demonstrates that an alkaline medium is really more aggressive for Pt/C electrocatalysts than an acidic one for the studied accelerated stress test (n = 150 cycles from E = 0.1 to 1.23 V *vs.* RHE). An impressive loss of ECSA (~60%) is observed only upon AST in 0.1 M NaOH, whereas the ECSA loss is limited to ~20% in acidic media (0.1 M H_2SO_4 or $HClO_4$). In the latter cases, Pt dissolution/redeposition and a low extent of particle detachment have been monitored. In contrast, the huge degradation observed in alkaline medium (with respect to the extremely small number of cycles performed, n = 150) follows the very large loss of Pt nanoparticles (~63%). Such detachment of nanoparticles from the carbon surface is moreover not due to extensive carbon corrosion, as demonstrated by combined ILTEM (no quantitative change of the carbon shape is detected after AST), Raman spectroscopy (no significant modification of the D1-band and G-band vibrational modes has been observed, even after n = 1000 voltammetric cycles in 0.1 M NaOH), and XPS results (the C1s band is literally unchanged upon any AST). A modification of the carbon (extreme) surface chemistry in alkaline media, which modifies the anchoring sites of the particles on the support, could explain such degradation. In the authors' opinion, this could follow not only the subtle modifications of the carbon surface chemistry in the vicinity of the platinum nanoparticle in alkaline medium, but also the harsher "transient" corrosion of the platinum surfaces in alkaline than in acidic medium [128], which was witnessed by Cherevko *et al.* for larger potential values (above E = 1.3 V *vs.* RHE) than in the present PhD work. More work would be necessary to prove so, but this could not be attempted in the timeframe of this PhD.

iv. Stability of commercial palladium electrocatalysts in alkaline medium

a. Results & Discussions

In this section, the investigations focus on two palladium electrocatalysts, the Pd/C#1 and Pd/C#2. The electrocatalyst Pd/C#1, composed of larger nanoparticles than Pd/C#2 (both supported on the same Vulcan XC-72 substrate), enables to study whether large palladium nanoparticles are less, similarly or more stable than smaller ones in both alkaline and acidic media. Then, the Pd/C#2 electrocatalyst, which is made of rather small nanoparticles that are well dispersed on the carbon support, allows a direct comparison with the platinum electrocatalyst studied in the previous section (same carbon support, rather similar average nanoparticles size and rather similar metal nanoparticles density at the carbon support). The morphology and the particle size distribution histogram (PSD) of the two (pristine) carbon-supported palladium electrocatalysts are shown in **FIGURE III-6**. It has to be noted that only isolated and spherical-shape nanoparticles have been taken into account in the determination of the PSD.

The Pd/C#1 electrocatalyst is composed of nanoparticles with a number-averaged diameter close to $\overline{d_N}$ ≈ 10.9 nm (which corresponds to a surface-averaged diameter $\overline{d_S}$ = 13.8 nm, and a volume-averaged diameter $\overline{d_V}$ = 14.9 nm) and the Pd/C#2 electrocatalyst is composed of nanoparticles with $\overline{d_N}$ ≈ 4.1 nm ($\overline{d_S}$ = 5.0 nm; $\overline{d_V}$ = 5.5 nm).

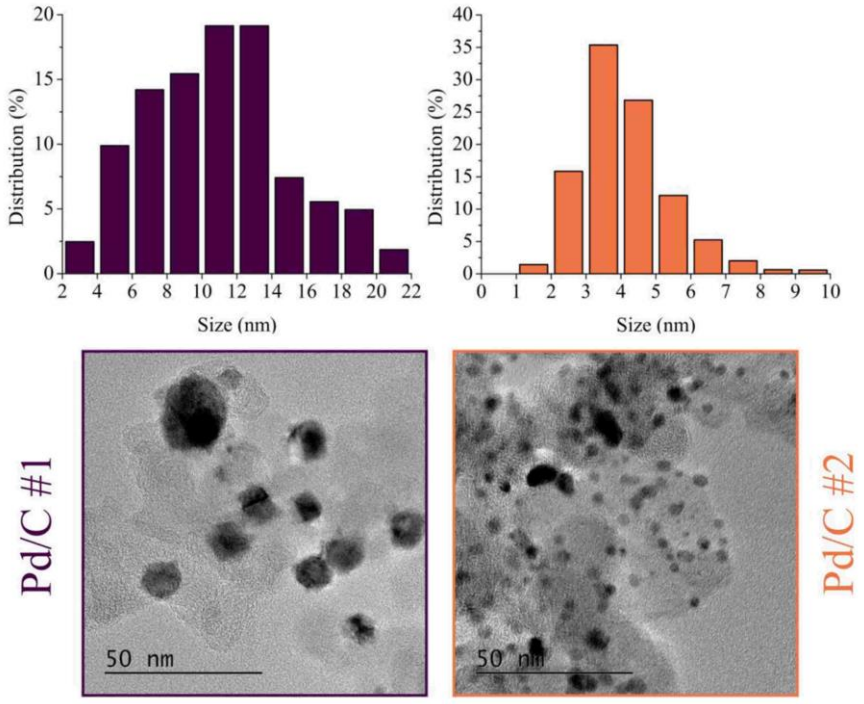

Figure III-6 Representative Transmission Electron Microscopy (TEM) micrographs and corresponding nanoparticles size distribution histograms for Pd/C#1 and Pd/C#2.

The average values of ECSA for a pristine electrode, measured with CO-stripping voltammetries, have been evaluated, assuming a charge density of 420 µC cm_{Pd}^{-2} for the carbon monoxide oxidation: one finds 42 $m^2 \cdot g_{Pd}^{-1}$ and 78 $m^2 \cdot g_{Pd}^{-1}$ for Pd/C#1 and Pd/C#2 respectively. The values correspond to an electrochemical average diameter of:

$$\overline{d_{\text{elec}}} = \frac{6000}{\rho \text{ x ECSA}}$$

With ρ = 12 g cm^{-3} (the density of palladium), one obtains $\overline{d_{\text{elec}}} \approx$ 12 nm and 6.4 nm for Pd/C#1 and Pd/C#2 respectively, in reasonable agreement with the values of $\overline{d_S}$ presented above.

Then, AST experiments were performed in both 0.1 M NaOH and 0.1 M H_2SO_4 supporting electrolyte solutions. **FIGURE III-7** shows the ESCA losses (measured by comparison of the data from CO-stripping CV prior and after the AST, see the examples of **FIGURE III-7-C&D**) plotted as a function of the degradation tests.

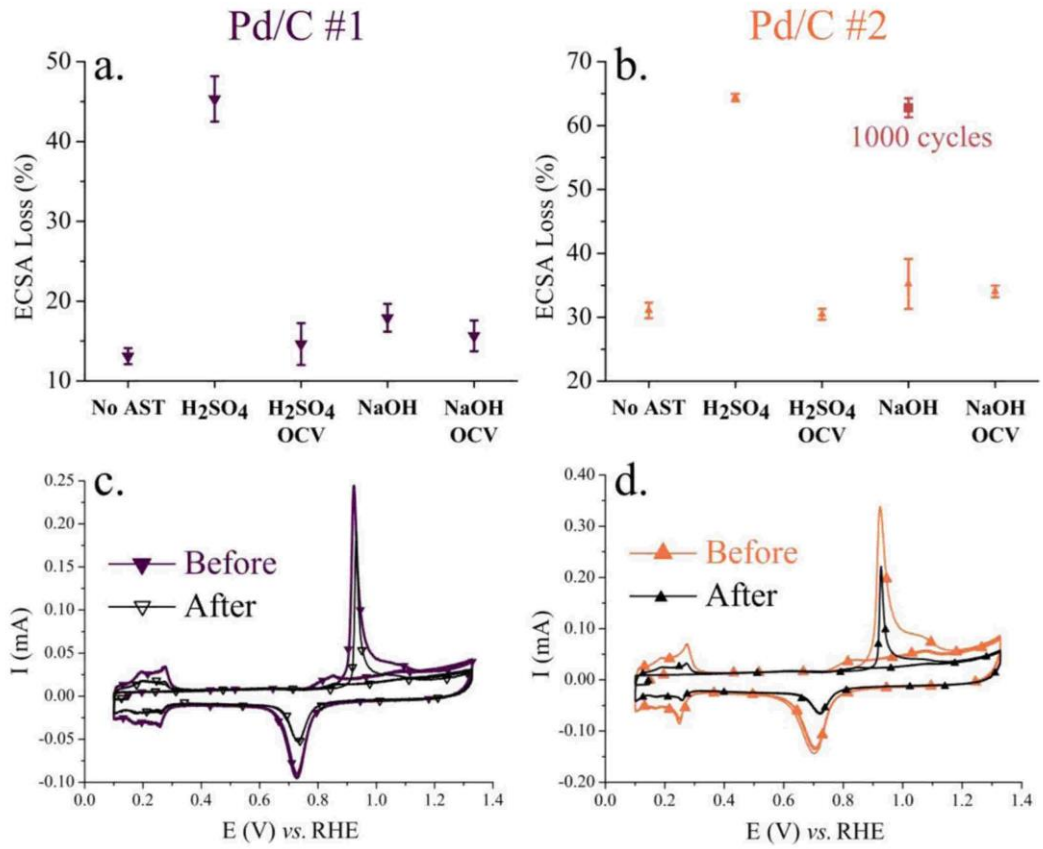

Figure III-7 (a-b) ECSA losses for the two Pd/C electrocatalysts in several conditions of degradation. "No AST" refers to a protocol where only the two characterization steps were performed (cycling and CO stripping in 0.1 M H_2SO_4 solution); "OCV" refers to a 1h30-long Open Circuit Voltage hold performed in acidic or in alkaline medium; "H_2SO_4" and "NaOH" correspond to the conjunction of the AST (150 CVs in the corresponding electrolyte) and of the characterization steps.
(c-d) CO-stripping cyclic voltammetries for the two Pd/C electrocatalysts, performed before and after an AST in 0.1 M H_2SO_4 (at T = 25°C).

The mentions "H_2SO_4" and "NaOH" correspond to the ASTs (n = 150 cycles in the corresponding electrolyte, or n = 1000 cycles when specified). The "OCV" experiment refers to a 1h30-long Open-Circuit Voltage hold (which corresponds to twice the duration of an AST) performed in acidic or in alkaline medium, which enables to characterize the calendar durability of the Pd/C electrocatalysts in open-circuit conditions. The "No AST" experiment corresponds to a protocol where neither degradation test nor OCV were performed; in this case, only the characterization steps (15 CVs and CO-stripping CVs in 0.1 M H_2SO_4 solution) are performed to check their effect on the degradation.

The extent of ECSA loss of **FIGURE III-7-A&B**, highlights the non-negligible and detrimental influence of a mild AST performed in alkaline medium for the two Pd/C electrocatalysts: the ECSA decreases by *ca*. 18% and 35% for Pd/C#1 and Pd/C#2, respectively. These values must however not be viewed as only the impact of the alkaline AST on the palladium materials. Indeed, the simple characterizations steps (CVs in supporting electrolyte and CO-stripping CVs, both performed in 0.1 M H_2SO_4 before and after the AST) and represented by the "No AST" data points, do impact the ECSA in a remarkable manner. This means that the characterization steps are also non-negligibly destructive by themselves. This destructiveness of the characterization steps has been reported previously by Castanheira *et al.* [79]; nonetheless, this effect seems even more pronounced for palladium-based material in acidic medium.

In this study, the characterization steps (without any AST) indeed yield *ca*. 10% and 30% of ECSA loss for Pd/C#1 and Pd/C#2, respectively, values which are nearly as high as the aforementioned ones for the conjunction of the characterization steps + AST (data points labeled "NaOH" in **FIGURE III-7**). Consequently, the real ECSA losses associated to the alkaline AST only (hereafter denoted as "characterization-free" and calculated as the difference of ECSA loss for the "NaOH" minus that for the "No AST" data points) can be recalculated and quantified to *ca*. 8% and 5% for Pd/C#1 and Pd/C#2, respectively, for the 150 CVs.

So, performing n = 150 cycles in alkaline electrolyte does only minorly alter the ECSA of the two electrocatalysts, and the same conclusion can be made for the results of the OCV hold for 1h30 in 0.1 M NaOH ("NaOH OCV" data points in **FIGURE III-7**).

This significant impact of the characterization steps in 0.1 M H_2SO_4 underlines the extreme instability of palladium nanoparticles in acidic electrolyte, in agreement with previous reports [88,99,128,148,149]. This extent of instability in acidic conditions, which by far exceeds that of Pt-based electrocatalysts [20,78,144,150,151], fully justifies that Pt remains the catalyst of choice in acidic PEMFC electrodes. This latter observation is confirmed by the results obtained for the AST performed in 0.1 M H_2SO_4, which yields a much larger ECSA loss: *ca*. 45% and 65% for Pd/C#1 and Pd/C#2, respectively. The instability of Pd/C in acidic medium is activated by the cycling in this potential window, while the absence of polarizations lets the palladium materials unchanged as suggested by the results of 1h30-long OCV holds in 0.1 M H_2SO_4 ("H_2SO_4 OCV" data points in **FIGURE III-7**).

Interestingly, a particle size effect is demonstrated for the stability of Pd/C; in acidic medium, the small palladium particles of Pd/C#2 are less stable than the large palladium particles of Pd/C#1. On the contrary, such effect is not pronounced in alkaline conditions. To summarize, the Pd/C electrocatalysts are relatively more stable in alkaline medium than Pt/C (which was demonstrated highly instable in similar conditions in the previous section); whereas the ECSA loss of Pt/C is as high as 60% after only 150 CVs in alkaline medium (steps of characterization included), it is 18% and 35% for Pd/C#1 and Pd/C#2, respectively (steps of characterization included) and even drops to *ca*. 8% and 5% for Pd/C#1 and Pd/C#2, respectively, steps of characterization excluded.

Then, a longer AST in alkaline medium was performed for Pd/C#2 (see **FIGURE III-8**); the ECSA loss after n = 1000 cycles in 0.1 M NaOH is plotted in **FIGURE III-7-B**. The "characterization-free" value of ECSA loss is *ca*. 32.5%, which is a non-negligible value at that stage. Since the intrinsic ("characterization-free") ECSA loss after n = 150 cycles is 5% for this electrocatalyst, the ECSA loss seems to be proportionally linked to the number of cycles. For n = 1000 cycles, 5% × 1000 / 150 ≈ 33% of ECSA loss may be expected, which is in agreement with the value of *ca*. 32.5% reported above. This indicates that although more stable than Pt/C in these conditions, Pd/C is however not durable for long-term cycling at T = 25°C: the ECSA loss scales near-linearly with the number of CV cycles performed in the present conditions, as remarkable on **FIGURE III-8**.

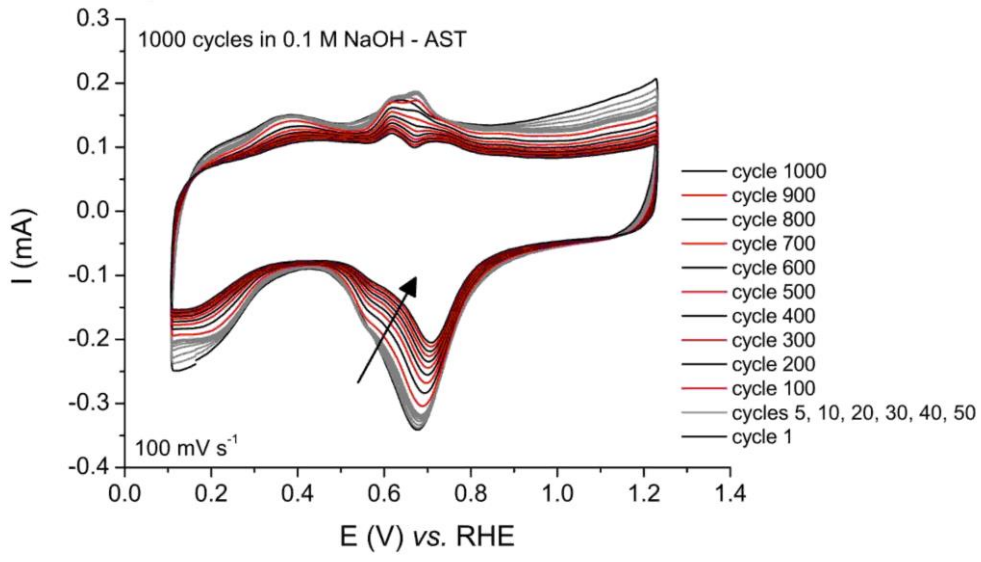

Figure III-8 Representative scans of the accelerated stress test performed in 0.1 M NaOH at T = 25°C for Pd/C#2.

One can see that the degradation rate (estimated by the decrease of area of the Pd-oxides reduction peak, at *ca.* E = 0.7 V *vs.* RHE in the negative scan) is slightly decreasing upon cycling. In addition, the

degradation rate is much slower than observed in the CV scans performed in acidic medium (**FIGURE III-9** and **FIGURE III-10**).

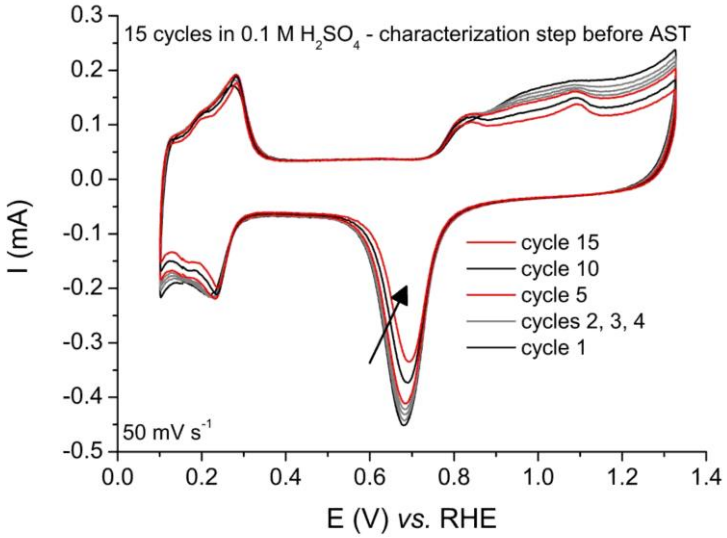

Figure III-9 Representative scans of the first characterization step performed in 0.1 M H_2SO_4 at T = 25°C for Pd/C#2.

The degradation rate (estimated by the decrease of area of the Pd-oxides reduction peak, at *ca.* E = 0.7 V *vs.* RHE in the negative scan) is initially fast and slowly decreases upon this initial CV cycling.

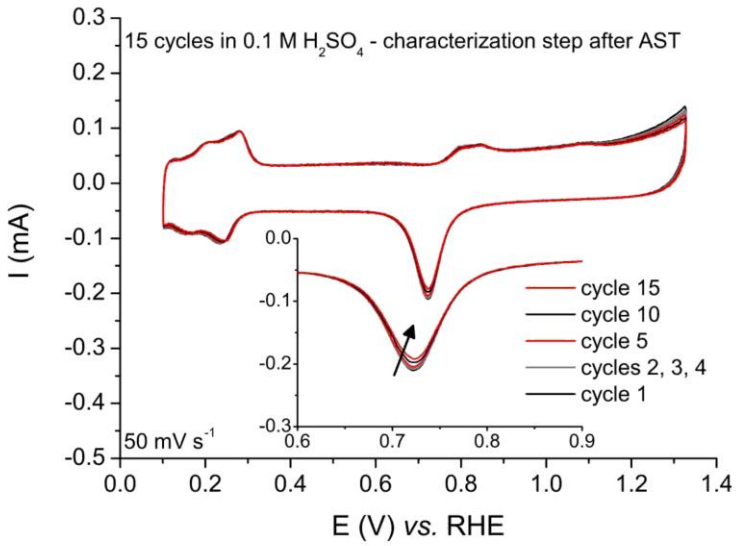

Figure III-10 Representative scans of the second characterization step performed in 0.1 M H_2SO_4 at T = 25°C for Pd/C#2, after the AST of Figure III-8.

One can see that the degradation rate (estimated by the decrease of area of the Pd-oxides reduction peak, at *ca.* E = 0.7 V *vs.* RHE in the negative scan) is slower but not negligible compared to the first characterization of **FIGURE III-9**. At that stage, the degradation rate per cycle is still larger than monitored at the end of the AST in 0.1 M NaOH.

It is well known, at least for AST performed on Pt/C electrocatalysts in acidic medium, that the degradations are harsher in the first cycles of AST (or characterization steps) than in the subsequent ones [79,152,153]. Besides, the deleterious effect of the characterization steps on the magnitude (and sometimes the mechanisms) of degradation has also been unveiled in these cases [152–154]. So, this puts into question the apparent linear decrease of ECSA per CV cycle in alkaline medium noted above for Pd/C. It is *a priori* not sure, that the knowledge derived from references [79,152,153], studies performed in acidic medium on Pt/C, can simply be translated to the case of Pd/C aging in alkaline solution (and neither to the case of Pt/C in alkaline solution). The first reason for the uncertainty is that the degradation mechanisms are very different: in acidic medium, Ostwald ripening and carbon corrosion are the dominant degradation processes for the potential interval investigated here; on the contrary, the present PhD work (for Pd/C, see the ILTEM results below) and (for Pt/C) demonstrates that it is mainly the particle detachment which is at stake in alkaline medium.

Unfortunately, one cannot make such electrochemical analyses without performing the characterizations steps in acidic medium, since it is thanks to these procedures that the ECSA loss is calculated. In fact, **FIGURE III-8** shows that the degradation rate (estimated by the decrease of area of the Pd-oxides reduction peak, at *ca.* E = 0.7 V *vs.* RHE in the negative scan) is very slightly decreasing upon cycling. In particular, the degradation rate is much slower and gradual than observed in the CV scans performed in acidic medium (**FIGURE III-9** and **FIGURE III-10**).

ILTEM observations were performed for the 1000-cycle-long AST in 0.1 M NaOH; some representative images are given in **FIGURE III-11.** These firstly enable to shed light into the morphological changes of Pd/C materials. Even at low magnification, the severe extent of degradation suffered by the Pd/C#2 electrocatalyst is confirmed. A very large fraction of the initial nanoparticles is lost. Some nanoparticles agglomeration is also occurring (although in a lesser extent) as observed at higher magnification.

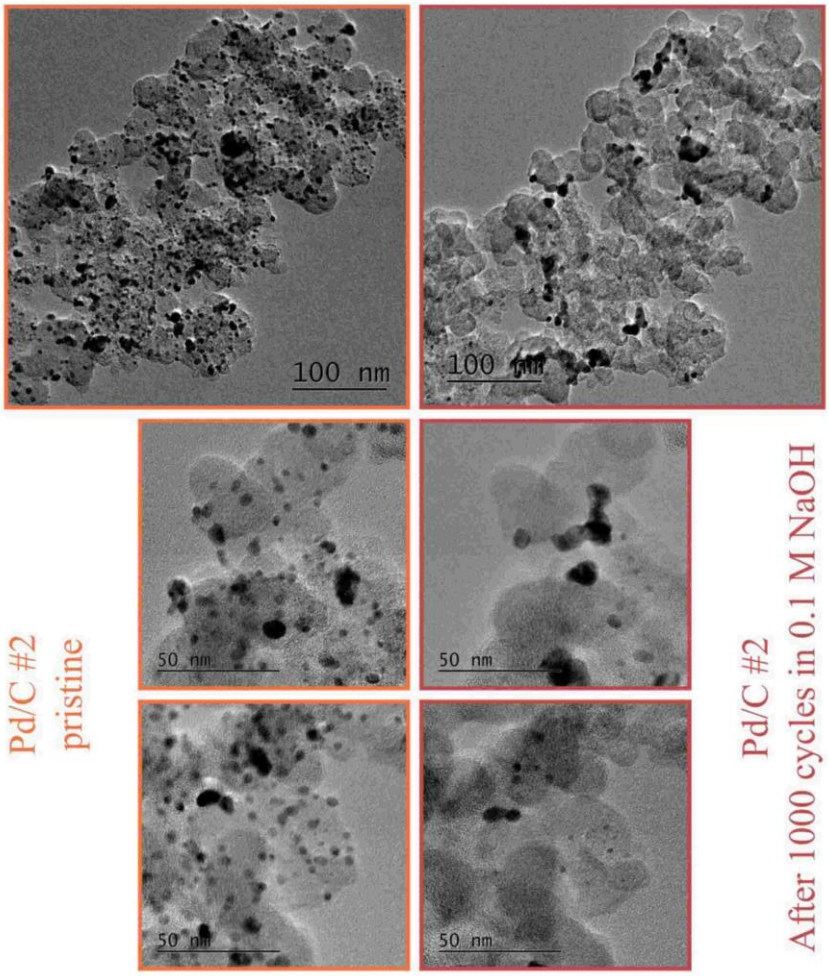

Figure III-11 ILTEM micrographs obtained before and after a 1000-cycle-long AST in 0.1 M NaOH between E = 0.1 and 1.23 V vs. RHE at T = 25°C for the Pd/C#2 electrocatalyst.

The ILTEM images obtained for the Pd/C#2 catalyst were exploited on a quantitative basis to build particle size distribution histograms before and after the 1000 CV-long AST and to determine average nanoparticle diameters (**FIGURE III-12**). More than 50% of the isolated particles counted initially have been lost (their number decreases from 1395 before the AST, to 676 after the AST), which is extremely dramatic after a mild AST of only a thousand CV cycles in a standard potential range ($0.1 < E < 1.23$ V *vs.* RHE) and a dilute (0.1 M) alkaline electrolyte at room temperature (T = 25°C).

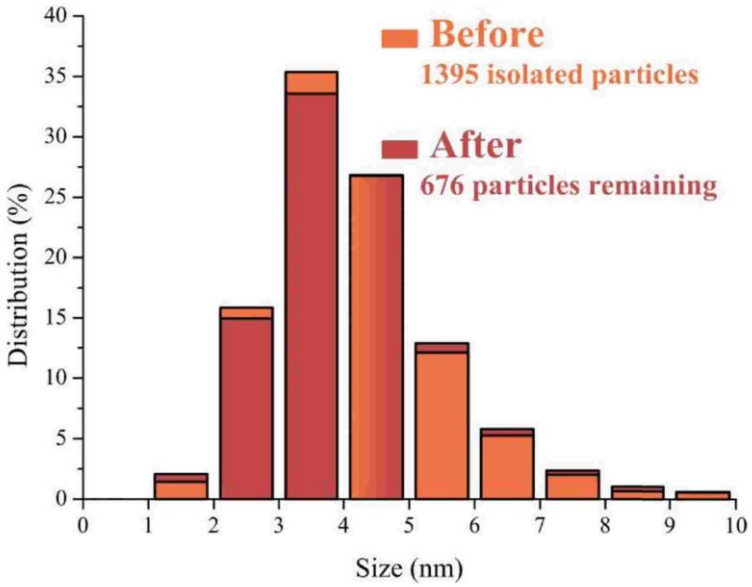

	Before AST (1000 cycles)	After AST (1000 cycles)
d_N / nm	4.1	4.2
d_S / nm	5.0	5.1
d_V / nm	5.5	5.6

Figure III-12 Particle size distribution histograms for Pd/C#2 based on the ILTEM images, taken before and after a 1000-cycle-long AST between E = 0.1 and 1.23 V vs. RHE in 0.1 M NaOH at T = 25°C. The legend indicates the evolution of the total number of isolated nanoparticles counted in similar region before and after the AST. The table indicates the evolution of the average diameters calculated only from the isolated nanoparticles observed in ILTEM.

Besides, the significant loss of nanoparticles is not accompanied by any major change in the particle size distribution; the same observation was made in the previous section for a Pt/C electrocatalyst. This result rules out the occurrence of a quantitative 3D-ostwald ripening for the isolated nanoparticles. The smaller nanoparticles, theoretically less stable (as predicted by the Gibbs-Thomson equation [155]), would be more subjected to 3D-ostwald ripening, but this is neither observed on **FIGURE III-11**, nor on **FIGURE III-12**.

If it is possible that dissolution partially explains the observed loss of nanoparticles (but we believe it is unlikely), it appears that no (re)-deposition happens in these conditions; indeed, the size distribution does neither indicate an increase of the nanoparticles diameter nor the apparition of new and very small nanoparticles on the carbon support. Finally, the shape of the carbon substrate is not modified, ruling out any quantitative carbon corrosion. Therefore, like for Pt/C nanoparticles, most of the damages caused by the repeated potential cycling in 0.1 M NaOH consist of massive detachment of particles, probably because their anchoring sites/groups to the carbon substrate are irreversibly destroyed.

The ILTEM experiments provide further insights into the amplitude of the aging upon the AST in 0.1 M NaOH. As stated above, the ILTEM experiments were performed right away for *n* = 1000 cycles in 0.1 M NaOH without any characterization steps before and after the AST. Assuming the slight change of the mean (isolated) particles diameter upon the AST ($\overline{d_S}$ varies from 5.0 nm to 5.1 nm, see **FIGURE III-12**), the ECSA loss for *n* = 1000 cycles can be estimated in first approximation (assuming there are only isolated nanoparticles in the sample before and after the AST) by **EQUATION III-1**:

$$\text{ECSA loss} = \frac{\left[\frac{N}{\overline{d_S}} - \frac{N'}{\overline{d_S}'}\right]}{\frac{N}{\overline{d_S}}}$$

Equation III-1

with *N* = 1395 and *N*' = 676 the numbers of nanoparticles before and after the AST (being admitted that the regions investigated in ILTEM are representative of the whole samples), and $\overline{d_S}$ =5.0 nm and $\overline{d_S}'$ = 5.1 nm, the surface-average diameters before and after the tests (**FIGURE III-12**).

In practice, the ECSA loss for *n* = 1000 cycles in 0.1 M NaOH is worth 52%, substantially larger than the 32.5% measured for the "characterization-free" value after *n* = 150 cycles of AST (see above). So it seems that the initial cycles of AST are also more degrading in alkaline environment when performed on a pristine Pd/C electrocatalyst, and that once the "easily corrodible" fraction of the Pd/C sample has been degraded, the remaining fraction degrade quasi-linearly as a function of the number of cycles of the AST (at least until *n* = 1000 cycles). However, the ECSA loss estimated from ILTEM may be subjected to some uncertainty, for two reasons: firstly, only the isolated Pd nanoparticles are counted in the ILTEM histograms of **FIGURE III-12**, and the practical ECSA determined after the AST should take into account the contribution of the agglomerates (and this is a very awkward task – the statistics on the agglomerates is small and their shape very irregular); secondly, the statistics of such ILTEM measurements (although more than 600 particles were counted, at minimum) is evidently much lower than for the electrochemical measurement in the previous section. What can be said at that stage is that the 52% ECSA loss for *n* = 1000 cycles in 0.1 M NaOH estimated from the ILTEM experiments is overestimated, but it is not known by how much. Finally, this discussion does not modify the main conclusion from this section: Pd/C electrocatalysts are more stable than their Pt/C counterparts in alkaline environment.

The stability of the Pd/C nanoparticles was further investigated in the presence of strong reducer in the electrolyte. Dissolved gaseous hydrogen and hydrazine borane (HB) were used to mimic the environment of a DHBFC (direct hydrazine borane fuel cell) anode. Hydrazine borane (like ammonia borane) is known to hydrolyze on palladium catalysts [156,157]; this parasitic reaction decreases the faradaic efficiency for HB direct oxidation reaction, but also leads to its decomposition into H_2 gas (and borates). For this reason, it seems important to investigate as well the effect of the presence of H_2 in solution on the catalyst stability.

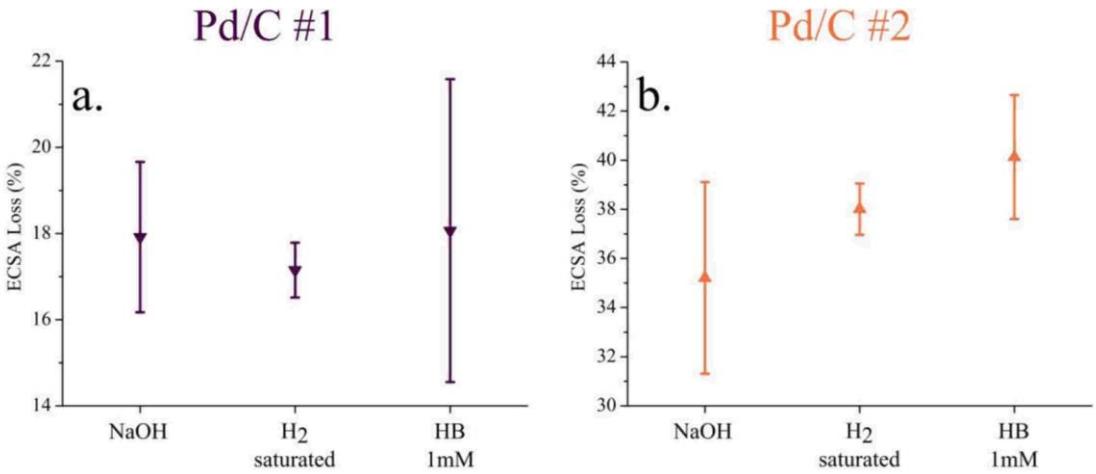

Figure III-13 ECSA losses for (a) Pd/C#1 and (b) Pd/C#2 in different reducing conditions of degradation. The AST consisted in 150 CV cycles between E = 0.1 and 1.23 V vs. RHE at T = 25°C in the considered alkaline electrolyte solution, and was preceded and followed by the usual characterization steps.

FIGURE III-13 shows the non-significant change in stability behavior for the large palladium nanoparticles (Pd/C#1) in presence of hydrogen or after the addition of hydrazine borane (1 mM) in the solution (the variations remain within the error bars). When smaller Pd nanoparticles are used (Pd/C#2), the picture changes: the ECSA losses are non-negligibly larger in presence than in absence of the fuel (strong reducer). This indicates the existence of some particle size effect on the durability of Pd/C nanoparticles in reducing alkaline environment. Moreover, a subtle increase of ECSA loss is monitored for the more reducing species (HB) *versus* hydrogen. It may be postulated that the repetitive cycling of the carbon-supported Pd nanoparticles from a stage of strong reduction (low potential in the presence of the strong reducer) to a stage of partial oxidation (large potential) promotes their instability; this strong reduction is more obvious for hydrazine borane than for H_2 (the former is a much stronger reducer than the latter), but also for small Pd nanoparticles than for larger ones (small nanoparticles are more oxophilic than large ones).

b. Intermediate milestone

The accelerated degradation of the two state-of-the-art and commercial Pd/C electrocatalysts was characterized and compared in dilute NaOH and H_2SO_4 electrolyte solutions at room temperature. Electrochemical measurements, combined with ILTEM, demonstrated that Pd/C catalysts are more robust than Pt/C in 0.1 M NaOH at T = 25°C, while palladium nanoparticles are severely damaged in acidic medium. If palladium electrocatalysts remain almost unchanged after a rather short accelerated stress test (n = 150 cycles between E = 0.1 and 1.23 V *vs.* RHE) in alkaline medium, an important degradation is nevertheless observed for a 1000-cycle-long AST in the same conditions. Indeed, 1000 cycles in 0.1 M NaOH at T = 25°C were found to be enough to monitor a significant loss of electrochemical surface area, because of high-extent detachment of particle (as well as agglomeration in a lesser extent); the corresponding ECSA loss in alkaline electrolyte scales rather proportionally to the number of CV cycles performed in the AST.

In addition, the presence of strong reducing species in the electrolyte (which would occur in a DLAFC anode) can trigger harsher degradation, and this effect is notable for smaller Pd/C nanoparticles. It can be inferred that the repeated alternation of the complete reduction of the carbon-supported metal nanoparticles and their partial oxidation promotes their detachment from the carbon substrate. This complete reduction is more likely for more reducing electrolytes, for smaller Pd/C nanoparticles than for larger ones, and for more noble metal nanoparticles (Pt/C), overall yielding larger extent of degradation in these cases. Finally, the results presented in this paper enable to forecast that carbon-supported palladium-based electrocatalysts may not be durable for long-term operation as anode electrocatalysts in direct liquid alkaline fuel cells such as DHBFC systems. Nevertheless, the relative stability of Pd/C materials (even in reducing conditions) *versus* similar Pt/C catalysts, at least for n = 150 cycles of AST, does guarantee their stability in the time frame of kinetic studies and therefore legitimates their utilization in such kinetic studies, as recently performed in [32], and as will be presented in chapter **"EFFECT OF THE NATURE OF THE BORANE FUEL ON THE ELECTROCATALYTIC ACTIVITY OF PALLADIUM"** of the present PhD manuscript.

v. Stability of cubic palladium nanoparticles in alkaline medium

Palladium exhibits great electrocatalytic performances and has gained a special interest for dehydrogenation process and for the electrooxidation of fuels such as ethanol, hydrazine [158,159] and boranes [32] and for the electroreduction of oxygen in alkaline medium [116,160,161]. A way to increase these intrinsic performances is to use shape-controlled Pd nanoparticles, which generally show significant (electro)catalytic enhancements following the predominance of more active facets [135,162]. Nevertheless, very few studies have been focused on the degradation of the nanoparticles shape as a consequence of their intensive use. To date, the group of Strasser [163] demonstrated that PtNi bimetallic octahedra was unstable in PEMFC environment, due to the preferential dissolution of Ni in super acidic electrolyte, whereas Abruña *et al.* demonstrated the instability of Pt hexagonal nanoparticles [164]. Alkaline environments are supposedly less aggressive and noble metals such as Pt or Pd in principle robust, but it was demonstrated in the two previous sections that even Pt and Pd carbon-supported nanoparticles are suffering degradation in alkaline medium, essentially owing to the destruction of the link between the carbon substrate and the metal nanoparticles. So, the aim of that present section is to investigate the stability of unsupported shape-controlled palladium-based nanoparticles.

a. Results & Discussions

FIGURE III-14-A shows the voltammogram (v = 5 mV s^{-1}) obtained in 0.1 M NaOH for cubic palladium nanoparticles. In addition to the typical oxide formation/reduction and hydrogen adsorption/desorption features of Pd surfaces, it exhibits two irreversible peaks corresponding to the specific {100}-orientation of the cubes. For example, Hoshi *et al.* studied the stability with Pd single crystals in alkaline medium and the peak ascribed to the presence of {100} sites can be observed [165]. Hereafter, ILTEM was performed for the same material to unveil a possible degradation of the cubic shape upon extensive cyclic voltammetry (CV) cycling. The widest potential window for the degradation tests was {0 < E < 0.9 V *vs.* RHE} which is a region of interest for fuel cell accelerated stress tests [20,150] and also a region where the oxidation reactions of non-carbonaceous fuels (such as $NaBH_4$, NH_3BH_3 and N_2H_4) are usually characterized [47,70,124]. In addition, this potential range enables to investigate the impact of hydrogen insertion/de-insertion which cannot be avoided with Pd materials.

FIGURE III-14-B exhibits the third CV sequence of the degradation test: the 15-min long chronoamperometry (CA) technique at E = 0 V *vs.* RHE leads to hydrogen insertion, these species being de-inserted and electrooxidized from the Pd surface in the subsequent CV cycles, and in particular in the first cycle (large peak at ca. E = 0.7 V *vs.* RHE in the first CV cycle of **FIGURE III-14-B**). The de-

insertion however proceeds (in a minor extent) in the subsequent cycles, owing to the slow solid-phase diffusion of Pd- hydrides from the bulk to the surface of the Pd nanocubes.

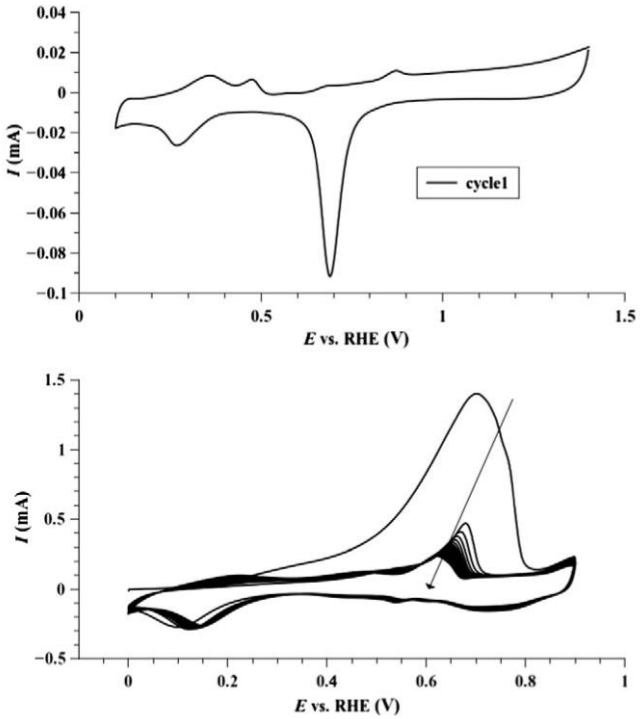

Figure III-14 (a) CV (v = 5 mV s^{-1}) between E = 0 and 1.4 V vs. RHE. (b) Third CV sequence (v = 100 mV s^{-1}) of the degradation test for {0 < E < 0.9 V vs. RHE} potential range, both performed in 0.1 M NaOH with Pd nanocubes deposited on glassy carbon electrodes.

FIGURE III-15-A clearly demonstrates the effective loss of cubic shape by cycling in 0.1 M NaOH electrolyte for a degradation test in the {0 < E < 0.9 V *vs.* RHE} potential range. **FIGURE III-15-B** corresponds to a benchmark sample on which only an Open Circuit Voltage technique has been performed, for an identical duration than for the latter degradation test (about 1 hour) in the same experimental conditions (0.1 M NaOH). Comparing **FIGURE III-15-A** and **FIGURE III-15-B** clearly demonstrates that cubic palladium nanoparticles do not withstand intensive (*ca.* n = 150 cycles) CV cycling in these conditions; nevertheless the origin of that dramatic degradation has to be identified.

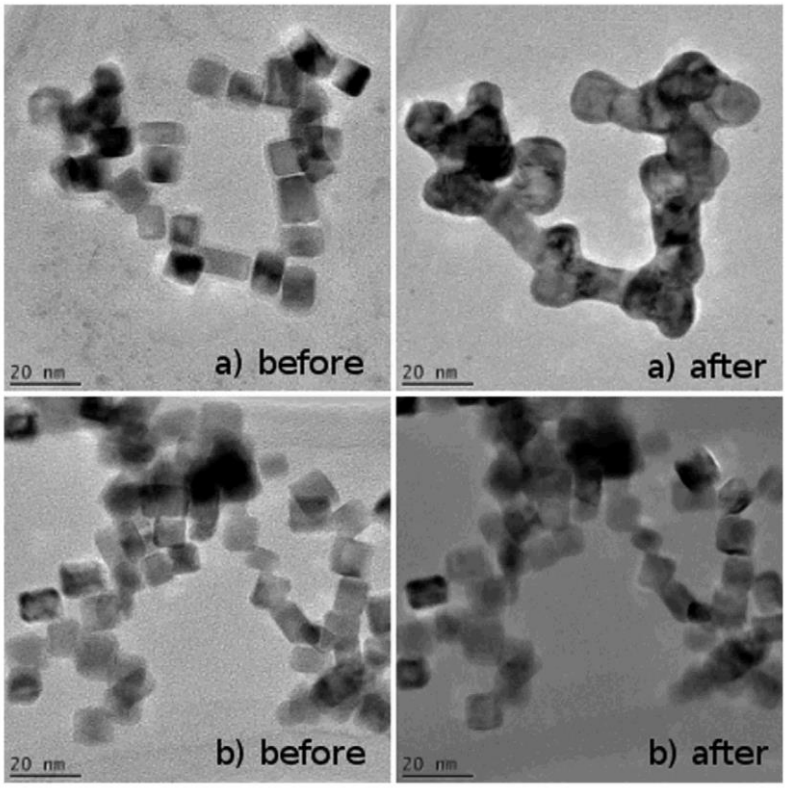

Figure III-15 Representative ILTEM micrographs of palladium cubic nanoparticles before/after for (a) a degradation test for a {0 < E < 0.9 V vs. RHE} potential range (b) an OCP technique with an identical duration (benchmark sample) than for a), both performed in 0.1 M NaOH

The formation/reduction of palladium oxides has been the first process suspected to modify the nanoparticle morphology. **FIGURE III-16** gives the ILTEM results obtained for a degradation test with a potential range from E_{low} = 0.4 V *vs.* RHE to E_{high} = 0.9 V *vs.* RHE; the CV associated curve, which presents one cycle for the corresponding "standard" electrochemical measurement on glassy carbon, clearly shows only the oxide region and confirms that no other process is involved in this potential range. After n = 150 cycles in 0.1 M NaOH, no significant change can be noticed on ILTEM images. This result excludes the oxide formation/reduction process as the most significant origin of the huge changes in nanoparticle morphology previously observed for intensive potential cycling between E = 0 and 0.9 V *vs.* RHE (**FIGURE III-15-A**).

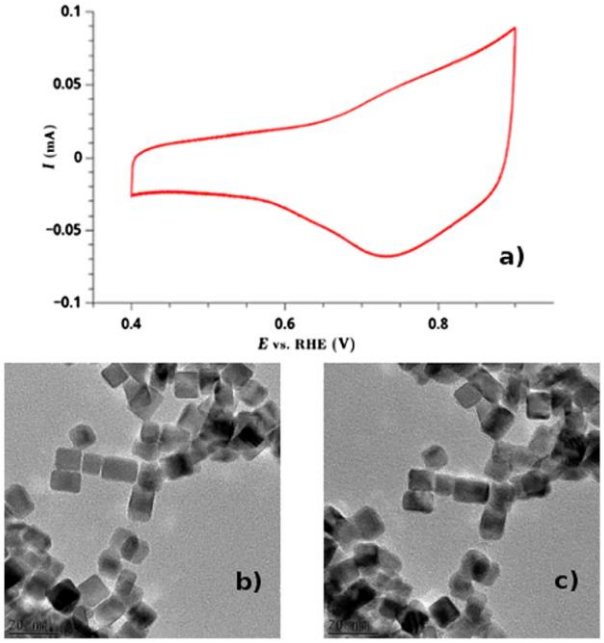

Figure III-16 Representative (a) CV and ILTEM micrographs of palladium cubic nanoparticles (b) before and (c) after a degradation test with a {0.4 < E < 0.9 V vs. RHE} potential range in 0.1 M NaOH.

Then, the palladium-hydride formation/reduction and hydrogen insertion processes have been investigated with a degradation test between E = 0 and 0.3 V *vs.* RHE; the ILTEM images of **FIGURE III-17-A&B** show that this degradation test does not lead to significant nanoparticle shape modifications, either. At that point, the shape-modification for that latter sample was followed by performing additional successive electrochemical measurements; after a chronoamperometry at E = 0 V *vs.* RHE for 15 minutes, a cyclic voltammetry at v = 100 mV s^{-1} between E = 0 and 0.9 V *vs.* RHE for ***n*** cycles has been performed. This procedure has been repeated 3 times with n = 10, 40 and 50 and ILTEM images acquired are giving insight into the rate of Pd nanocube modification. These images confirm again the instability of the cubic shape, which cannot sustain more than n = 100 cycles (at v = 100 mV s^{-1}) in the widest potential window {0 < E < 0.9 V *vs.* RHE} (**FIGURE III-17,C-E**). In addition, cycling the potential between E = 0 and 0.9 V *vs.* RHE has a more significant impact than both {0 < E < 0.3 V *vs.* RHE} and {0.4 < E < 0.9 V *vs.* RHE} restricted potential windows.

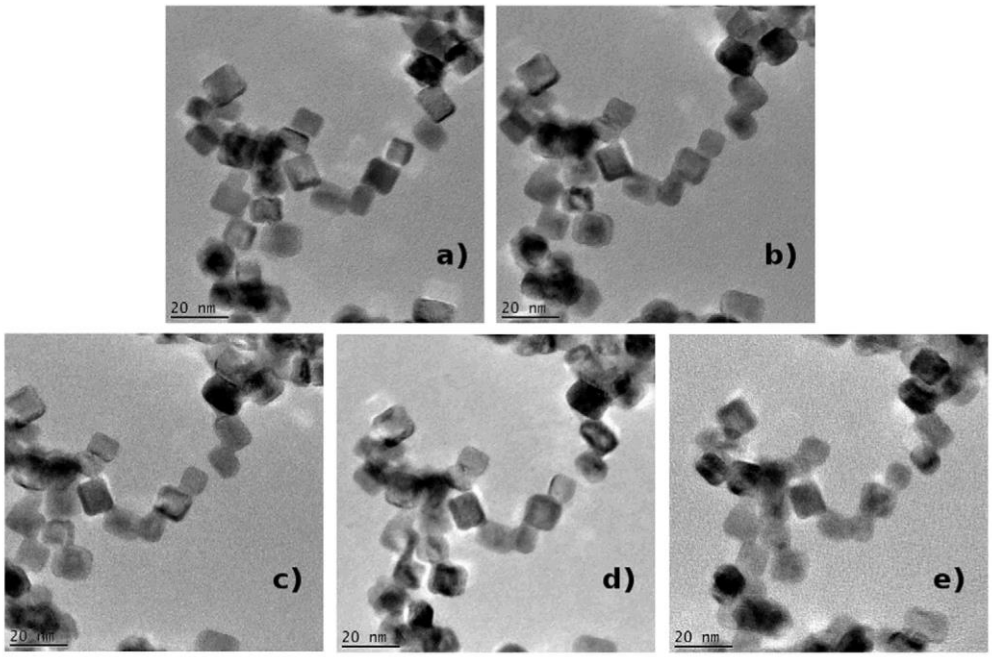

Figure III-17 Representative ILTEM micrographs of palladium cubic nanoparticles performed (a) before any experiment (b) after a degradation test for a { 0 < E < 0.3 V vs. RHE} potential range and after (c) 10 (d) 50 (e) 100 additional CV cycles between E = 0 and 0.9 V vs. RHE at v = 100 mV s^{-1}. All experiments performed in 0.1 M NaOH.

So, shape modifications are related to the cycling between very low and very high potential values. Obviously, the hydrogen generated at low potential, which acts as an electrochemical reagent only at high potential values, for both its de-insertion and its electrooxidation (Fig. 1b), can be a factor of degradation; indeed, the successive insertion/de-insertion of hydrogen (which can generate mechanical stress) or its electrooxidation on Pd can enhance the degradation of the nanoparticles and their change of morphology. Nevertheless, it remains sure that the cubic shape is neither stable nor sustainable for a usual potential range of study in 0.1 M NaOH electrolyte.

b. Intermediate milestone

The instability of cubic palladium nanoparticles was studied upon electrochemical experimentation. ILTEM micrographs demonstrated that less than a hundred cycles in 0.1 M NaOH at $v = 100$ mV s^{-1} can significantly modify the cubic shape into coalesced and near-spherical nanoparticles. The degradation of the cubic shape is due to re-organization of the surface atoms to diminish the number of edge atoms and to "smooth" the nanoparticle, leading to a spherical particle. This study also demonstrates that Pd is subjected to other degradation phenomena than evidenced for the Pd/C samples, and in particular that Pd dissolution/redeposition must be at stake in alkaline medium (the change of shape of the nanocubes cannot be accounted for without such mechanism of degradation). In consequence, special care must be taken on post-test characterization of the nanoparticle shape to assert that the tailored structure has sustained or not, even for noble metals.

vi. Chapter three conclusion

The results presented in that chapter bring important evidence of the aggressiveness of alkaline electrolytes towards noble electrocatalyst materials, based on platinum and palladium. It is now confirmed that stability issues have to be taken into account in alkaline medium even for "standard" electrochemical/kinetic studies. Indeed, one saw in that chapter that platinum-based carbon-supported electrocatalysts are highly degraded after only n = 150 cycles between E = 0.1 and 1.23 V *vs.* RHE in 0.1 M NaOH (at T = 25°C). Therefore, even a "long" kinetic study can be affected (and so its conclusions) if the experimenter is cycling too much the potential in his characterizations.

However, the degradation of platinum electrocatalysts can be nuanced for real alkaline fuel cell applications; indeed, it was observed that most of the degradation is due to particle detachment and those detached particles could have been retained in a thick electrocatalytic layer (as designed in real fuel cell systems). Nevertheless, it seems clear that alkaline fuel cells based on these catalysts are not sustainable for long-term operation, especially if one tries to decrease as much as possible the quantity of electrocatalyst used. Then, even if the palladium-based carbon-supported nanoparticles are relatively more stable than platinum ones, the same conclusions can be made; palladium electrocatalysts do not seem suitable for long-term operation in alkaline systems. However, their relatively better stability (than platinum) enables to use them for "trustable" and "reliable" kinetic study in alkaline medium.

Also, if it is possible to enhance the electrocatalytic activity of a given electrocatalyst by changing its morphology, the experimenter must also investigate the sustainability of that morphology in alkaline medium. Taking the example of a cubic-palladium electrocatalyst, it was observed that the cubic shape is not stable after only n = 150 cycles between E = 0 and 0.9 V *vs.* RHE in 0.1 M NaOH (T = 25°C). The degradation of the cubic shape is due to re-organization of the surface atoms to diminish the number of edge atoms and to "smooth" the nanoparticle, leading to a spherical particle.

Whereas Pd dissolution/redeposition must be at stake in the change of shape of the nanocubes, it is worth noting that for platinum and palladium carbon-supported electrocatalysts, no consequent dissolution/redeposition process is happening during the degradation: only particle detachment and agglomeration processes are witnessed. Moreover, neither carbon corrosion nor a "general" change in carbon chemistry are monitored and so responsible of their impressive degradation. It is believed, that the degradation takes place in the "vicinity" (region of contact) between the metal-based particle and its surface. This scenario is strengthened by the fact that the monitored degradation rate depends on the nature of the material while it is independent on the particle size: indeed, the palladium electrocatalysts (less noble than platinum) are more stable than platinum electrocatalysts, and no major difference has been remarked between the two palladium electrocatalysts (different in particle size distribution).

Besides, a slight (and detrimental) effect of the presence of reducer in solution was observed for palladium.

Nickel-based electrocatalysts for Direct BBM Fuel Cell

IV. Nickel-based electrocatalysts for Direct BBM Fuel Cell

i. Goals of the investigation

This chapter investigates the electroactivity of nickel-based carbon-supported electrocatalysts (Ni_3Ag/C, Ni_3Pd/C and Ni_3Co/C) for the direct electrooxidation of ammonia borane (AB) and hydrazine borane (HB) in alkaline medium.

Most of the experiment data presented here focus on AB, even if this PhD work is targeting an application for DHBFC systems. The choice to also work with AB was motivated by several reasons:

- Due to the very little literature available on the borane electrooxidation reaction (BH_3OR) for fuel cell application, it seemed relevant to bring new results to the scientific community. AB was chosen because it is an easy-to-find BBM; so, other groups could continue the work started in that PhD work;
- Working with AB instead of HB allows to remove the contribution of the hydrazine fragment, and doing so, to understand what is happening for the electrooxidation of the borane fragment separately.

The direct borane electrooxidation reaction (BH_3OR), using AB, is firstly investigated on Ni_3Ag/C, Ni_3Pd/C and Ni_3Co/C electrocatalysts. Then, because of its promising electroactivity toward the BH_3OR, the durability of Ni_3Co/C is investigated in real AFC conditions and also in alkaline supporting electrolyte for sake of comparison with the results obtained for Pt/C and Pd/C electrocatalysts (see the previous chapter). Finally, the activity of Ni_3Co/C for the HB electrooxidation reaction (HBOR) is investigated to see if the presence of hydrazine (instead of ammonia) modifies the electrooxidation of the borane fragment.

ii. Specific experimental section

a. For nickel-based electrocatalyst synthesis

The carbon-supported nickel-based nanoparticles were synthesized by thermal reduction of nickel, cobalt or palladium nitrates ($Ni(NO_3)_2*6H_2O$, $Co(NO_3)_2*4H_2O$, $Pd(NO_3)_2*xH_2O$, Sigma Aldrich) on the surface of a commercially available carbon support (KetJen Black 600J, KB600J, AkzoNobel). The loading of the final catalyst was calculated to be 50 wt%, while the desired atomic ratio between Ni and the second metal (M = Co, Ag and Pd) was kept constant at 75:25. The calculated amounts of metal nitrates were dissolved in 5 mL of de-ionized (DI) water and KB600J was added to transparent solution under stirring. The water was evaporated on a heat-plate pre-set to T = 85°C. The dry composite mixture was loaded into an agate jar (volume of 50 mL) with 10 agate balls (diameter 10 mm) and was ball-milled in a planetary ball-mill at ω = 450 rpm for 60 minutes. The resulting powder was placed into a porcelain boat and reduced for 2 hours at T = 400°C in a tube furnace under a flow of 7 at% H_2 at 100 cm^3 min^{-1}. After natural cooling down to room temperature, the hydrogen gas was switched to a 1 at% O_2 stream, and the Ni_3-M/C materials were passivated at T = 25°C for 6 hours. Extreme caution must be taken while removing the samples from the tube furnace without passivation: nano-dispersed non-passivated Ni_3-M/KB600J materials are pyrophoric and can be self-ignited upon contact with air. The synthesized samples are denoted below as Ni_3M/C (M = Co, Ag and Pd). These syntheses were performed by the author at the University of New Mexico (USA).

b. For nickel-based electrocatalyst characterization

From the electrocatalyst powders, the X-ray diffraction patterns were obtained; the crystallite size and relative phase composition were determined through Whole Pattern Fitting (WPF) in the MDI JADE 2010TM software. Then, Brunauer-Emmet-Teller (BET) surface areas were calculated from four-point measurements (all samples being outgassed with N_2 at T = 120°C for at least 8 hours prior the measurements). Finally, surface chemical analysis was completed with X-ray photoelectron spectroscopy (XPS). Three areas per sample were analyzed. Further details are available in the chapter **"GENERAL EXPERIMENTAL SECTION".**

Electrocatalyst inks were prepared by mixing 10 mg of each catalyst powder with 800 µL of ultrapure water, 50 µL of Nafion® solution (5 wt.% in water and light alcohols, Electrochem. Inc.®) and 150 µL of isopropanol. Thin-film rotating-disk electrodes (RDEs) were prepared by depositing 10 µL of the catalyst ink on a 5 mm-diameter glassy-carbon electrode, in order to reach a surface metal loading approximating *ca*. 255 μg_{Ni3M} cm^{-2} (with M = Ag, Co or Pd).

iii. Nickel-based electrocatalysts characterizations

The initial morphology and the particle size distribution histogram (PSD) of the three pristine carbon-supported nickel-based electrocatalysts are shown in **FIGURE IV-1**. Only isolated and spherical-shape nanoparticles have been taken into account in the determination of the PSD.

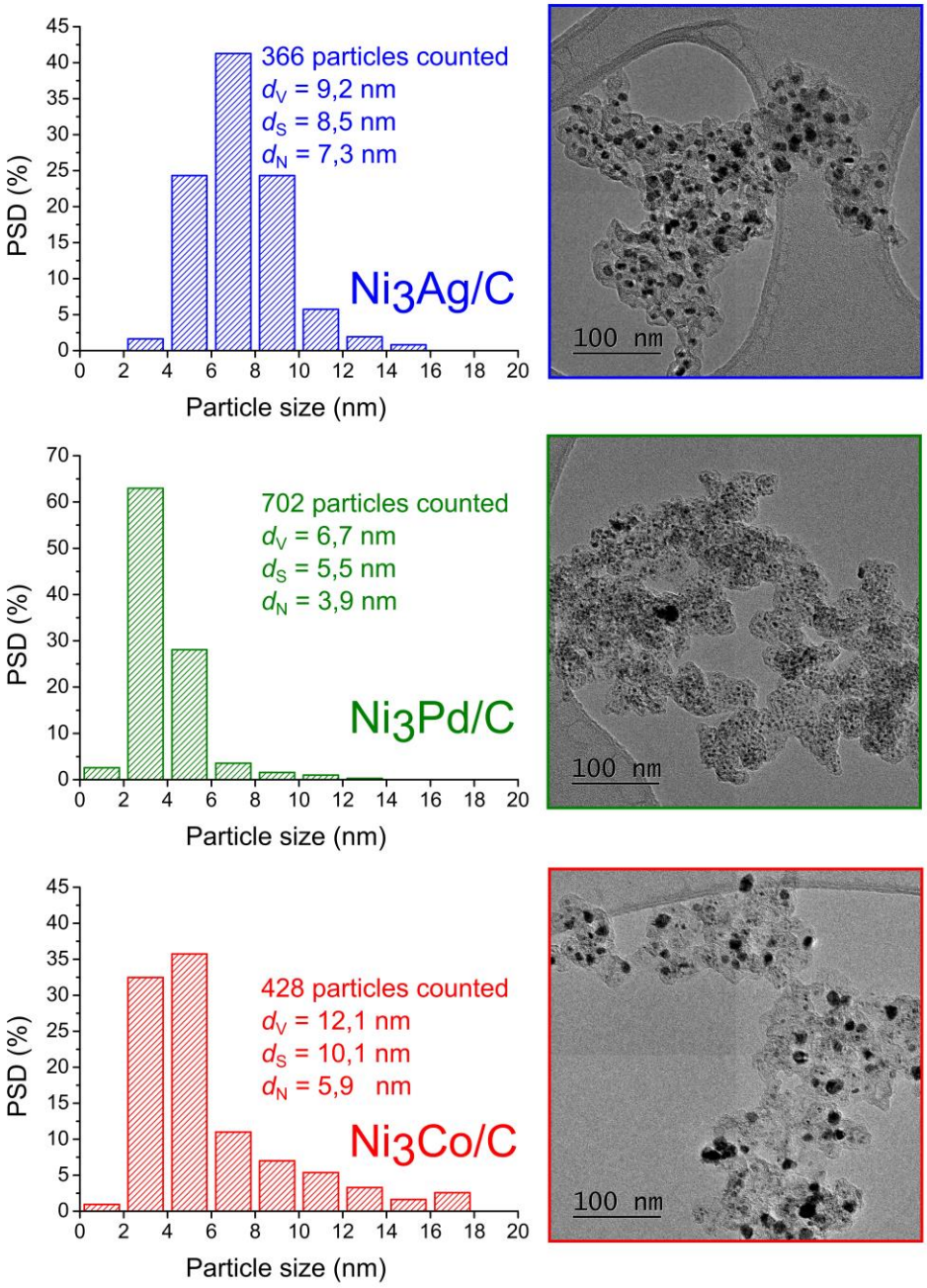

Figure IV-1 Particle Size Distributions (PSD) and representative TEM images of Ni_3Ag/C, Ni_3Pd/C and Ni_3Co/C electrocatalysts

The Ni_3Ag/C, Ni_3Pd/C and Ni_3Co/C electrocatalysts are composed of nanoparticles with a number-averaged diameter close to $\overline{d_N} \approx 7.3$, 3.9 and 5.9 nm respectively (which corresponds to a surface-averaged diameter $\overline{d_S}$ = 8.5, 5.5 and 10.1 nm respectively, and a volume-averaged diameter $\overline{d_V}$ = 9.2, 6.7 and 12.1 nm respectively). When M is noble (Pd), the nanoparticles are rather small and homogeneous in size, whereas when M is non-noble (Co), both larger nanoparticles and agglomerates (not counted in PSD) are observed. The case of Ni_3Ag/C is intermediate between these two extremes with small and large (but spherical and counted) nanoparticles. The presence of agglomerates in the case of Ni_3Co/C is explained by the relatively low temperature of formation of a fully miscible solid solution, which leads to particle growth and agglomeration during the prolonged synthesis [166]. **FIGURE IV-2** presents the powder diffractograms of the three Ni_3M/C electrocatalysts. They clearly demonstrate the composite nature of the three materials: separate peaks of nickel phase and M phase are observed in all cases. In other words, the materials are not pure alloys. Such a phase segregation can be explained by the selected temperature of the synthesis (T = 400°C), which is substantially below of the temperature of alloy formation ($T \approx$ 1000°C). The utilization of such a lower temperature is justified as a trade-off between the partial alloy formation and the prevention of particle growth and agglomeration (which is inevitable at T = 1000°C). Peaks at 2 Theta = 44°, which are attributed to metallic nickel, were broad due to contribution from silver alloying in Ni_3Ag/C (**FIGURE IV-2-TOP**) and palladium alloying in Ni_3Pd/C (**FIGURE IV-2-BOTTOM**). In the latter case, the signature of metallic palladium was also found in the diffractogram. Both the Ni_3Ag/C and Ni_3Pd/C samples had an insignificant amounts of surface oxide due to partial oxidation of nickel to NiO (peak at 2 Theta = 37°) under the exposure of materials to air.

TABLE IV-1 summarizes the data from XRD and BET measurements. For Ni_3Pd/C and Ni_3Co/C, the crystallite size is larger for the nickel fraction than for the palladium and cobalt one, the trend being opposite for the Ni_3Ag/C sample. Overall, the crystallite sizes are slightly larger than the volume-average diameters ($\overline{d_V}$) estimated from TEM (see **FIGURE IV-1**), which originates from the fact that only isolated and spherical-shape particles were counted in the PSD statistics (and that larger non-spherical nanoparticles and agglomerates were observed occasionally). In summary, the large particles in the three samples are rich in nickel for Ni_3Pd/C and Ni_3Co/C, and rich in silver for Ni_3Ag/C.

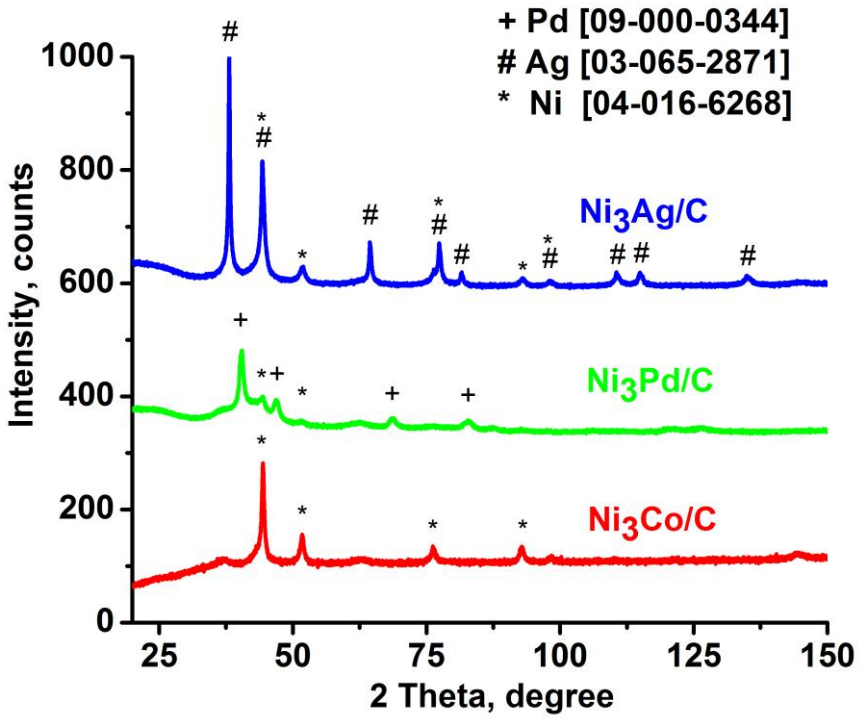

Figure IV-2 XRD data of the Ni_3Ag/C, Ni_3Co/C and Ni_3Pd/C catalysts with symbols showing peak assignments. The data was not background subtracted

Table IV-1 Surface area from multipoint BET measurements; catalyst component weight percent and crystallite size calculated with WPF from XRD

Electro Catalyst	BET Surface Area ($m^2\ g^{-1}$)	Ni (wt%)	NiO (wt%)	M (wt%)	Ni Size (nm)	NiO Size (nm)	M size (nm)
Ni_3Ag/C	450	49	11	40	7.9	10.4	15.7
Ni_3Co/C	360	28	19	53	33.3	7.9	8.5
Ni_3Pd/C	465	14	38	48	9.3	8.3	8.4

The top surface (*ca*. 2.5 nm) of each material was analyzed by X-ray Photoelectron Spectroscopy; a typical high resolution Ni 2p spectrum is shown in **FIGURE IV-3**. For all samples, approximately half of the total nickel detected is due to alloy and half is due to oxides. For Ni_3Co/C, ~60% of the total Co exists as oxide and for the Ni_3Pd/C sample, ~25% of the total Pd exists as oxide. From the elemental atomic ratio of the non-oxidized fraction of Ni to other metals in the alloy, the surface composition of the alloy can be calculated (**TABLE IV-2**). Only for Ni_3Co/C, the surface composition is close to the stoichiometric $Ni_{75}Co_{25}$. For both Ni_3Ag/C and Ni_3Pd/C, the nanoparticles surface is depleted in Ni and enriched with the other metal (Ag or Pd) in comparison with the stoichiometric ratios.

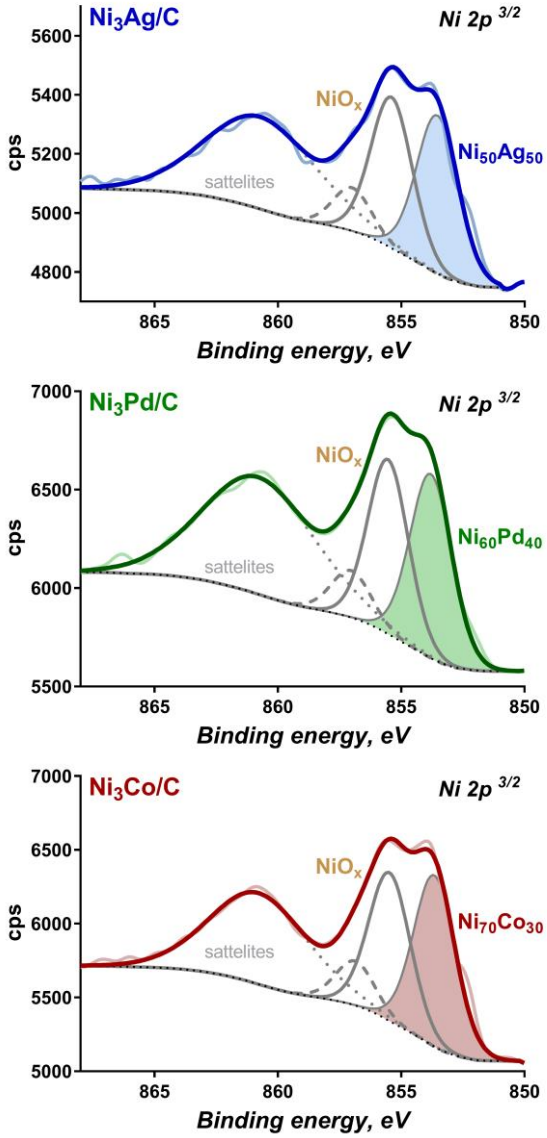

Figure IV-3 XPS spectrums obtained for each Ni_3M/C (M = Ag, Pd or Co) electrocatalyst material with emphasis on nickel oxide and nickel alloys/compounds formation.

Table IV-2 Surface speciation of catalysts derived from XPS analyses.

Electrocatalyst	**Surface alloy/compound composition**	**Surface NiO (at%)**	**Surface MO_x (at%)**
$Ni_{75}Ag_{25}$ (Ni_3Ag/C)	$Ni_{50}Ag_{50}$	51.8	0.0
$Ni_{75}Co_{25}$ (Ni_3Co/C)	$Ni_{70}Co_{30}$	52.8	58.6
$Ni_{75}Pd_{25}$ (Ni_3Pd/C)	$Ni_{60}Pd_{40}$	53.3	26.7

iv. Nickel-based electrocatalysts for AB electrooxidation

FIGURE IV-4 shows the electrocatalytic performances of the three nickel-based electrocatalysts for the electrooxidation of 5 mM AB in 0.1 M NaOH at T = 25°C, measured for a revolution rate of ω = 1600 rpm (hydrodynamic regime). The onset of reaction, defined for I = 0 A, is E_{onset} = -30, -50 and -90 mV *vs.* RHE for Ni_3Pd/C, Ni_3Ag/C and Ni_3Co/C, respectively. This indicates that the pure noble-metal-free electrocatalyst, Ni_3Co/C, presents a better ability to electrooxidize AB at low potential. Moreover, those values are all negative, which indicates that the reaction involved is (at least to some extent) the direct AB electrooxidation at those very low potential values, and not (only) the electrooxidation of the hydrogen generated by the AB hydrolysis at the electrode; this statement is confirmed by the poor activity of the electrocatalysts to oxidize hydrogen in a H_2-saturated solution (round symbols in **FIGURE IV-4**).

It is worth noting that the Hydrogen Evolution Reaction (HER) is also inhibited in presence of ammonia borane: the HER is shifted at lower potential value for every electrocatalyst material and this inhibition is even harsher for Ni_3Co/C.

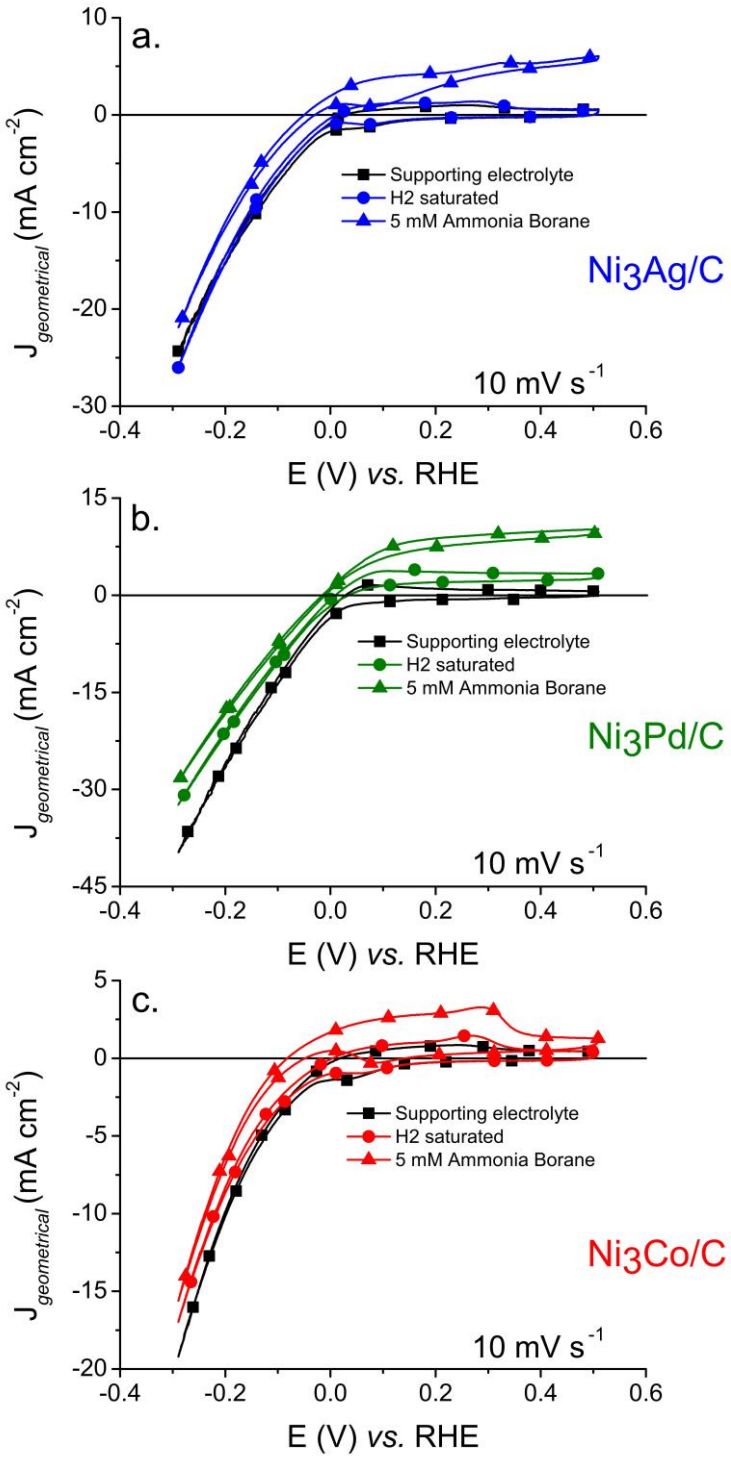

Figure IV-4 Cyclic voltammograms recorded on the Ni_3Ag/C, Ni_3Pd/C and Ni_3Co/C electrocatalysts in supporting 0.1 M NaOH (■) electrolyte, and after H_2 saturation (which corresponds to a concentration of ca. 1 mM H_2 [167], ●) or with addition of 5 mM Ammonia Borane (▲). In all cases, the potential was varied between -300 < E < 500 mV vs. RHE at $v = 10\ mV\ s^{-1}$, T = 25°C and $\omega = 1600$ rpm.

For the Ni_3Co/C electrocatalyst (the least noble material), an electrochemical pre-treatment is needed to activate the surface for AB electrooxidation. **FIGURE IV-5-A** shows the increase of the AB electrooxidation activity by cycling the electrode in the electrolyte in presence of ammonia borane at v = 50 mV s^{-1} for n = 25 cycles between -300 < E < 500 mV *vs.* RHE.

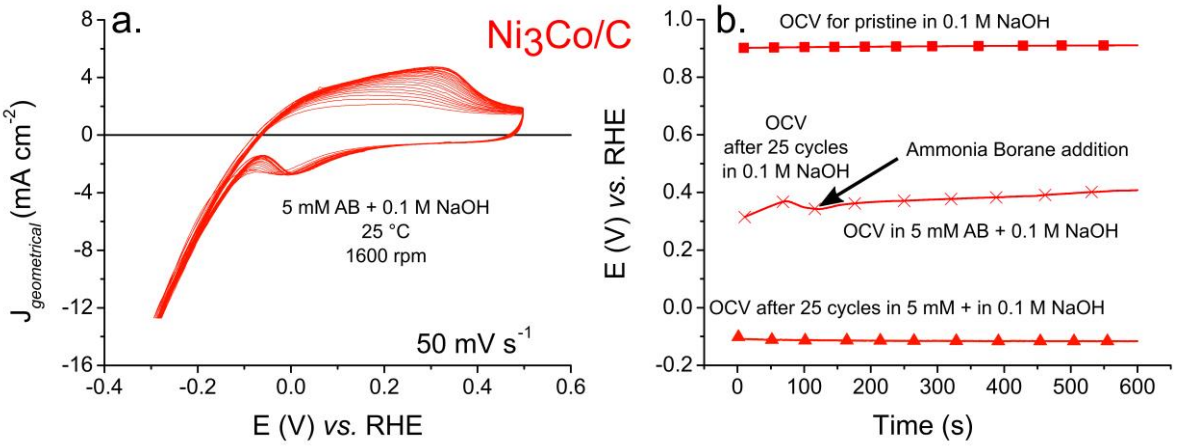

Figure IV-5 (a) Electrochemical pre-treatment required for the activation of the Ni_3Co/C electrocatalyst for the electrooxidation of AB. 25 cycles in 5 mM AB + 0.1 M NaOH at v = 50 mV s^{-1}, T = 25°C and ω = 1600 rpm. (b) Effect of the addition of AB and of the potential cycling on the evolution of the open-circuit voltage (OCV) measured for the Ni_3Co/C electrocatalyst.

It can be postulated at that stage that the open-circuit potential on the three Ni_3M/C materials is a mixed potential, as recently demonstrated [32,42,168] and modelled [36] for the electrooxidation of borohydride or ammonia borane at various noble electrocatalysts; this mixed potential is an equilibrium between two reactions, the BH_3OR (using AB) and the HER (electroreduction of water into H_2). As observed on **FIGURE IV-5-B**, before any electrochemical test, the OCV value for pristine Ni_3Co/C electrocatalyst is around E = 900 mV *vs.* RHE in supporting electrolyte. After cycling between -300 < E < 500 mV *vs.* RHE in supporting electrolyte (cleaning step), this value drops at E = 400 mV *vs.* RHE (which denotes for the partial reduction of the Ni_3Co/C sample, probably through partial reduction of its surface oxides). This value remains approximately constant, even after addition of ammonia borane; in other words, the presence of AB in solution (at 5 mM) is not enough to completely reduce (depassivate) the Ni_3Co/C electrocatalyst.

Interestingly, this behavior is not observed for the two partially noble electrocatalysts (M = Pd or Ag), which is in perfect agreement with the data obtained by surface XPS analysis. While the surface of Ni_3Co/C is covered by mixed oxides of nickel and cobalt that can be only partially reduced at the experimental conditions described above, the surfaces of Ni_3Ag/C and Ni_3Pd/C have substantially lower amount of second metal oxide and are easily depassivated. For those latter electrocatalysts, the OCV value drops as soon as the ammonia borane is added and remains close or lower than E = 0 mV *vs.* RHE

(see **FIGURE IV-6-A** and **FIGURE IV-6-B** for Ni_3Ag/C and Ni_3Pd/C, respectively). The easy depassivation of Ni_3Ag/C and Ni_3Pd/C upon the presence of only 5 mM AB in solution signs the clear influence of their partially noble nature. Finally, the OCV value also drops around E = -100 mV *vs.* RHE for Ni_3Co/C after the potential cycling (activation) in presence of AB (see **FIGURE IV-5-A**). These results show the major role played by the noble metals (Ag and Pd) in the passivation/depassivation process of the base metal component (Ni).

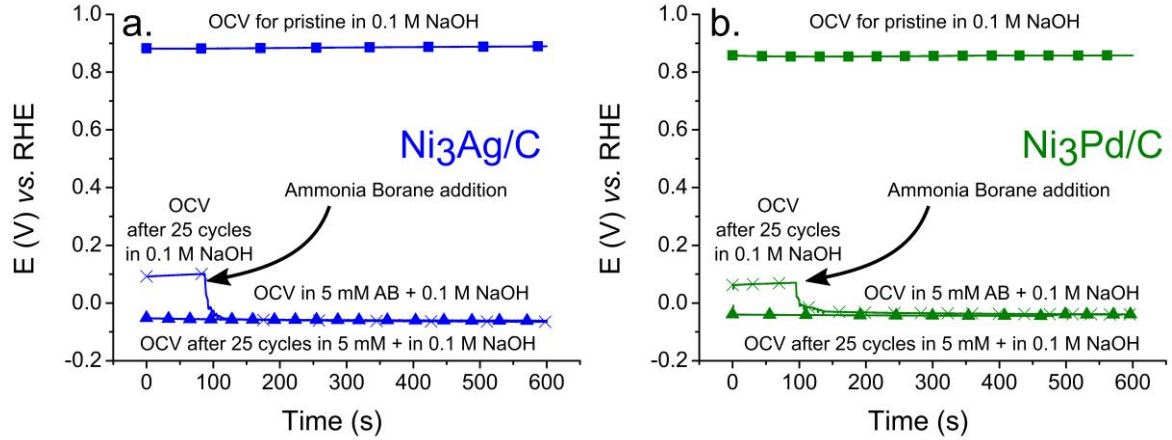

Figure IV-6 Evolution of OCV values and effect of CV cycling in supporting electrolyte for (a) the Ni_3Ag/C electrocatalyst and (b) the Ni_3Pd/C electrocatalyst.

FIGURE IV-7 presents the electrocatalytic stability of the three electrocatalysts. It has been investigated by performing the following electrochemical sequence:

- Initially, a polarization for 3 minutes at E = -300 mV *vs.* RHE (to pre-reduce the samples);
- Then, a polarization for 15 minutes at E = 100 mV *vs.* RHE to measure the steady-state activity for the borane electrooxidation reaction (using AB);
- Finally, a polarization for 5 minutes at E = 500 mV *vs.* RHE followed by a polarization for 3 minutes at E = 100 mV *vs.* RHE.

The final step allows to investigate a possible re-passivation of the electrocatalysts at high potential values (E > 500 mV *vs.* RHE) and a possible loss of activity when returning at lower potential values.

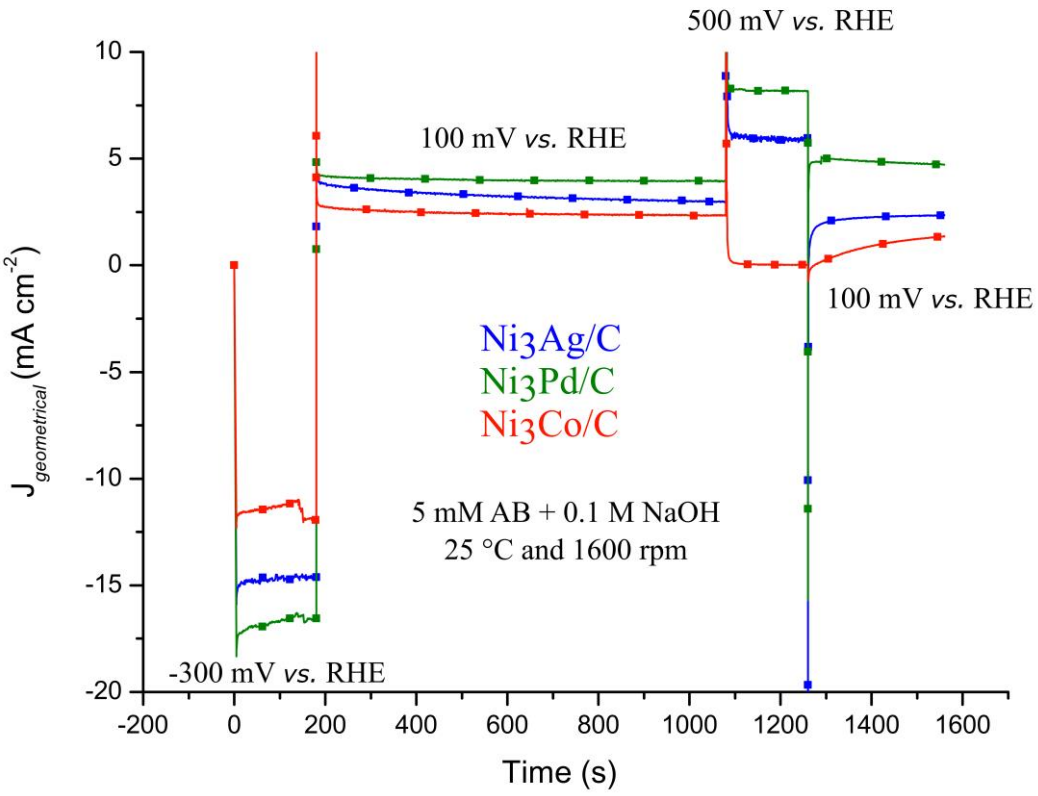

Figure IV-7 Stability of the borane electrooxidation reaction (using AB) steady-state performance for the three Ni_3M/C electrocatalysts, measured at T = 25°C and ω = 1600 rpm in 0.1 M NaOH + 5 mM AB.

Each electrocatalyst presents a non-negligible steady-state activity for BH_3OR (using AB); moreover, the anodic current is stable when the electrode potential is held at E = 100 mV *vs.* RHE for 15 minutes, which demonstrates the absence of severe deactivation of the catalyst materials. It must be recalled here that Au and Pt electrocatalysts are severely deactivating during the low-potential electrooxidation of $NaBH_4$ [36,40,41,63], a drawback obviously not experienced here.

Then, the electrocatalysts were investigated at higher potential: E = 500 mV *vs.* RHE, which mimics the situation experienced for a DABFC anode at large load. The effect of a 2-minute hold at this potential is markedly different for the three electrocatalysts. On the one hand, it is enough to passivate the Ni_3Co/C electrocatalyst (the borane electrooxidation current almost completely and instantly levels off at E = 500 mV *vs.* RHE), and this passivation somewhat maintains upon return to E = 100 mV *vs.* RHE: the Ni_3Co/C electrocatalyst struggles to recover its initial electrocatalytic activity.

On the other hand, the nobler Ni_3Pd/C electrocatalyst and in a minor extent Ni_3Ag/C are not affected by the incursion at E = 500 mV *vs.* RHE: their electrocatalytic activity increases with the electrode potential, and the return to E = 100 mV *vs.* RHE only slightly inhibits the Ni_3Ag/C electrocatalyst and even further

activates Ni_3Pd/C. That latter observation signs that Ni_3Pd/C is (slightly in the present conditions) self-polluting upon AB electrooxidation, likely by boron-based intermediate species, as observed (in a much larger extent) for $NaBH_4$ electrooxidation on noble metals [36,40,41,63]. These results underline, again, the importance of the materials' conditioning on their AB electrooxidation performance, and the influence of the nobleness of the M metal on the overall behavior of the Ni_3M/C electrocatalysts. Besides, these observations during borane electrooxidation (using AB) agree with the results obtained for the variation of OCV values and the required (or not) activation pre-treatment for three electrocatalysts (**FIGURE IV-5** and **FIGURE IV-6**). This behavior notably indicates the necessity to control the oxidation state of the noble-metal-free Ni_3Co/C material surface to get optimal activity in real application, which is not so required when noble metals are added to the nickel base.

The tests of performance stability have been reproduced at least 4 times with fresh electrodes for each electrocatalyst. An average value of the steady-state electrocatalytic activity has been measured at E = 100 mV *vs.* RHE which is the potential of interest for the alkaline fuel cell application (**FIGURE IV-8,LEFT-Y-AXIS**). The borane electrooxidation (using AB) onset potential, which is another relevant parameter to compare the activity of different electrocatalysts, is also shown in **FIGURE IV-8,RIGHT-Y-AXIS.**

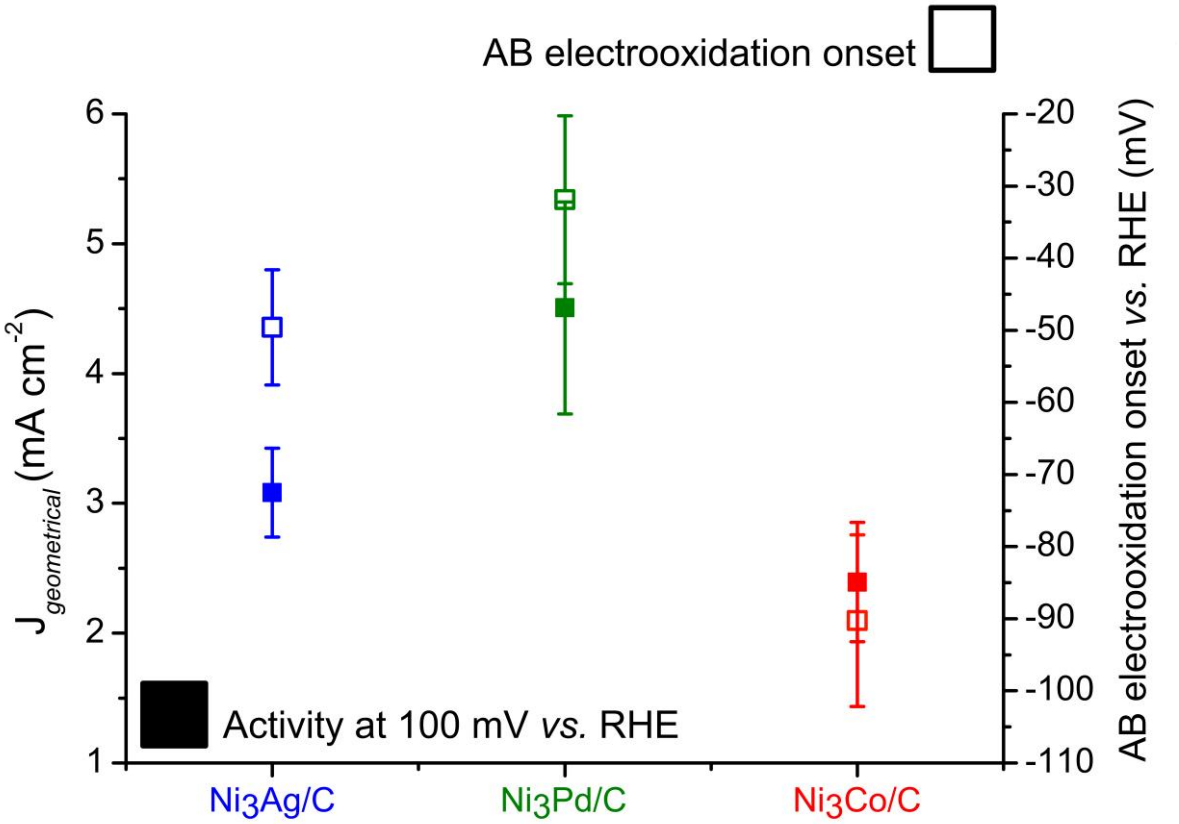

Figure IV-8 Comparison of the electrocatalytic activity for Ammonia Borane electrooxidation in 5 mM AB + 0.1 M NaOH measured at E = 100 mV vs. RHE, T = 25°C and ω = 1600 rpm for the Ni_3Ag/C, Ni_3Pd/C and Ni_3Co/C electrocatalysts.

The borane electrooxidation activity can be ranked as follows when measured at E = 100 mV *vs.* RHE:

Ni_3Pd/C (*ca.* 4.5 mA cm^{-2}) > Ni_3Ag/C (*ca.* 3 mA cm^{-2}) > Ni_3Co/C (*ca.* 2.5 mA cm^{-2})

Nevertheless, it is worth noting that the activity of Ni_3Pd/C is only twice higher than the electroactivity of Ni_3Co/C, the latter material being significantly cheaper and more available than the others, because it contains no noble metals. Besides, as noted above, Ni_3Pd/C is subjected to self-deactivation at low potential.

Now, when the onset potential of borane electrooxidation (using AB) is considered, Ni_3Co/C is the most interesting electrocatalyst, followed by Ni_3Ag/C and then Ni_3Pd/C. This ranking is exactly opposed to the trend observed at E = 100 mV *vs.* RHE. In particular, the BH_3OR starts on Ni_3Co/C at a *ca.* 65 mV lower potential than on Ni_3Pd/C, but proceeds slower at E = 100 mV *vs.* RHE. This likely demonstrates a trade-off of (electro)catalytic properties: the Pd component of Ni_3Pd/C is very active for the catalytic decomposition of AB and for the HER, but is capable to electrooxidize H_2 in a fast manner (above E = 0 mV *vs.* RHE); on the contrary, Ni_3Co/C is less active for these reactions, overall enabling to valorize

AB in a more direct and complete manner at lower electrode potential. The Ag-containing sample has an intermediate behavior. Those results highlight that the Ni_3Co/C electrocatalyst is a material of choice for direct AB fuel cells, and will be studied in more details below.

Also, **FIGURE IV-9-A** shows a clear mass-transport dependency of the borane electrooxidation (using AB) current measured at E = 100 mV *vs.* RHE: the current density increases in a near-linear manner with the square root of the electrode rotation rate. This suggests that the BH_3OR (using AB) is not only limited by the charge transfer kinetics, even at such low potential, again demonstrating the interest of Ni_3Co/C for the DABFC anode. **FIGURE IV-9-B** presents two borane electrooxidation (using AB) voltammograms measured in hydrodynamic conditions at T = 25°C and 60°C. The effect of the temperature is dual. On the one hand, a larger temperature is detrimental to the onset of the BH_3OR; this phenomenon is explained by the AB hydrolysis. Indeed, increasing the temperature enhances the kinetic of the AB hydrolysis into gaseous hydrogen, which cannot be valorized for E < 0 mV *vs.* RHE (and for which Ni_3Co/C is not so active, as shown in **FIGURE IV-4**). On the other hand, the mass-transport and direct AB electrooxidation kinetics are also faster at high temperature, therefore increasing the maximum anodic current density at T = 60°C. The same behavior has been reported for DABFC anodes based on Pt/C and Pd/C [32]. Concerning the passivation above *ca.* E = 0.35 V *vs.* RHE, the temperature does not seem to have any significant effect.

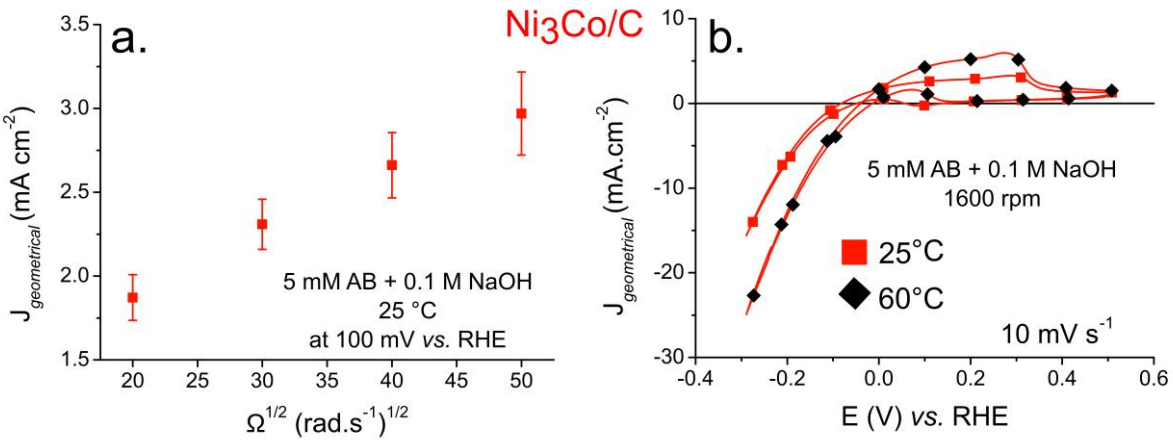

Figure IV-9 Effect of a- the electrode rotation speed and b- the solution temperature on the electrocatalytic performance of Ni_3Co/C for borane electrooxidation (using AB) in 5 mM AB + 0.1 M NaOH.

v. Durability of nickel-based electrocatalysts in alkaline media

The durability of the Ni_3Co/C electrocatalyst was surveyed in alkaline media. At first, a "mild" degradation test was performed in AB-containing electrolyte (5 mM AB) at T = 25°C. The electrochemical protocol consisted of:

1. An activation pre-treatment (n = 25 cycles between -300 < E < 500 mV *vs*. RHE at v = 50 mV s^{-1}) followed by;
2. A 6 hour-long chronoamperometry at E = 100 mV *vs*. RHE.

The micrographs of **FIGURE IV-10**, obtained at a magnification of ×50,000 and ×200,000, do not enable to detect any degradation of the Ni_3Co/C electrocatalyst. Neither clear loss of Ni_3Co nanoparticles, nor change of their size and /nor shape are witnessed; besides, the shape of the carbon substrate is essentially unaffected by this electrochemical treatment. In other words, neither the Ni_3Co nanoparticles nor the carbon substrate do experience any detectable corrosion in these conditions, thereby demonstrating the stability of Ni_3Co/C electrocatalyst in AB-electrooxidation conditions.

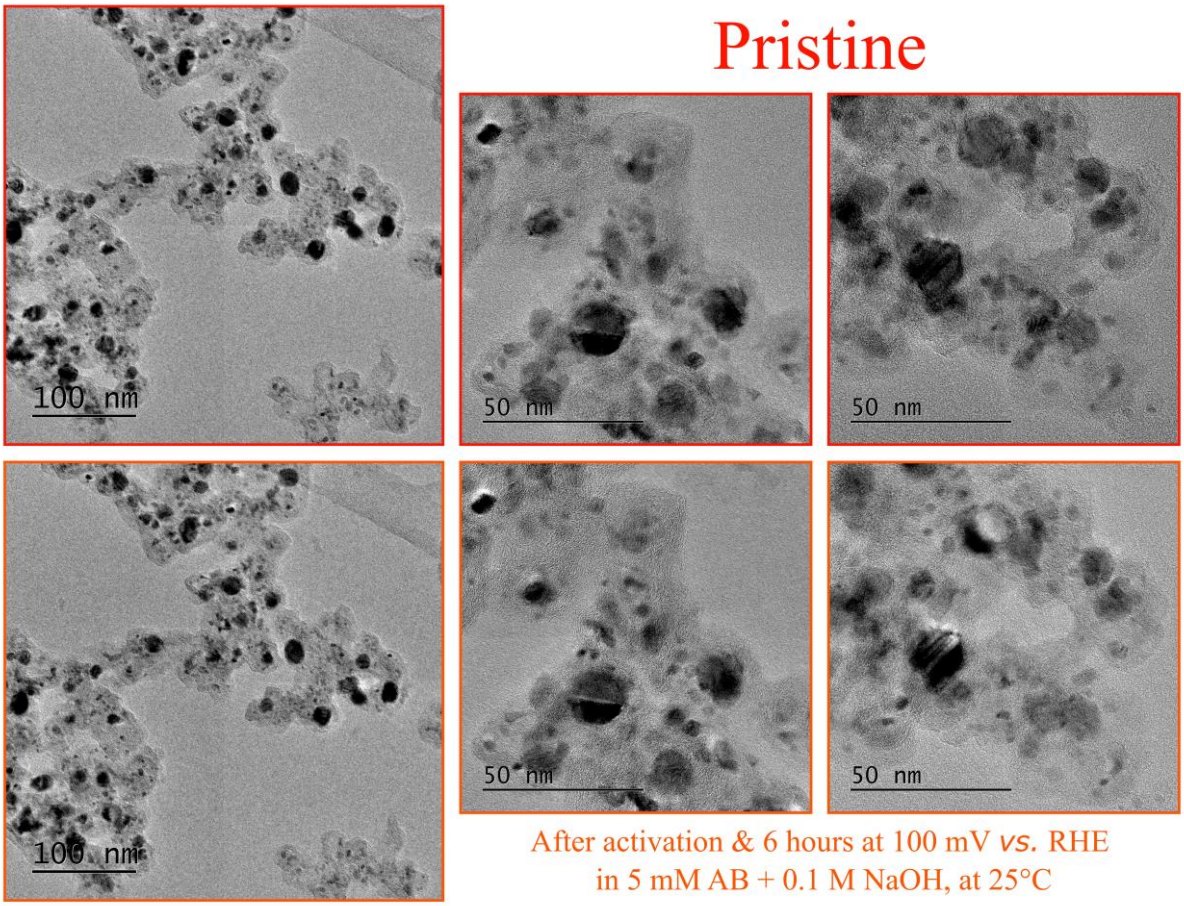

Figure IV-10 Representative ILTEM images of the Ni_3Co/C electrocatalyst obtained before and after electrochemistry; the electrochemical treatment consisted of a pre-treatment (activation) and a 6-hour-long steady-polarization at E = 100 mV vs. RHE in a 5 mM AB + 0.1 M NaOH electrolyte at T = 25°C.

A second accelerated stress test (AST) was then performed; it consists of repetitive cycling (n = 150 and then 1000 cycles) performed between E = 0.1 and 1.23 V *vs*. RHE at v = 100 mV s^{-1} and T = 25°C in supporting electrolyte (0.1 M NaOH).

This allows to compare the stability of Ni_3Co/C in these conditions with the previous results for Pd/C and Pt/C (presented in the previous chapter); ILTEM images have been made after n = 150 cycles and n = 1000 cycles (**FIGURE IV-11**). They demonstrate the stability of the Ni_3Co/C electrocatalysts in alkaline medium: no morphology changes can be noticed on the ILTEM images. It must be recalled the results presented in the previous chapter: Pt/C and in a lesser extent Pd/C electrocatalysts experience severe degradations in these conditions [80,100,101]. For example, about 60% Electro-Chemical Surface Area (ECSA) loss was measured for Pt/C, demonstrating the extreme weakness of this electrocatalyst in alkaline medium; this loss was mainly due to nanoparticles detachment and agglomeration processes, and this was observed after only n = 150 cycles. Pd/C was relatively more stable in these conditions [101],

but not as much as the present Ni_3Co/C electrocatalyst. Again, the instability of Pd/C was mainly due to nanoparticles detachment.

So, contrary to the case of Pd/C and Pt/C electrocatalysts, neither massive nanoparticle detachment nor agglomeration processes are observed for Ni_3Co/C on **FIGURE IV-10** and **FIGURE IV-11**. Coupled with the stability of the AB electrooxidation current measured on this material at low electrode potential (**FIGURE IV-7**), this result further demonstrates the interest of Ni_3Co/C for the DABFC anode.

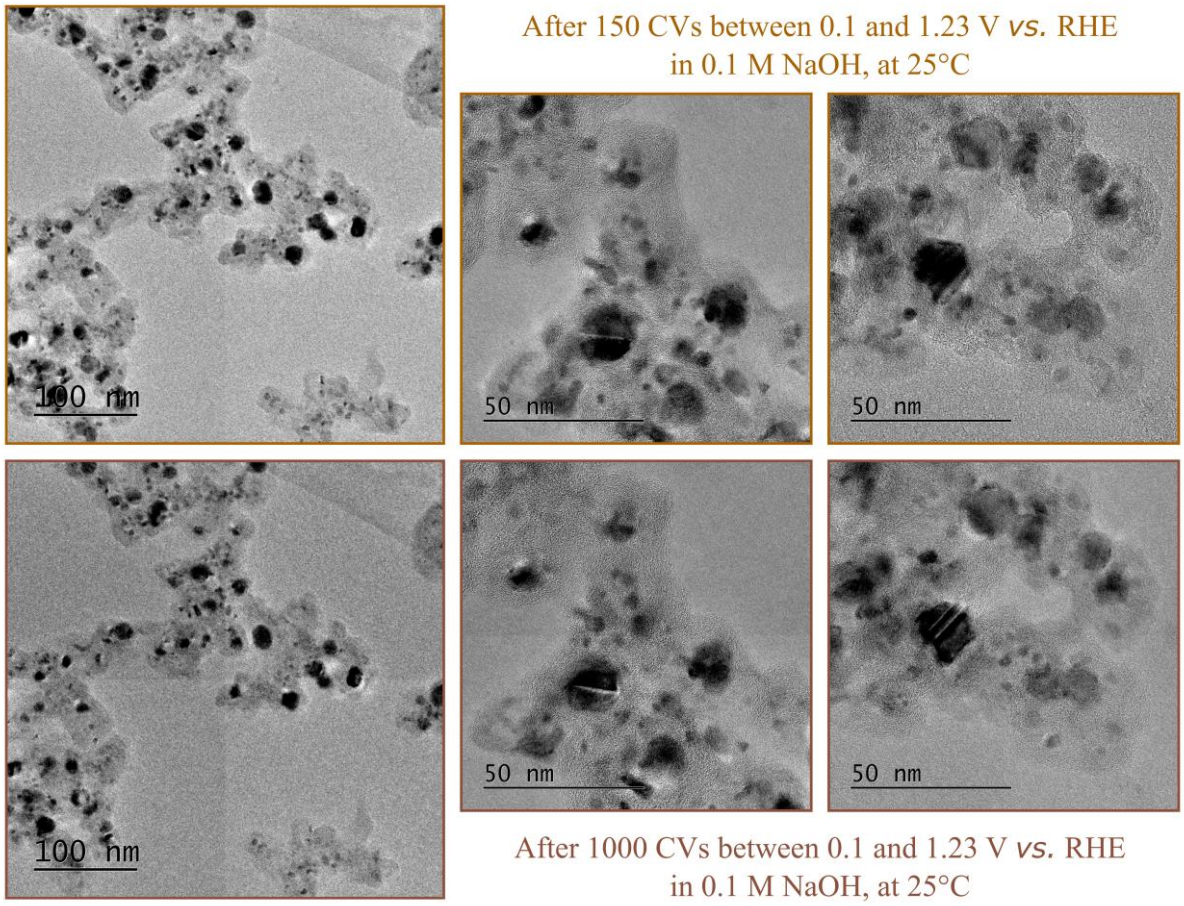

Figure IV-11 Representative ILTEM images of the Ni_3Co/C electrocatalyst obtained before and after electrochemistry; the electrochemical treatment consisted of repeated cycling between $0.1 < E < 1.23$ V vs. RHE in 0.1 M NaOH at T = 25°C.
The regions presented here are the same than on Figure IV-10

vi. Application for HB electrooxidation

The electroactivity of the Ni_3Co/C electrocatalyst for the electrooxidation of HB has also been investigated. The **FIGURE IV-12** shows the electrocatalytic performance in 0.1 M NaOH + 5 mM of ammonia borane or hydrazine borane, at ω = 1600 rpm and *T* = 25°C.

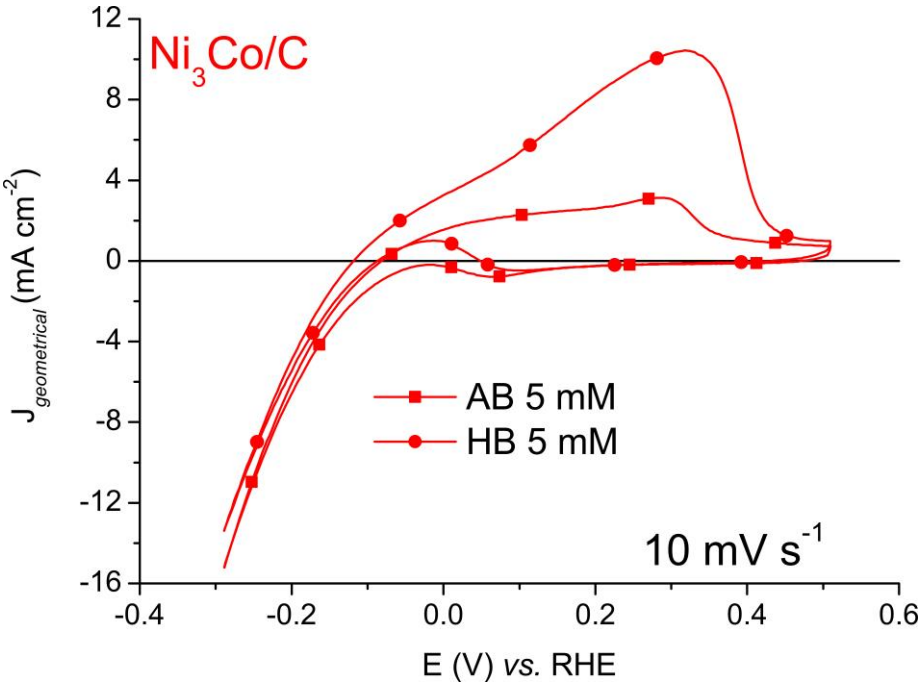

Figure IV-12 Cyclic voltammograms for the Ni_3Co/C electrocatalyst in 0.1 M NaOH + 5 mM of ammonia borane or hydrazine borane, at v = 10 mV s^{-1}, T = 25°C and ω = 1600 rpm.

As remarkable, Ni_3Co/C remains a very good electrocatalyst for the BH_3OR using HB; the onset of reaction is even lower when this latter borane fuel is used: the BH_3OR begins at *E* = -85 mV against -120 mV *vs.* RHE for AB and HB respectively. Then, when the maximum current density is measured around 2.50 mA cm^{-2} for AB, this value reaches *ca.* 10 mA cm^{-2} for HB; this can be related to a better electrochemical kinetics for BH_3OR and also to the electrochemical activity of nickel-based electrocatalysts for the hydrazine electrooxidation reaction (HHOR); indeed, the HB electrooxidation reaction is in fact the addition of BH_3OR and HHOR. In recent studies performed in similar conditions [169,170], the groups of Finkelstein and Strasser, have brought evidences of the electroactivity of Ni-based, Co-based and NiCo-based (supported on carbon or not) electrocatalysts for the HHOR in very similar experimental conditions. They recorded an onset of reaction between *E* = -100 and 100 mV *vs.* RHE, depending on the amount in nickel and in cobalt for a given electrocatalyst. So, it is very probable that

the BH_3OR and the HHOR happen simultaneously at negative potential (< E = 0 *vs.* RHE) which is a very good result for the DHBFC systems.

The **FIGURE IV-12** also indicates that the utilization of HB instead of AB diminishes the passivation of the Ni_3Co/C electrocatalyst surface; the passivation phenomenon appears around E = 300 mV against 500 mV *vs.* RHE for AB and HB respectively, which is another advantage of the utilization of HB in direct liquid alkaline fuel cell systems.

vii. Chapter four conclusion

Nickel-based carbon-supported electrocatalysts (Ni_3Ag/C, Ni_3Pd/C and Ni_3Co/C), were synthesized and thoroughly characterized by a complete set of physicochemical and electrochemical methods. They all consist of composite nickel (and nickel oxide) and M (Pd, Ag or Co) nanoparticles. Their activity was tested for the borane electrooxidation reaction (BH_3OR, using AB) in alkaline medium. All the Ni_3M/C electrocatalysts demonstrate interesting performances for the BH_3OR. Even if the highest faradic current of electrooxidation is observed on the Ni_3Pd/C and Ni_3Ag/C electrocatalysts, the Ni_3Co/C electrocatalyst also exhibits appreciable activity: the current density measured at E = 100 mV *vs.* RHE on Ni_3Co/C is only twice lower than measured for Ni_3Pd/C, the best electrocatalyst at that potential. Moreover, the reaction onset is the lowest on Ni_3Co/C (it is *ca.* E = -90 mV *vs.* RHE); at such low potential value, the BH_3OR is direct and cannot proceed *via* the decomposition of AB into H_2 followed by H_2 electrooxidation, which is interesting in terms of energy density and faradaic efficiency. This could lead to high operating voltage value with a Ni_3Co/C-based anode in liquid alkaline fuel cell systems fed with borane fuel. Finally, the Ni_3Co/C electrocatalyst has shown promising durability for rather long-term borane electrooxidation (in 5 mM AB + 0.1 M NaOH electrolyte) and for accelerated stress tests in supporting electrolyte. In particular, ILTEM experiments demonstrated the absence of any consequent degradation for Ni_3Co/C, which confirms a much larger material stability than reported in the previous chapter for platinum and palladium based carbon-supported nanoparticles.

The electroactivity of Ni_3Co/C for the BH_3OR using hydrazine borane has also been confirmed; actually, the kinetic performances are improved and the onset of the BH_3OR is even lower (E ~ -120 mV *vs.* RHE) with HB. This latter result can be explained by an enhancement in BH_3OR kinetics with HB (probably because the electrocatalyst surface is not hindered by any presence of ammonia in that case) and by the simultaneous valorization of the hydrazine fragment at very low potential value.

To summarize, with a promising electroactivity for AB or HB electrooxidation reactions and with a higher stability in real conditions, the Ni_3Co/C noble-free electrocatalyst appears to be a material of choice for the anode of DABFC or DHBFC systems.

Effect on the borane origin on palladium electrocatalytic activity

V. Effect of the nature of the borane fuel on the electrocatalytic activity of palladium

i. Goals of the investigations

This chapter investigates the borane electrooxidation reaction (BH_3OR) in alkaline medium. The investigations are mainly performed on a carbon-supported palladium electrocatalyst, because it is a "noble" material allowing to have a model surface for kinetic experiments; besides, as seen in the chapter **"DEGRADATION OF NOBLE ELECTROCATALYSTS IN ALKALINE MEDIUM"**, palladium electrocatalysts can be considered 'relatively stable' in alkaline medium if only a few voltamperometric cycles are performed, conditions which will be fulfilled in the present chapter.

The BH_3OR has not been intensively studied in the literature so far; in addition, no half-cell study was performed with experimental conditions close to those in real liquid alkaline fuel cell systems (concentrated anolyte, temperature above $T = 25°C$, carbon-supported electrocatalysts [32]). Besides, most of the data are related to gold smooth or textured surface for which the BH_3OR onset is higher than $E = 0$ *vs.* RHE (at pH ≥ 13), which is, to the author's opinion useless for DLAFC applications. Despite the fact that gold is absolutely not a suitable electrocatalyst for the DHBFC system (because of the combination of its expensiveness and of its inability to valorize the borane fuel at low potential value), the data related to BH_3OR studies on gold has permitted to provide first insights into the BH_3OR mechanism on this model metal. For instance, Finkelstein *et al.* [119], using dimethylamine borane (DMAB) as a fuel, have formalized the BH_3OR mechanism has a CE (Chemical-Electrochemical) process, following the equations:

$$(C_{Finkelstein}) \qquad (CH_3)_2NBH_3 + OH^- \leftrightarrow (CH_3)_2N + BH_3OH^-$$

Followed, at low potential values by:

$$(E_{Finkelstein}, low) \qquad BH_3OH^- + 3OH^- \leftrightarrow B(OH)_4^- + \frac{3}{2}H_2 + 3e^-$$

Or, at high potential values by:

$$(E_{Finkelstein}, high) \qquad BH_3OH^- + 6OH^- \leftrightarrow B(OH)_4^- + 3H_2O + 6e^-$$

NB: Sometimes, others authors prefer to use BO_2^- (metaborate) instead of $B(OH)_4^-$ for the final product of BH_3OR, but in practice the difference between these two compounds is only a matter of 2 H_2O molecules in the latter compound and does not significantly change the reaction mechanisms.

According to that mechanism, the BH_3OR electrooxidation generates $n_{e^-} = 3$ electrons at low potential (this pathway includes H_2 loss *via* borane hydrolysis – gold is not capable to valorize efficiently H_2) or $n_{e^-} = 6$ electrons at high potential (complete electrooxidation of BH_3OH^-). Experimentally however, Finkelstein *et al.* measured a number of $n_{e^-} = 1.8$ exchanged electrons (respectively $n_{e^-} = 3.6$) at low potential values (respectively high potential values). They measured those smaller numbers of exchanged electrons than theoretically expected *via* electrochemical mass-transport limited techniques (Levich theory), using the same diffusion coefficient for hydroxiborane (BH_3OH^-) and sodium borohydride ($D_{NaBH4} = 1.67 * 10^{-5}$ cm^2 s^{-1}). However, Finkelstein *et al.* clearly explained that the number of exchanged electron per borane moiety would be equal to $n_{e^-} = 3$ and 6 (*i.e.* equal to the theory) if they had used a smaller hydroxiborane diffusion coefficient value ($D_{BH3OH^-} \sim 8 * 10^{-6}$ cm^2 s^{-1}), as reported in the previous works of Sargent *et al.* and Nagle *et al.* [45,60]. Actually, there is still no consensus on the value of the (hydroxi)borane diffusion coefficient, as summarized in **TABLE V-1**. This bias will be addressed later in this chapter.

Table V-1 Diffusion coefficient values available in the literature for borane fuels.

Year	Authors	Ref	Assumed or reported	Borane diffusion coefficient (cm^2 s^{-1})
2001	Sargent *et al.*	[56]	Reported for DMAB	$8.55 * 10^{-6}$
2005	Nagle *et al.*	[60]	Reported for DMAB	$7.48 * 10^{-6}$
2006	Nagle *et al.*	[45]	Reported for AB	$8.45 * 10^{-6}$
2009	Zhang *et al.*	[46]	Assumed probably from [45]	$8.45 * 10^{-6}$
2009	Finkelstein *et al.*	[119]	Assumed that $D_{BH3} = D_{NaBH4}$	$1.67 * 10^{-5}$
2011	Plana *et al.*	[51]	Reported for DMAB	$1.7 * 10^{-5}$
2011	Plana *et al.*	[52]	Reported for DMAB	$2.3 * 10^{-5}$ $1.6 * 10^{-5}$
2013	Concha *et al.*	[47]	Assumed	$8 * 10^{-6}$

For Finkelstein *et al.*, those reported values are too low in comparison to the value reported for sodium borohydride and they prefer not to use them for the calculation of the number of exchanged electrons.

Then, Nagle *et al.* have generalized the electrochemical processes as:

$$(E_{Burke}) \qquad BH_3OH^- + nOH^- \leftrightarrow B(OH)_4^- + \left(3 - \frac{n}{2}\right)H_2 + (n-3)H_2O + ne^-$$

where n_{e^-} is a value between 3 and 6 depending of the electrode potential. Actually, Nagle *et al.* measured experimentally (on a gold microdisk) n_{e^-} = 3 exchanged electrons per BH_3OH^- species at low potential values and n_{e^-} = 6 at higher potential values, using their own measured diffusion coefficient values (see table **TABLE V-1**). To be more specific, Nagle *et al.* measured the diffusion coefficient of DMAB [60] or AB [45] using chronoamperometric measurements at the gold microdisk, following a method introduced by Bard *et al.* [171]; its interest is that it does not require prior knowledge of the number of exchanged electrons per reacting species, unlike for the well-known and widely used Levich method. The results obtained by Nagle *et al.* are close for both AB and DMAB (for AB: D_{BH3OH^-} = 8.45 * 10^{-6} cm² s^{-1}; for DMAB: D_{BH3OH^-} = 7.48 * 10^{-6} cm² s^{-1}), which is in agreement with the well accepted hypothesis of a chemical (and total) dissociation of AB and DMAB into hydroxiborane (BH_3OH^-) species plus the counter-borane (either ammonia or dimethylamine). Plana *et al.* [51] also agreed with the same mechanism and found n_{e^-} = 3 and 6 exchanged electrons at low/high potential values, but this time using larger diffusion coefficient values (see **TABLE V-1)**.

More recently and also for gold electrodes, Molina Concha *et al.* [47] have brought confirmation of the BH_3OR mechanism (using AB as a fuel). They monitored the potential-dependent H_2 production while the BH_3OR was happening on a gold electrode (sputtering) by DEMS experiment, as remarkable on **FIGURE V-6**. At low potential value (when the number of exchanged electrons is n_{e^-} = 3), an important quantity of hydrogen is released, which leads to a loss of faradic efficiency (hydrogen is irreversibly lost to electrochemistry, as gold cannot ionize it). At higher potential values (E ~ 0.8 V *vs.* RHE), almost n_{e^-} = 6 exchanged electrons are produced and no hydrogen gas is detected by the mass spectrometer; those results agree with the BH_3OR mechanism previously proposed by Fikelstein *et al.* In the case of Molina Concha *et al.* [47] though, the values of n_{e^-} were calculated from several techniques: Levich and Koutecki-Levich methods (assuming a diffusion coefficient for BH_3OH^- of 8 * 10^{-6} $cm^2 s^{-1}$), and directly via DEMS measurements (see **FIGURE V-6** below – a technique which does not require any knowledge of D_{BH3OH^-}); the agreement between the various values demonstrates that the diffusion coefficient of BH_3OH^- must be close to 8 * 10^{-6} $cm^2 s^{-1}$, in agreement with the values of Sargent *et al.*, Nagle *et al.* and Zhang *et al.* (see **TABLE V-1**). This statement also shows that the agreement between the theoretical mechanism of BH_3OR (n_{e^-} = 3 {6} electrons at low {high} potential values) and the experimental values of n_{e^-} of Finkelstein *et al.* is very good (using the proper value of D_{BH3OH^-}, *i.e. ca.* 8 * 10^{-6} $cm^2 s^{-1}$), despite their doubts [119].

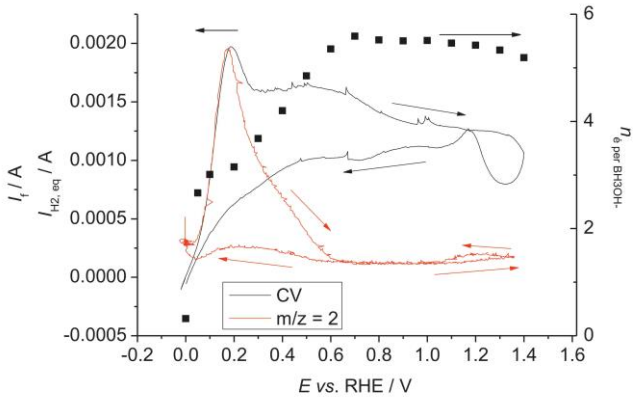

Figure V-1 Borane electrooxidation reaction (using Ammonia Borane). BH_3OR faradaic current (If) vs. E and resulting absolute value of the equivalent HER current ($|IH_{2,eq}|$) obtained by correction of the $I_{m/Z=2}$ signal using the DEMS calibration constant K and corresponding variation of $n_{e\text{-}perBH3OH\text{-}}$. Extracted form Molina Concha et al. [47]

If most of the literature on BH_3OR deals with gold materials, one study has however been carried out on platinum. In [119], Finkelstein *et al.* have carried out some experiments of BH_3OH^- electrooxidation at smooth Pt surfaces. The BH_3OR electrooxidation was not dependent on the rotation rate of the RDE, and they assumed that the BH_3OR mechanism on Pt was controlled by surface oxidative adsorption rather than by mass-transport at Pt surfaces; in consequence, they postulated that the BH_3OR mechanism was different on platinum versus on gold, without questioning the possible interaction between the counter-borane fragment (dimethylamine, DMA in their study) and the platinum surface. This is probably not so wise, as detailed below.

To be more specific, this chapter pretends to answer whether the nature of the borane fuel has an impact on the BH_3OR mechanism proceeding at a given electrocatalyst. If one puts a mindful eye on the data available in the literature, it is possible to find the first pieces of answer; indeed, despite the very little studies dealing with borane compounds and BH_3OR, some results have underlined an influence of the nature of the borane fuel (generally ammonia borane {AB} or dimethylamine borane {DMAB}) on the shape of BH_3OR cyclic voltammograms (CVs).

For instance, in [45] Nagle *et al.* have studied the electrooxidation of borane (using both AB and DMAB) and sodium borohydride ($NaBH_4$) at a gold microdisk in 1 M NaOH. They demonstrated the negative influence of an addition of DMA into a solution only containing ammonia borane initially. When DMA is added in the AB-containing solution (**FIGURE V-2**), the second plateau of AB electrooxidation progressively levels off upon increase in DMA concentration. They suggested that the magnitude of the second electrooxidation wave decreases due to the adsorption of DMA on the gold microdisk surface,

the DMA having an influence on the borane electrooxidation reaction on gold by non-faradaic surface interactions at the electrode surface. Interestingly, in the same paper, the authors presented another graph (**FIGURE V-3**) in which a non-negligible difference in the borane electrooxidation reaction onset potential is observed between an electrolyte containing AB or DMAB.

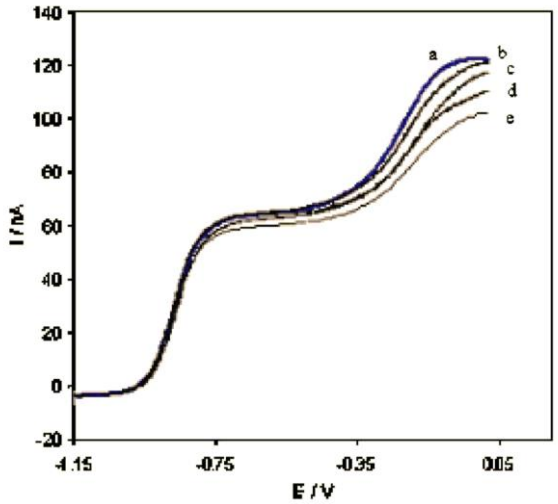

Figure V-2 Cyclic-voltammogram (-1.14 to -0.02 V vs. Ag/AgCl) in 10 mM AB with (a) 0, (b) 10, (c) 30, (d) 100 and (e) 200 mM of dimethelamine added at gold microdisk in 1 M NaOH at v = 100 mV s^{-1}. Extracted form Nagle et al. [45]

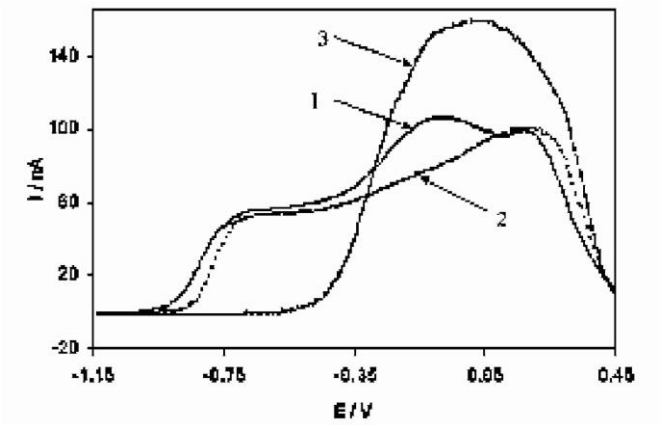

Figure V-3 Linear sweep voltammograms (-1.15 to 0.45 V vs. Ag/AgCl) in (1) 10 mM AB, (2) 10 mM DMAB and (3) 8 mM $NaBH_4$ at gold microdisk in 1 M NaOH at v = 100 mV s^{-1}. Extracted form Nagle et al. [45]

As remarkable on **FIGURE V-3**, the borane electrooxidation begins at lower potential values when AB is used. This major result has not been commented by the authors and has nevertheless constituted the starting point of the investigations presented in this chapter. However, the results reported by Nagle *et al.* might be subjected to caution; indeed, even if the microdisk electrode is in principle suitable to work in steady-state conditions, it has to be mentioned that gold can hydrolyze the borane fuel and so release

hydrogen, as clearly demonstrated by the DEMS measurement of Molina Concha *et al.* [47] ; knowing the very small surface area of the gold microdisk electrode, and the fact it is static, one can wonder about the possible accumulation of hydrogen near/at the electrode, which could yield nucleation of H_2 bubbles that could block a fraction of the surface and lead to possible modifications in the shape of the voltammograms. This bias was clearly put forth by Chatenet *at al.* while performing the electrooxidation of $NaBH_4$ at Au microdisk [61]. From this latter study, Chatenet *et al.* (and more recently, Oliveira *et al.* [138,139]) concluded that the best manner to study the electrooxidation of $NaBH_4$ (and this should be valid for other BBMs) is to use hydrodynamic conditions (using RDE measurement system), to prevent any accumulation of gaseous or dissolved products of the electrooxidation (and chemical decomposition or hydrolysis) reactions taking place at the electrode with the BBM.

Whatever this bias, the above results demonstrated that the DMA fragment can be detrimental to the BH_3OR, even when a gold electrode is used (it is more obvious when Pt is used). On the contrary, ammonia borane has been considered as a "non-poisonous" borane fuel for gold electrodes by Nagle *et al.* [45] or Molina Concha *et al.* [47]. In particular, the latter found no evidence (both by DEMS and *in situ* Fourier Transform InfraRed spectroscopy, FTIR) of dehydrogenated ammonia adsorbates in 0.1 M KOH solution between E = 0 and 1.5 V *vs.* RHE [47,172]. Although this has been demonstrated for gold, it must be stated that palladium and all the more platinum surfaces do interact differently than gold with the ammonia fragment in alkaline medium; these metals could therefore be prone to interaction with ammonia and formation of deleterious adsorbates for the BH_3OR [172 173].

To comply with this issue, the present chapter investigates the nature of the borane compound used as a fuel for utilization in DLAFC systems. Because, palladium catalysts have demonstrated great activity for the BH_3OR (using ammonia borane as a fuel) and a reasonable stability in these conditions, palladium has been selected as the primary catalyst to study the impact of the nature of the borane fuel on the observed performances. Experiments have been carried out using various borane fuels: ammonia borane, hydrazine borane, dimethylamine borane and also hydrazine bis-borane. For the sake of comparison, a commercial platinum-based carbon-supported electrocatalyst has also been studied, to check whether the influence of the nature of the borane is "electrocatalyst-sensitive" or not. In the specific case of hydrazine borane and hydrazine bis-borane electrooxidation, it is however good to remember that the hydrazine electrooxidation reaction (named after, HHOR) must be taken into account as well, because, unlike for other boranes (AB or DMAB), the hydrazine "counter-borane" fragment is also valorizable; specific studies have indeed focused on the hydrazine electrooxidation in alkaline medium on palladium-based electrocatalysts [169,174–177].

Another originality of this chapter is to provide RDE results for carbon-supported electrocatalysts; in the literature, the utilization of metal-based carbon-supported electrocatalysts for the BH_3OR is only done for experimentations on complete direct borane fuel cell. So, using a real commercial electrocatalysts (Pd/C and Pt/C) will make the present results relevant for the targeted direct (hydrazine) borane fuel cell technology. Actually, if the hydrazine and the borane electrooxidation processes are very complex, working with thin-layer deposit adds another difficulty; for instance, it is well known that borane hydrolysis is catalyzed on palladium surface (and on platinum surfaces as well); this hydrogen produced can remain trapped in the thin-layer deposit, and so can the products of HHOR and BH_3OR, resulting in complex mass-transport and residence time effects [32,36,42]. Of course, real systems will face such situations, and this chapter, by combined experimentations of DEMS and electrochemistry, will track products of the catalytic decomposition and heterogeneous hydrolysis of the fuel, which shall provide insights into relevant ways to design Direct Hydrazine Borane Fuel Cell anodes and systems.

Finally, it is worth recalling that, all the knowledge obtained during that PhD concerning the platinum or palladium nanoparticle stabilities and presented in the previous chapter enabled to set up relevant procedures for the kinetic experiments. To be more specific, in order not to be bothered by the instability of these electrocatalysts, it was chosen to perform the minimum CV cycles possible, in order to limit as much as possible the potential degradation of the electrocatalysts.

ii. Specific experimental section

The palladium electrocatalyst used is Pd/C#2, as presented in the chapter **"DEGRADATION OF NOBLE ELECTROCATALYSTS IN ALKALINE MEDIUM"**. Unlike the platinum-based carbon-supported electrocatalyst used in this chapter **"DEGRADATION OF NOBLE ELECTROCATALYSTS IN ALKALINE MEDIUM"**, the Pt/C used herein has a weight percentage in platinum of *ca*. 10% and is supported on Vulcan XC-72 (same metal weight percentage and same support as the Pd/C#2 electrocatalyst); it will be named Pt/C#2, to differentiate it from the previous Pt/C sample. The Pd/C#2 and Pt/C#2 samples are very similar in terms of particle size distribution (PSD), dispersion and nature of the carbon support (**FIGURE V-4**). The Pt/C#2 electrocatalyst PSD has been presented by Olu *et al.* in [32] (the PSD of the Pd/C#2 electrocatalyst, made by the same experimenter is also given).

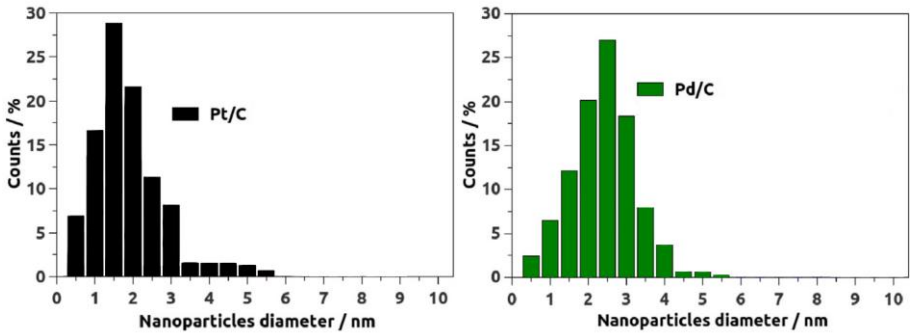

Figure V-4 Pt/C#2 and Pd/C#2 electrocatalyst particle size distribution histograms. Extracted from Olu et al. in [32]

The electrocatalyst inks were prepared by mixing 10 mg of catalyst powder, 6.74 mL of MQ-grade water (18.2 MΩ cm, < 3 ppb total organic carbon, Elix + Milli-Q Gradient, Millipore), 48.3 µL of 5 wt% Nafion® solution (Electrochem. Inc.), and 33.9 µL of isopropyl alcohol.

After 30 min of ultrasonic stirring before each experiment, a given volume (20 µL) of the chosen electrocatalyst ink (Pt/C#2 or Pd/C#2) was deposited on a 5 mm-diameter glassy-carbon electrode. Therefore, for every electrocatalysts, the loading in metal on the working electrode surface is about 15 $\mu g_{Pt\ or\ Pd}\ cm^{-2}$. For the DEMS experiments, 50 µL of the electrocatalyst ink was deposited on a carbon cloth, as explained in chapter **"GENERAL EXPERIMENTAL SECTION"**.

All the experiments were carried out in 0.1 M NaOH solutions at T = 25°C, using a carbon plate as counter-electrode and an Hg/HgO reference electrode (*cf.* chapter **"GENERAL EXPERIMENTAL SECTION"**).

The electrochemical experiments were performed using a VSP Biologic potentiostat and the tests were mainly cyclic voltammograms (CVs) performed between E = -0.3 and 1.3 V *vs.* RHE. Except in DEMS,

the working electrode was a rotating disk electrode, which enables controlling the diffusion-convection near the electrode surface. Experiments were generally performed at ω = 1600 rpm (except for the DEMS experiments which are static, as explained in chapter "General experimental section") and v = 10 mV s^{-1} as potential sweep rate. This potential sweep rate was chosen as a compromise between a slow scan rate to enable quasi-stationary CVs (at least in RDE configuration), and a fast scan rate to yield "short experiments", in order to avoid severe formation of bubbles at the electrode surface and issues with its contamination by reaction products.

iii. Borane electrooxidation on carbon-supported platinum and palladium nanoparticles

FIGURE V-5 presents the impact of the nature of the borane fuel (hydrazine bis-borane (HBB), hydrazine borane (HB), ammonia borane (AB) or dimethylamine borane (DMAB)) on the borane electrooxidation reaction on platinum-based carbon-supported electrocatalyst. On this figure the 5th cycle of CV is plotted in each case.

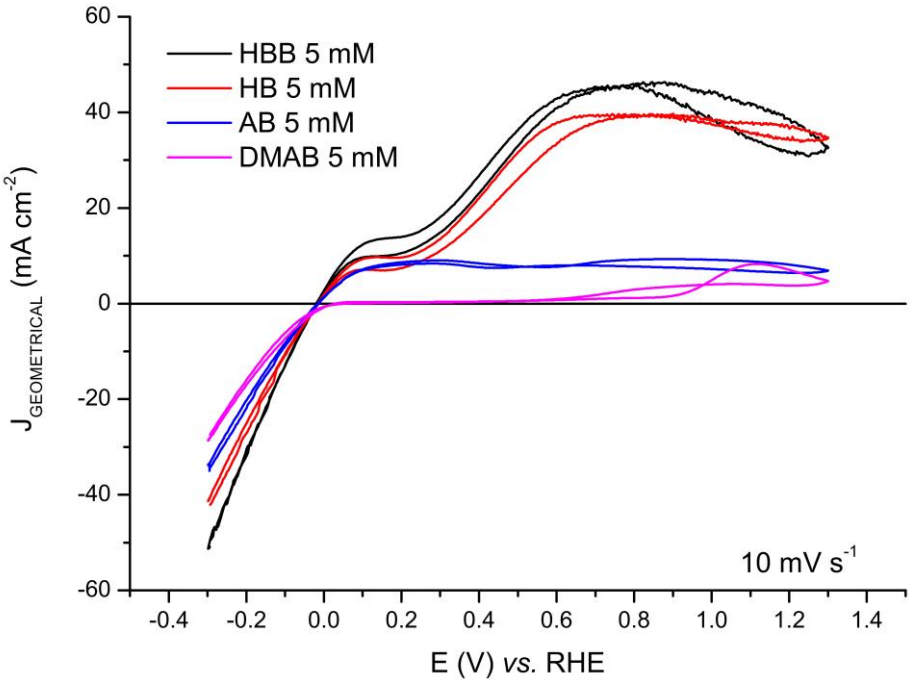

Figure V-5 BH3OR on Pt/C#2. CVs obtained in 0.1 M NaOH + 5 mM of HBB, HB, AB or DMAB. All performed at T = 25°C, at ω = 1600 rpm and ν = 10 mV s^{-1}

The cyclic-voltammograms (CVs) are dramatically different depending on the nature of the borane fuel chosen; obviously, a higher maximum current density value is expected with HBB and HB, since these fuels contain an electroactive "counter-borane" fragment (hydrazine) and platinum is an active electrocatalyst material for the hydrazine electrooxidation reaction (HHOR) [169,174,176]. Nonetheless, the CVs related to AB and DMAB electrooxidation are also very different, while only the BH_3OR is proceeding in those cases, as reported by Nagle *et al.* [45]; this difference is the first evidence of the influence of the origin of the borane fuel on the BH_3OR mechanism for platinum electrocatalyst materials. This sensitivity could be explained by the detrimental interaction between the "counter-borane" fragment and the platinum surface. In particular, when DMAB is used, the presence of the DMA "counter-borane" fragment leads to a very small value of anodic current density for the 5th cycle.

Actually, it is interesting to see how the BH_3OR with DMAB changes upon repetitive potential cycling (**FIGURE V-6**): the CV shape is severely modified between the first cycle and the 5th one. One can observe a gradual but nonetheless pronounced decrease in oxidation current density upon cycling in the "low-potential" region ($0 < E < 0.8$ V *vs.* RHE), and also a gradual levelling-off in the HER region; both trends can be explained by a progressive pollution of the platinum surface by the DMA "counter-borane" fragment. This hypothesis has been mentioned previously by Nagle *et al.* [45], who worked with DMAB, and it is curious to see that more recent works kept this observation quiet in their discussion. For example, in the study (on platinum material) reported by Finkelstein *et al.* [119], one can legitimately wonder if the non-dependence of the borane electrooxidation plateau (using DMAB) on the rotation rate of the electrode cannot be explained by a total pollution of the surface.

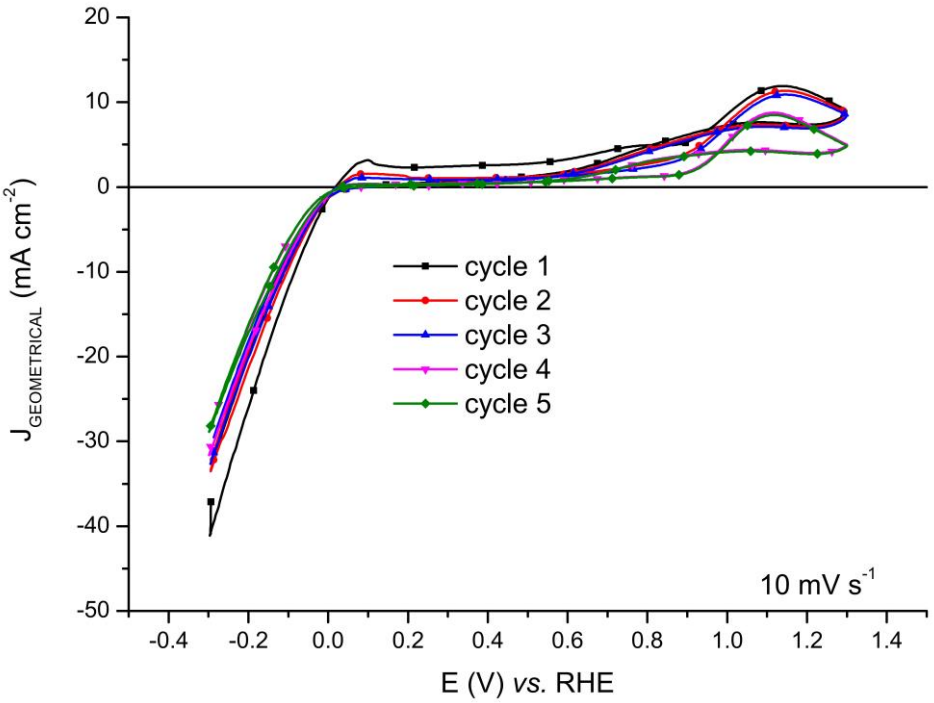

Figure V-6 The 5 first CV cycles of BH_3OR on Pt/C#2 obtained in 0.1 M NaOH + 5 mM DMAB. Performed at T = 25°C, at ω = 1600 rpm and v = 10 mV s^{-1}

Another piece of information given by **FIGURE V-5** is that, independently from the borane fuel chosen, the onset of electrooxidation is around $E = 0$ *vs.* RHE (or sometimes at higher potential values when the pollution is severe). This is explained by a high ability of platinum to hydrolyze boranes into hydrogen; this chemical reaction is so favored that the platinum is mostly performing the hydrogen electrooxidation reaction (HOR) instead of any BH_3OR, shifting the electrooxidation onset for the borane complex towards the HOR onset. This behavior was reported previously by Olu *et al.* [36] and Jusys *et al.* [168] in the case of $NaBH_4$. On platinum materials, seeking the best borane fuel seems useless in term of gain in onset potential, since boranes are inevitably electrooxidized at the hydrogen potential ($E = 0$ *vs.* RHE).

FIGURE V-7 presents results obtained in the same condition for the Pd/C#2 electrocatalyst. Once again, one can see the dramatic influence of the choice of the borane fuel on the CV shape, both in the high and low potential regions.

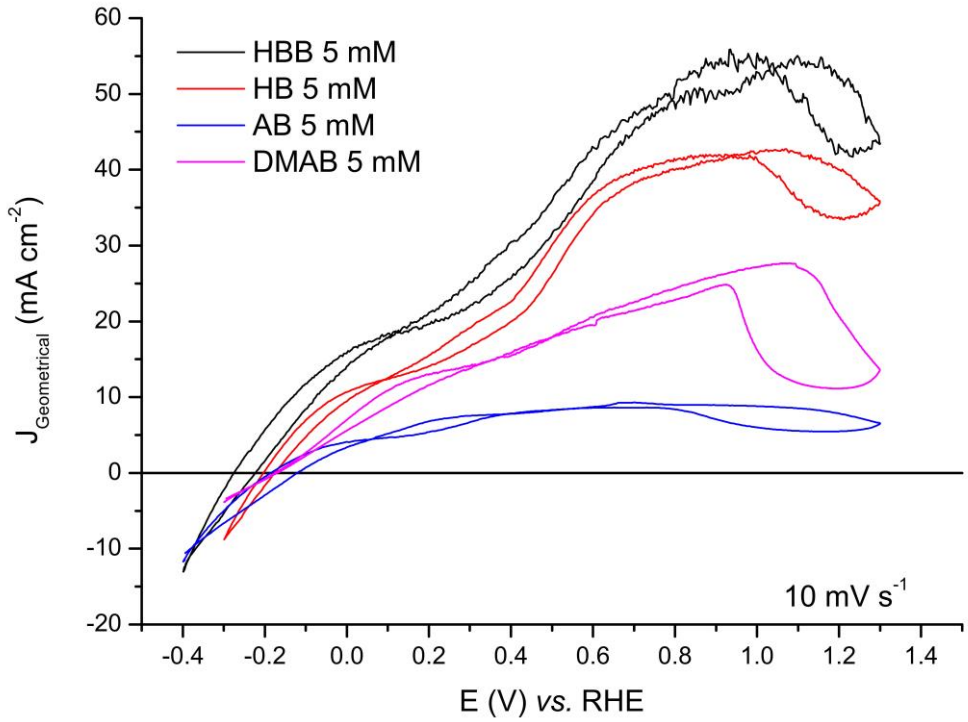

Figure V-7 BH_3OR on Pd/C#2. CVs obtained in 0.1 M NaOH + 5 mM of HBB, HB, AB or DMAB. All performed at T = 25°C, at ω = 1600 rpm and v = 10 mV s^{-1}

As observed for the Pt/C#2 electrocatalyst, the maximum anodic current density (at large potential values) is higher for HBB and HB due to the activity of palladium for the HHOR. In addition, unlike for Pt/C#2, the DMAB electrooxidation seems more facile on palladium than AB electrooxidation. The opposite trend measured on Pt/C#2 may be accounted for by a lower interaction between the DMA "counter-borane" fragment with palladium surfaces than with platinum surfaces.

The most striking feature of these CVs is however noted in the onset potential region. A significant difference in onset potential of reaction is witnessed between the different borane fuels. The lowest onset values are obtained with HBB and HB, with a value of E = –275 and -200 mV *vs.* RHE respectively, which is close to the thermodynamic value expected for the BH_3OR (*ca.* E = -0.4 V *vs.* RHE). This ability of palladium to initiate the BH_3OR at negative potential value (considering the RHE scale) indicates that the BH_3OR pathway is mostly direct, since hydrogen cannot be electrooxidized below E = 0 V *vs.* RHE. Those results underline, once again, the spectacular electrocatalytic activity of palladium materials for the BH_3OR and make of it a material of choice for DLAFC systems using boron based materials as fuel.

To sum up, from the results obtained, the borane fuels can be ranked for the BH_3OR on palladium surface as follows:

HBB > HB > AB > DMAB

The higher anodic current densities obtained with HBB could make more interesting the development of direct hydrazine bis-borane fuel cells (DHHBFCs) over DHBFCs; nonetheless, HBB was found to be hazardous: it may explode violently if heated rapidly much beyond T = 100°C and may also be detonated by impact. Though not clearly specified, one may guess that such phenomena would also occur under inert atmosphere, and further, HBB would be extremely flammable in oxygen-containing environments. For those reasons, HBB is less suitable than HB for real applications, especially when the safety and ease of fuel storage are amongst the main reasons for the development of DHBFC. Surprisingly, the above results are compatible with a direct BH_3OR favored on palladium, when it is reported by Hannauer *et al.* [157] that palladium is even a better electrocatalyst for borane heterogeneous hydrolysis into H_2. Indeed, the present observations on the Pd/C#2 electrocatalyst show that the anodic reaction is not initiating E = 0 V *vs.* RHE, demonstrating that the heterogeneous hydrolysis on this material is far from being complete and predominant.

FIGURE V-8 presents the CVs performed on the Pd/C#2 electrocatalyst in presence of each "counter-borane" fragment, in 0.1 M NaOH solution; 5 mM of hydrazine hydrate (HH), DMA or NH_4OH are used to probe their possible interaction with the palladium surface (at T = 25°C and ω = 1600 rpm).

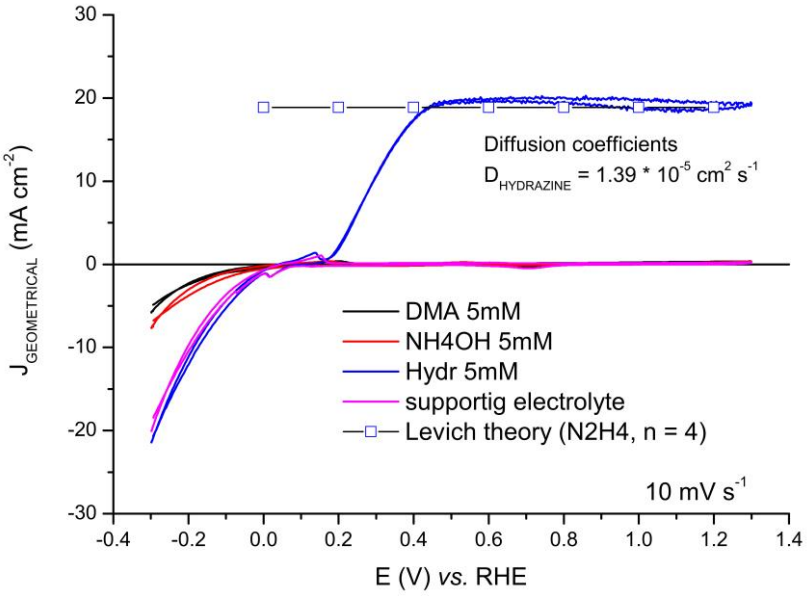

Figure V-8 Effect of the nature of the "counter-borane" fragment on Pd/C#2. CVs obtained in 0.1 M NaOH supporting electrolyte with (or without) 5 mM of DMA free, NH_4OH or hydrazine hydrate. All performed at T = 25°C, at ω = 1600 rpm and v = 10 mV s^{-1}

By comparing the shape of hydrogen evolution reaction (HER) between the CVs in supporting electrolyte and with DMA or NH_4OH, it can be remarked the blocking effect of the ammonium and dimethylamine fragments: the palladium surface is largely inhibited for the hydrogen evolution reaction (HER) in presence of these two compounds. The case of hydrazine hydrate underlines the interest of using HB over DMAB and AB; indeed, the HHOR begins at the Pd/C#2 at rather low potential (E = 200 mV *vs.* RHE) and can lead to the production of n_{e^-} = 4 additional electrons (at potential values exceeding E = 0.4 V *vs.* RHE, as calculated using the results plotted on **FIGURE V-8** and $D_{N2H4} = 1.39 * 10^{-5}$ cm² s^{-1} for the diffusion coefficient of hydrazine in 0.1 M NaOH solutions [178]). This indicates that the hydrazine is totally valorized beyond E = 400 mV *vs.* RHE, making of it an appropriate "counter-borane" fragment compared to DMA and NH_3 (unlike these two latter fragments, hydrazine is also a fuel that can be valorized in a DLAFC). Besides, the onset potential value monitored is in perfect agreement with recent results obtained by Finkelstein *et al.* [169] for HHOR experiments on palladium bulk electrode in similar conditions (0.1 M NaOH + 5 mM N_2H_4): the HHOR onset potential was measured at E = 177 mV *vs.* RHE.

From the results obtained with hydrazine hydrate, it can be said that, using HB as borane fuel:

1. Any oxidation current below E = 200 mV *vs.* RHE is only related to the BH_3OR;
2. BH_3OR and HHOR proceed simultaneous above E = 200 mV *vs.* RHE;
3. Hydrazine is totally valorized above E = 400 mV *vs.* RHE.

Obviously, these statements can be deeply dependent on the experimental conditions and should probably be updated (or even not considered) for other concentration values in OH^- and HB, other hydrodynamic regime (here ω = 1600 rpm) or other configurations/geometries of electrodes, as studied below.

Further experiments were performed to probe the HBOR on Pd/C#2; several parameters such as the temperature, the HB concentration or the loading in palladium were varied to observe their influence on the HBOR CVs.

FIGURE V-9 presents the effect of the temperature on the HBOR in 0.1 M NaOH + 5 mM HB solution with a temperature controlled at T = 25, 40, 60 or 80°C (at ω = 1600 rpm).

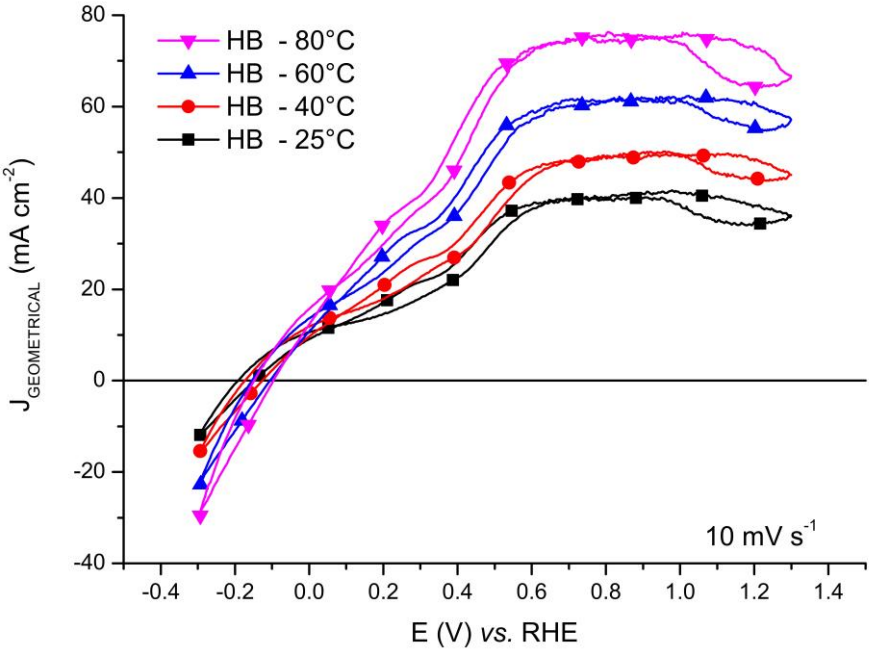

Figure V-9 Effect of temperature on Pd/C#2. CVs obtained in 0.1 M NaOH + 5 mM HB at T = {25, 40, 60 or 80°C}. All performed at ω = 1600 rpm and ν = 10 mV s^{-1}.

Clearly, the temperature has a dual effect on the apparent efficiency of the HBOR at Pd/C#2. On the one hand, larger temperatures enable reaching larger current densities at high potential values. This can be ascribed to the increase of the mass-transport kinetics of the fuel; for the sake of comparison, in [61] Chatenet *et al.* have measured and reported for a solution of 0.1 M NaOH + 1 mM $NaBH_4$, a value of ν = 0.0146 cm² s^{-1} for the kinematic viscosity and a value of D_{NaBH4} = 2.78 cm² s^{-1} for the sodium borohydride diffusion coefficient at T = 10°C, against ν = 0.0075 cm² s^{-1} and D_{NaBH4} = 4.49 cm² s^{-1} respectively at T = 40°C. On the other hand, one can observe the detrimental effect of the temperature on the BH_3OR onset potential; the HBOR onset potential shifts by 100 mV toward more positive potential values when T increases from 25 to 80°C. This detrimental effect of the temperature has already been observed by Olu *et al.* [32] for the BH_3OR using AB as borane fuel; this prejudicial effect is explained by the detrimental enhancement of borane hydrolysis at higher temperature, leading to a lower concentration in borane (and so a higher concentration in hydrogen) near to the electrode, that renders more predominant the HOR over the BH_3OR and triggers the apparent onset potential closer to E = 0 V *vs.* RHE.

Another way to confirm the latter statement is to investigate the effect of an increase of the HB concentration; **FIGURE V-10** presents the CVs obtained in 0.1 M NaOH with a concentration in HB corresponding to 1, 5, 10 or 50 mM (at T = 25°C and ω = 1600 rpm).

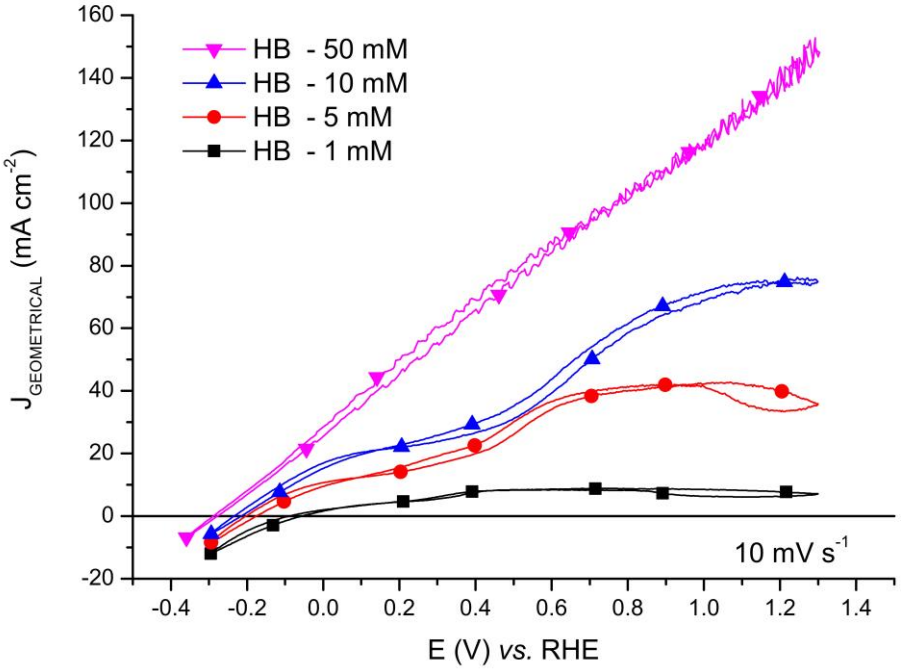

Figure V-10 Effect of HB concentration on Pd/C#2.
CVs obtained in 0.1 M NaOH + HB concentration = {1, 5, 10 or 50 mM}.
All performed at T = 25°C, at ω = 1600 rpm and ν = 10 mV s^{-1}

On **FIGURE V-10**, one can notice that the increase of HB concentration induces an expected decrease of the BH_3OR onset potential, going from *E* = -90 mV *vs.* RHE for 1 mM to *E* = -290 mV *vs.* RHE for 50 mM. Moreover, from 1 to 10 mM in HB, the CVs have mainly the same shape exhibiting 2 waves of electrooxidation, but at 50 mM in HB the electrooxidation leads to very high values of current densities (> 80 mA cm^{-2}) for which the diffusion-convection theory of Levich seems no longer applicable. In that latter case, the charge-transfer kinetics likely overwhelms the results, and the mass-transport limitation is no-longer predominant, even at large overpotential values (the overall process may be limited by the kinetics of the charge transfer and not by mass-transport). Besides, it is worth noting that the Ohmic drop was corrected numerically by the potentiostat at 85%, so with the very high current densities measured, the non-compensated part of the Ohmic drop probably becomes non-negligible at all. Whatever this bias (and knowing that in the present case, the surface loading of electrocatalysts is *ca.* 10 times smaller than for state-of-the-art fuel cell electrodes), those results are promising for the DHBFC systems, for which the HB concentration shall probably be higher than 50 mM; according to these results, a higher concentration will ensure a very low BH_3OR onset potential value.

Then, the impact of the loading in Pd/C#2 electrocatalyst was investigated for the BH_3OR using HB as borane fuel. Knowing that the working electrode was the same 5 mm-diameter glassy carbon rod, a change in electrocatalyst loading means a change in the number of palladium sites available for the

BH_3OR (and HHOR) and a change in the electrocatalyst layer thickness. **FIGURE V-11** presents the CVs obtained in 0.1 M NaOH + 5 mM HB solution (at T = 25°C and ω = 1600 rpm) with a loading in palladium equal to 3.74, 14.96 or 29.91 μg_{Pd} cm^{-2} (corresponding to a deposition of 5, 20 or 40 µL of the Pd/C electrocatalyst ink on the glassy carbon supporting electrode, respectively).

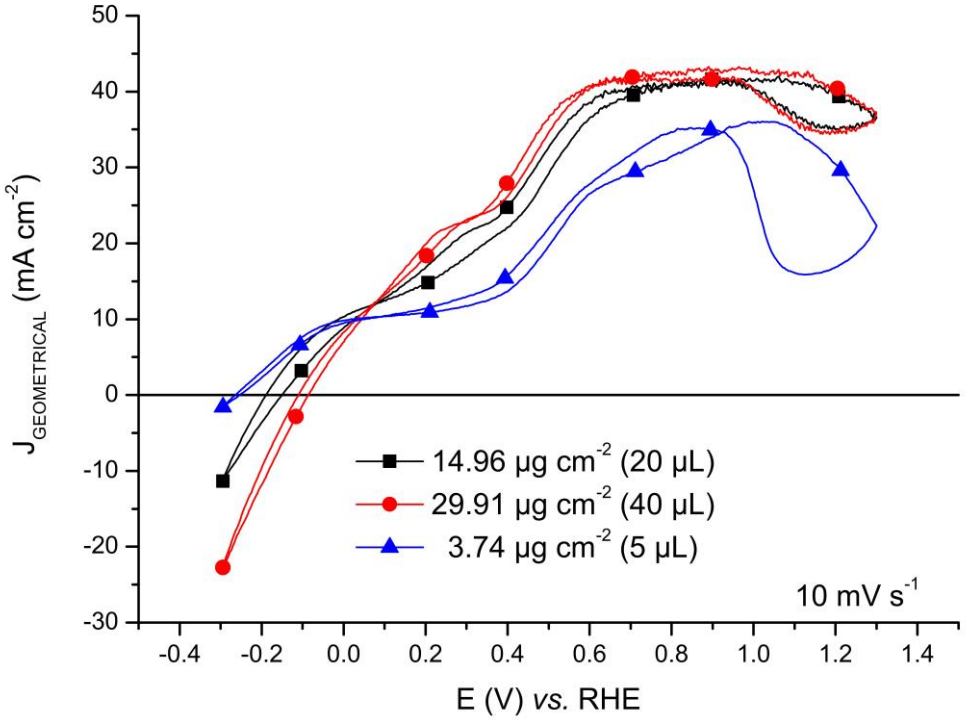

Figure V-11 Effect of the electrocatalyst loading of Pd/C#2. CVs obtained in 0.1 M NaOH + 5 mM HB for a loading in palladium of {3.74, 14.96, or 29.91 $\mu g_{Pd}\, cm^{-2}$}. All performed at T = 25°C, at ω = 1600 rpm and v = 10 mV s^{-1}.

Increasing the loading of Pd/C#2 leads to a significant increase in BH_3OR onset potential, which is detrimental for the DHBFC systems (from E = -110 mV *vs.* RHE for 29.91 μg_{Pd} cm^{-2} to E = -270 mV *vs.* RHE for 3.74 μg_{Pd} cm^{-2}). Those results indicate that using HB as borane fuel does not induce significant (and detrimental) active site pollution by an intermediate or a by-product of the borane electrooxidation, which would have been much more visible for the lowest palladium loading. An explanation of this loading effect on CVs is that a higher loading lead to more hydrogen production by borane hydrolysis (more palladium sites) and a longer hydrogen residence time inside the electrocatalyst layer. So, the competition between HOR and BH_3OR is favored for thicker deposits and higher palladium loadings, and the HOR becomes predominant for large loadings (the same effect was witnessed in **FIGURE V-10** for the smallest concentration of fuel).

To sum up, the effects of the electrolyte temperature, fuel concentration and palladium loading are converging to the same conclusion: the BH_3OR can be in competition with HOR. An increase in temperature, in OH^-/borane ratio or in electrocatalyst loading leads to an enhancement in hydrogen production that favors the HOR over the BH_3OR and induces an increase on BH_3OR onset potential value, which is detrimental for DHBFC systems when the maximum operating voltage is targeted (corresponding to the lowest BH_3OR onset potential value). In [63,179] Freitas *et al.* studied "residence time" effects of the fuel, and described such influence of hydrogen or reaction products trapped within the electrocatalyst layer; performing experiments in 0.1 M NaOH + 1 mM $NaBH_4$ with platinum-based carbon-supported nanoparticles, they observed that for the same loading in platinum, thicker electrocatalyst layer (obtained with the addition of non-active carbon material) leads to higher electrocatalytic performances for the complex sodium borohydride electrooxidation reaction (BOR) for which the completion of its multi-step reaction requires (i) sufficient catalyst loading (amount of catalytic sites) as well as (ii) sufficient residence time for the intermediates (with thicker electrocatalytic layer). However, this "trapping" has a positive effect for the BOR on platinum, because it simply enables to valorize better the hydrogen formed by the very fast catalytic decomposition of the fuel on Pt. This effect is however detrimental for the BH_3OR on palladium, because it favors such catalytic decomposition of the fuel at the expense of its direct electrooxidation (an electrochemical reaction which was not favored at Pt surfaces).

All those results underline the complexity to optimize the DHBFC performances. The same applies to DLAFC using others boron based materials (such as ammonia borane or sodium borohydride), for which the open circuit voltage hardly exceeded 1 V in practice [32,65] despite the promises of three-electrode cell experiments.

Finally, investigations focused on the mechanism of BH_3OR in 0.1 M NaOH + 5 mM HB solutions. **FIGURE V-12** presents the CVs obtained for a rotation rate corresponding to ω = 2500, 1600, 900, 400 or 0 rpm.

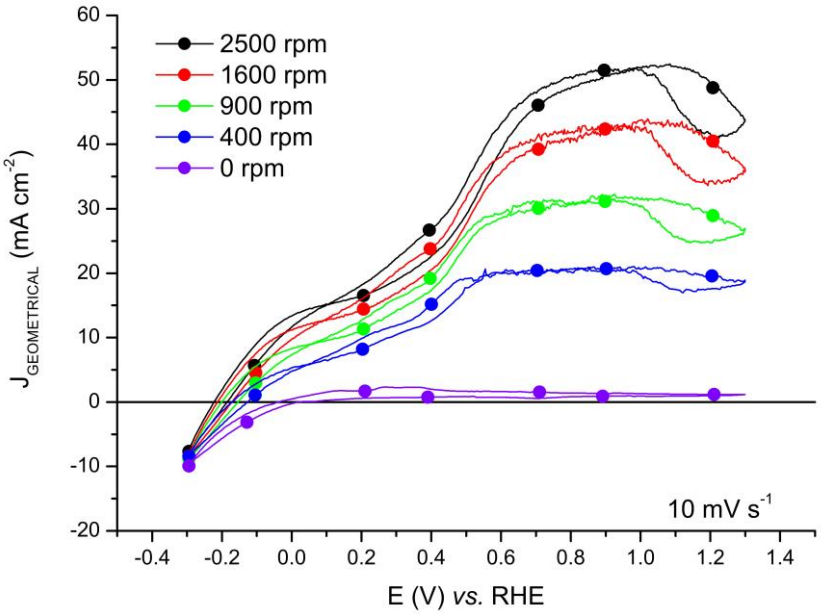

Figure V-12 Effect of rotation speed on Pd/C.CVs obtained in 0.1 M NaOH + 5 mM at ω = {2500, 1600, 900, 400, or 0 rpm}.All performed at T = 25°C, and v = 10 mV s^{-1}

FIGURE V-12 demonstrates a clear dependence of the CV on the rotation speed, as expected in conditions of diffusion-convection limitation (the concentration in HB, 5 mM, is very low to enable depletion at the electrode surface at sufficient overvoltage). One can distinguish two main waves on the CV obtained in hydrodynamic regime (*i.e.*, not for ω = 0 rpm); the first one begins around *E* = -300 mV *vs.* RHE and stops around *E* = 200 mV *vs.* RHE. The previous sections of the chapter showed that the electrooxidation of the hydrazine fragment begins at *E* = 200 mV *vs.* RHE, so it was decided to perform some steady-state chronoamperometries (CAs) at *E* = 100 mV *vs.* RHE with a variation of the rotation speed, *i.e.* in a potential region where the hydrazine fragment cannot be electrooxidized. The results are presented on **FIGURE V-13:** the linear dependence of the measured steady-state current densities with the square root of the rotation speed agrees with the Levich theory. So, using the Levich theory and gathering the values available in the literature for the kinematic viscosity (ν = 0.0114 cm² s^{-1} [61]) and the borane diffusion coefficient (D_{Borane} = 8 * 10^{-6} cm² s^{-1} [47]), the number of exchanged electrons per borane moiety can be calculated; it equals *ca.* n_{e^-} = 3.7 exchanged electrons at this potential. This value is higher than the value of n_{e^-} = 3 exchanged electrons previously reported in [45,47,60,119] ; nonetheless, those latter studies were carried out with gold rod electrodes, which is a bad electrocatalyst for the HOR. Indeed, as previously mentioned, in the present conditions, the palladium is a good electrocatalyst for the HOR, in particular

at E = 100 mV *vs.* RHE; the electrocatalytic layer of Pd/C#2 can therefore trap the hydrogen produced from heterogeneous hydrolysis (or formed during the BH_3OR) and valorize this H_2 above the hydrogen potential. So, in addition to the BH_3OR, the HOR can simultaneously happen at E = 100 mV *vs.* RHE, leading to a total exchanged electron number higher than n_{e^-} = 3 (*i.e.* n_{e^-} = 3 for the direct borane electrooxidation and additional ones for the valorization of some H_2). It is also possible that the direct borane electrooxidation proceeds in a more complete manner on Pd than on Au surfaces.

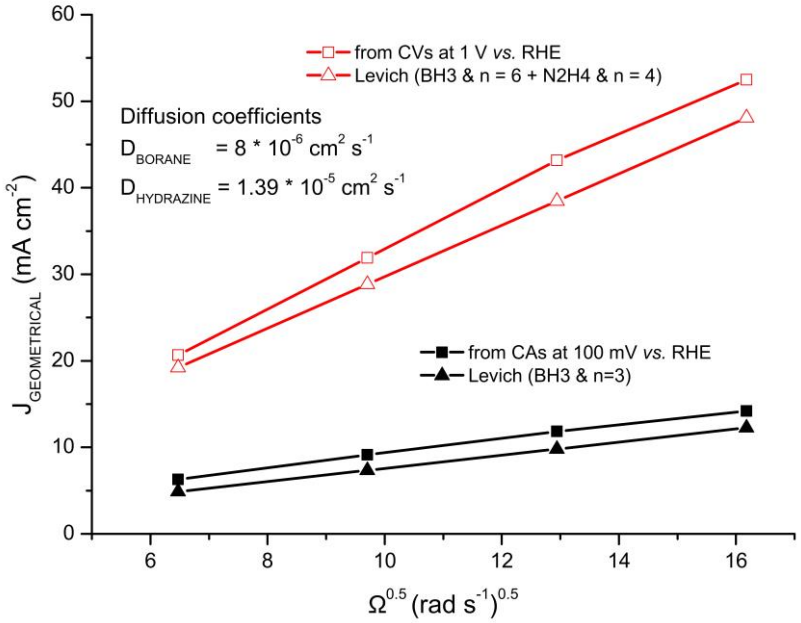

Figure V-13 Comparizon between experimental results (CVs & CAs) and the Levich theroy. Experiments were performed in 0.1 M NaOH + 5 mM HB at ω = {2500, 1600, 900, 400, or 0 rpm} All performed at T = 25°C, and v = 10 mV s^{-1}

FIGURE V-13 also presents the current density values obtained on the CVs at E = 1 V *vs.* RHE (in the second wave plateau) as a function of the square root of the rotation rate. Here again, the results are in agreement with the Levich theory (the profiles are linear), if one assumes that BH_3OR and HHOR are both mass-transport limited and concomitant (which means that there are enough palladium sites available for the two reactions). Assuming n_{e^-} = 6 and 4 exchanged electrons at maximum for the BH_3OR and HHOR respectively, one can see here again that the total exchanged electron numbers is slightly higher than the n_{e^-} = 10 expected. The explanation is probably the same than for the CAs performed at E = 100 mV *vs.* RHE.

However, it seems important to mention that the hydrogen production by hydrolysis (or electrochemical reaction in the preceding negative scan) is only related to the borane fragment, since the results of **FIGURE V-7** demonstrated complete HHOR on the Pd/C#2 electrocatalyst and an onset potential larger than the hydrogen potential. This has been confirmed by differential electrochemical mass spectrometry

(DEMS) experiments. **FIGURE V-14** presents the calibration tests for Pd/C in 0.1 M NaOH (at room temperature and in static condition).

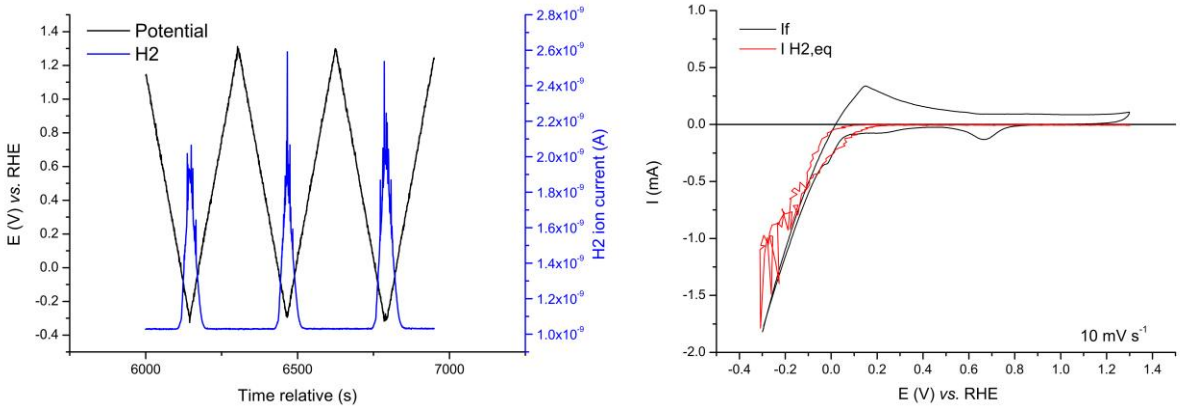

Figure V-14 (a) DEMS for the calibration with Pd/C#2 electrocatalyst in 0.1 M NaOH at room temperature and in static condition. (b) HER calibration; the intensity of the m/z = 2 signal was adjusted so as to fit the faradaic HER current using the DEMS calibration constant (in that case, If = $I_{H2,eq} = -1.22 \times 10^{-9} * I_{m/z=2}$)

FIGURE V-14 shows the perfect match between the potential of the Pd/C#2 electrocatalyst and the production of hydrogen *via* HER. At potential value lower than E = 0 V *vs.* RHE, hydrogen is detected by the mass spectrometer (MS) and the value of hydrogen ion current ($I_{m/z\,=\,2}$) reaches 1 * 10^{-9} $A_{ion\ current}$ (after subtraction of the baseline around 1 * 10^{-9} $A_{ion\ current}$) when the Pd/C is around E = -300 mV *vs.* RHE. So, dividing the potential-dependent HER faradic current by the intensity of the m/z = 2 signal yields the DEMS calibration constant:

$$K = \frac{I_f}{I_{m/z=2}}$$

with I_f in mA and $I_{m/z\,=\,2}$ in $A_{ion\ current}$.

The DEMS calibration constant is worth K = -1.22 × 10^{-9} in the case of **FIGURE V-14-A**. Using this value of K, one can "convert" the MS current for m/z = 2 into an equivalent HER current (noted as $I_{H2,eq}$ hereafter) as graphically plotted in **FIGURE V-14-B.**

Now, if HB (5 mM) is introduced in the supporting electrolyte, some production of hydrogen by the hydrolysis of HB at the palladium surface is observed at open circuit (**FIGURE V-15**).

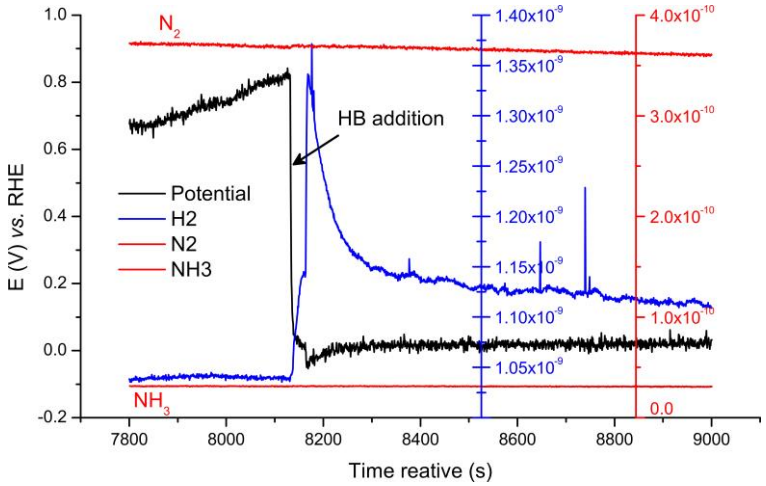

Figure V-15 DEMS detection of HB hydrolysis on Pd/C electrocatalyst in 0.1 M NaOH at room temperature and in static condition

More specifically, **FIGURE V-15** demonstrates that as soon as HB is added to the solution, the potential of the Pd/C electrocatalyst drops from E = 0.8 to 0 V *vs.* RHE, and concomitantly, hydrogen is produced. Because no ion current signal is detected for N_2 gas or ammonia (NH_3), it can be assumed that the hydrazine fragment is almost not suffering any decomposition on palladium material at this potential value (in agreement with the results of **FIGURE V-3** that showed HB was only reacting above E = 0.2 V *vs.* RHE). After a large peak of hydrogen detection, the signal stabilizes around $I_{m/z\,=\,2}$ = 7.0769 * 10^{-11} $A_{ion\ current}$ after the subtraction of the baseline, which corresponds to an equivalent HER faradic current of $I_{H2,eq}$ = -0.0865 mA.

Polarization CVs, performed between E = -300 and 1300 mV *vs.* RHE, were then attempted to see how the BH_3OR and the HHOR take place on the Pd/C electrocatalyst (**FIGURE V-16**).

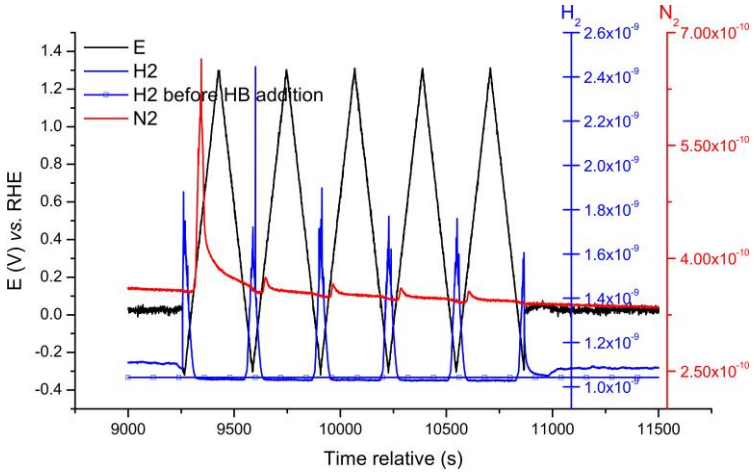

Figure V-16 DEMS detection for BH3OR on Pd/C electrocatalyst in 0.1 M NaOH + 5 mM HB at room temperature and in static condition

FIGURE V-16 clearly exhibits some detection of N_2 and H_2 for several successive CV cycles; the response is almost the same for all of them, and only a higher current of N_2 is detected for the first cycle; this is likely due to the static condition in which the DEMS experiments were performed: for the first CV, more hydrazine fragment is present in the electrocatalytic layer, and then, the concentration gradually decreases over time (the experiments are not performed in quasi-stationary conditions). **FIGURE V-17,** in which the gas detection is plotted as a function of electrode potential, gives further insight into the mechanism.

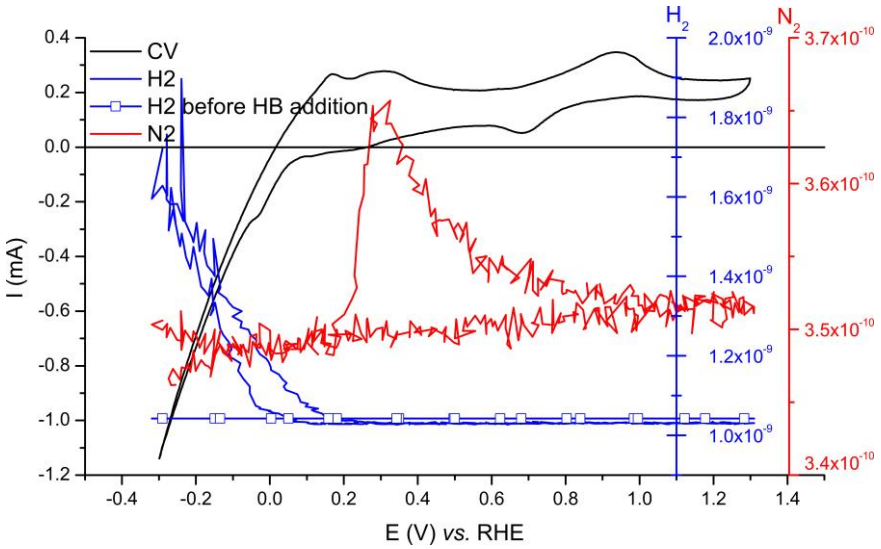

Figure V-17 Single CV of DEMS detection for BH3OR on Pd/C#2 electrocatalyst in 0.1 M NaOH + 5 mM HB at room temperature and in static condition

For potential values higher than E = 0 V *vs.* RHE, almost no hydrogen gas is detected by the MS: the hydrogen ion current is around the value measured before the addition of HB in solution. This means that either the hydrogen is fully valorized (electrooxidized) or that no hydrogen is produced during the BH_3OR above E = 0 V *vs.* RHE. To be more specific, the fact that some H_2 is detected up to E = 0.1 V *vs.* RHE in the forward scan is probably more the result of the transient residence of H_2 bubbles at the Pd/C#2 following the period at ocp than to the production of H_2 until this potential value; the fact that in the backward scan, H_2 is only detected below E = 0 V *vs.* RHE, seems to confirm this, and suggests that H_2 is produced by HER at these potentials more than by major catalytic decomposition of the borane fragment. Such behavior was measured by Jusys *at al.* in the case of the BOR at Pt electrocatalysts [168]. Then, the detection of a N_2 ion current is happening around E = 200 mV *vs.* RHE, which agrees with the results previously presented (**FIGURE V-3**) and corresponds to the total electrooxidation of the hydrazine fragment above E = 200 mV *vs.* RHE.

Ultimate experiments have been carried out with hydrazine hydrate to confirm the absence of decomposition of the hydrazine on Pd/C. Firstly, calibration test in supporting electrolyte were performed, as presented in **FIGURE V-18**.

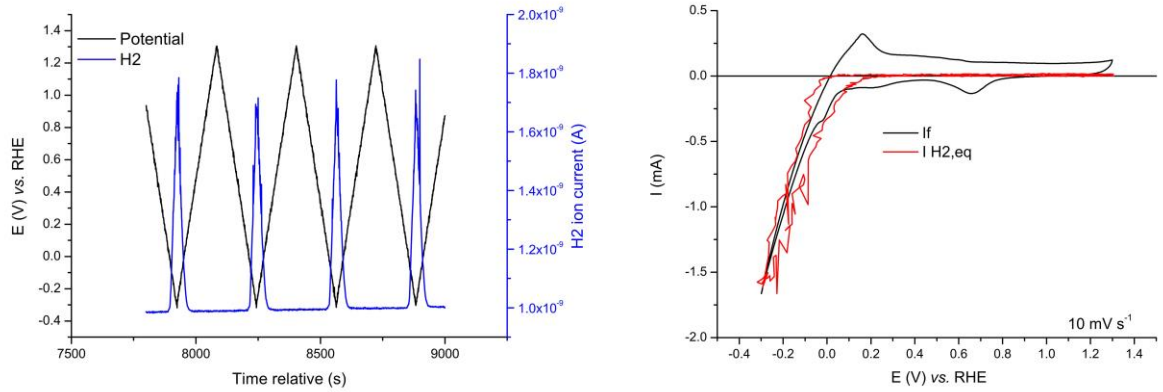

Figure V-18 (a) DEMS for the calibration with Pd/C#2 electrocatalyst in 0.1 M NaOH at room temperature and in static condition. (b) HER calibration; the intensity of the m/z = 2 signal was adjusted so as to fit the faradaic HER current using the DEMS calibration constant (in that case, $I_f = I_{H2,eq} = -2.31 \times 10^{-9} * I_{m/z=2}$)

Here again, the detection of H_2 during the HER matches perfectly this the potential value of the Pd/C electrocatalyst; the magnitude of H_2 ion current is around $I_{m/z\ =\ 2} = 0.8 * 10^{-10}$ $A_{ion\ current}$ after the subtraction of the baseline line ($K = -2.31 \times 10^{-9}$ in that case). This indicates that the approximately the same quantity/volume of electrocatalyst layer is probed by the MS between each DEMS experiment. Then, hydrazine hydrate was added to investigate its potential hydrolysis on the palladium catalyst (**FIGURE V-19)**.

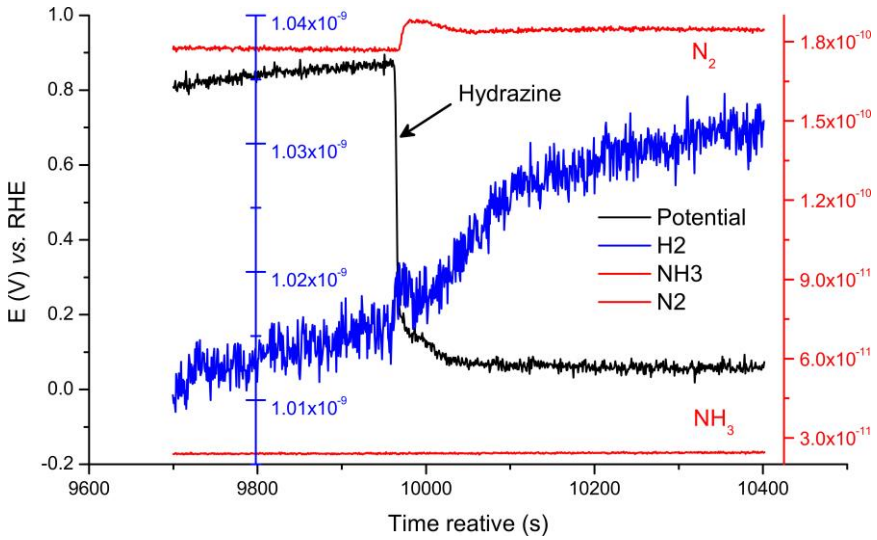

Figure V-19 DEMS detection of hydrazine hydrate hydrolysis on Pd/C#2 electrocatalyst in 0.1 M NaOH at room temperature and in static condition

FIGURE V-19 shows the progressive (and small) apparition of a H_2 ion current at ocp, with a magnitude of $I_{m/z = 2}$ = 0.02 * 10^{-9} $A_{ion\ current}$ (*vs.* a magnitude of $I_{m/z = 2}$ = 0.3 * 10^{-9} $A_{ion\ current}$ upon addition of HB), and the concomitant apparition of a N_2 ion current of very low magnitude; at that stage, it must be stated that such signals were not observed with HB. Those results suggest that hydrazine hydrate can be hydrolyzed on palladium into H_2 and N_2, but that this process is not quantitative on palladium and likely masked by the electroactivity of the material towards the reactions with borane when the fuel is HB. Moreover, CVs performed in 0.1 M NaOH + 5 mM hydrazine hydrate confirmed that the HHOR begins around E = 200 mV *vs.* RHE on Pd/C and that no hydrogen is observed after (above) E = 100 mV *vs.* RHE, as presented in **FIGURE V-20**. In general, this confirms that hydrazine hydrate (or by extension, the hydrazine fragment of HB) is most probably totally valorized electrochemically, leading the n_{e-} = 4 exchanged electrons above E = 200 mV *vs.* RHE, again, making of HB the perfect borane fuel for a DLAFC.

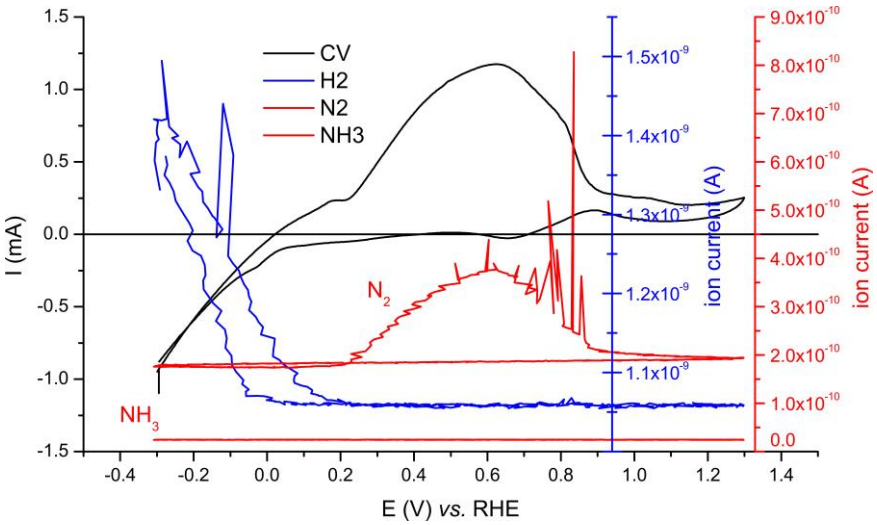

Figure V-20 Single CV of DEMS detection for HHOR on Pd/C#2 electrocatalyst in 0.1 M NaOH + 5 mM hydrazine hydrate at room temperature and in static condition

iv. Chapter five conclusion

The results presented in that chapter put the palladium as a material of choice for the borane electrooxidation in alkaline medium and so as anode in DLAFC systems fed with boranes. However, the nature of the borane fuel has been demonstrated to be an important parameter to reach the best performances for the BH_3OR; evidences have been brought that hydrazine borane is the best borane fuel over hydrazine bis-borane (which suffers safety issues) and ammonia borane or dimethylamine borane (both are impeded by poisoning issues by the "counter-fragment" and/or electroinactivity of the latter). Using HB as borane fuel with palladium material, the onset potential of BH_3OR can be as low as E = -300 mV *vs.* RHE (while its values is E = 0 V *vs.* RHE on platinum and on gold), demonstrating a superior electrocatalytic property of palladium over alternative electrocatalyst materials. Interestingly, the nature of borane fuel has no impact on the BH_3OR onset potential when platinum electrocatalyst is used, because Pt favors the complete decomposition of the fuel into H_2, followed by the HOR; conversely, this influence is very pronounced with palladium.

On carbon-supported palladium, the hydrazine "counter-borane" fragment is valorized beyond E = 200 mV *vs.* RHE *via* the HHOR; this reaction is found to be complete (no hydrogen produced) and therefore leads to n_{e^-} = 4 exchanged electrons per hydrazine moiety. The exchanged electron number was found to be (transiently) higher than expected when the BH_3OR happens either at low or high potential values; this has been assumed to be related to the electrooxidation of the hydrogen produced by the hydrolysis of HB since palladium is a good electrocatalyst for HOR. This activity marks another interest of palladium for the DHBFC anode: Pd does not yield severe H_2 production by the catalytic decomposition/heterogeneous hydrolysis of the fuel, but can nevertheless electrooxidize/valorize any H_2 produced within the electrode. This influence of hydrogen appears favorable, but the effect is transient in the present experimental conditions, because this additional hydrogen produced during the HER at low potential value (< E = 0 *vs.* RHE) or by borane hydrolysis happening just before our electrochemical measurements is trapped in the electrocatalyst layer and shall be fully removed (electrooxidized) in real steady-state conditions (in real DHBFC operation). In addition, hydrogen trapping has been found detrimental for DHBFC systems because (i) it leads to an increase of the system (HOR/BH_3OR) onset potential and (ii) the HOR can only proceed above E = 0 V *vs.* RHE.

Besides, the effects of the temperature, the HB concentration and the palladium loading have been found to be extremely remarkable, which denotes for the competition between the direct electrooxidation of the fuel (BH_3OR) and its catalytic decomposition followed by potential valorization of H_2 (HOR), and the overall effect of the time of residence of the reactants on the completion (and nature) of the reactions.

All those results indicate how difficult will be the task to optimize the DHBFC systems. Hopefully, they also brought evidence that on suitable electrocatalyst and with suitable borane fuel, the BH_3OR thermodynamic onset potential value can nearly be reached, and, that the $n_{e^-} = 10$ electrons can be exchanged in appropriate conditions at reasonably low anode potential.

General Conclusion

VI. General conclusion

This PhD work made a first step into the technological development of an original liquid alkaline fuel cell system, the direct hydrazine borane fuel cell (DHBFC). This work also gave first insights into stability issues of carbon-supported electrocatalysts in alkaline medium, a knowledge which is more general and re-suable for the improvement of other alkaline technologies.

It was demonstrated that "classical" and "state-of-the-art" electrocatalyst of platinum are highly unstable in alkaline medium. Carbon-supported platinum nanoparticles (Pt/C) suffer 60% of electrochemical surface area (ECSA) loss after only n = 150 cycles between E = 0.1 and 1.23 V *vs.* RHE in 0.1 M solution at T = 25°C. This intrinsic instability rules out any utilization of Pt/C materials for alkaline fuel cells (at least for electrodes with low loading of platinum – a trend followed nowadays). The impressive degradation fates observed render the kinetic studies performed on such materials "quite" unreliable (the degradation is already non-negligible for very little number of CV cycles performed, *i.e.* even for "classical cleaning and activation steps), while a lot of papers have been published using Pt/C in alkaline conditions. Carbon-supported palladium nanoparticles (Pd/C) have shown a relatively better stability in alkaline medium; they seem at least stable enough for kinetic studies in alkaline medium, but do not seem the most suitable for a real utilization in direct alkaline fuel cell conditions. The results obtained during that PhD are also questioning the general tendency to "tailor" the electrocatalysts in order to provide shaped nanoparticles that exhibit preferential facets (crystallographic orientations) found more electroactive for a given electrochemical reaction. The case of palladium cubic nanoparticles (unsupported) has been investigated and the cubic shape appeared highly unstable in alkaline conditions; indeed, the particles "turned spherical" after only n = 150 cycles between E = 0 and 0.9 V *vs.* RHE in 0.1 M NaOH at room temperature (T ~ 25°C). More generally, this PhD work has finally underlined that the stability issues in alkaline medium are probably largely underestimated in the scientific community. These results are the first ones related to stability issues of classical electrocatalysts in alkaline medium, and the author believes that the future works targeting an application in AFC systems will (and shall) integrate the durability to provide sustainable and active electrocatalysts.

Then, it was demonstrated that nickel-based carbon-supported electrocatalysts (Ni_3Ag/C, Ni_3Pd/C and Ni_3Co/C) have an interesting electroactivity for the borane electrooxidation reaction (BH_3OR) in alkaline medium. All those electrocatalysts are very active for the BH_3OR. Interestingly, even if the highest faradic current of electrooxidation is observed on the Ni_3Pd/C and Ni_3Ag/C electrocatalysts, the Ni_3Co/C electrocatalyst also exhibits appreciable electroactivity: the maximum current density with Ni_3Co/C is only twice lower than measured for Ni_3Pd/C, while Ni_3Co/M is a "low-cost" material. Moreover, the reaction onset is the lowest on Ni_3Co/C (it is *ca.* E = -90 mV *vs.* RHE); at such low potential value, the BH_3OR must be direct and cannot proceed *via* the decomposition of AB into H_2

followed by H_2 electrooxidation, which is interesting in terms of energy density and faradaic efficiency of a DLAFC. This could lead to high operating voltage value with a Ni_3Co/C-based anode in liquid alkaline fuel cell systems fed with borane fuels.

Concerning the specific development of DHBFC systems, the kinetic performances of Ni_3Co/C for BH_3OR using hydrazine borane (HB) are improved compared to the results obtained with AB, and the onset of BH_3OR is even lower with HB (it is *ca.* E = -120 mV *vs.* RHE). This latter result can be explained by an enhancement in the BH_3OR kinetics with HB and by the simultaneous valorization of the hydrazine fragment at very low potential value. For a real utilization in DHBFC systems, durability must also be assessed. ILTEM experiments demonstrated the absence of any consequent degradation for Ni_3Co/C, which exhibits a much larger material stability than observed for Pt/C and Pd/C electrocatalysts. So, with the combination of a promising activity for HB electrooxidation and a high stability in operation, the Ni_3Co/C noble-free electrocatalyst appears to be a material of choice for DHBFC systems.

Finally, despite their electrocatalytic activity and their durability for DHBFC systems, the nickel-based carbon-supported electrocatalysts may not be the best ones to further investigate the BH_3OR mechanism; they are indeed neither pure, nor perfectly homogeneous and they have a very complex and sensitive surface chemistry (oxidation, passivation *etc.*), features that do not render them "model electrocatalysts" to understand complex reaction mechanisms. So the borane electrooxidation reaction (BH_3OR) in alkaline medium was investigated on a Pd/C electrocatalyst. Obviously, the instability of such material has been taken into account to provide relevant and trustable data (no extensive CV cycling was performed on the Pd/C electrodes). On Pd/C, the nature of the borane fuel was demonstrated to be a critical parameter to reach the best BH_3OR performances: hydrazine borane is the best borane fuel tested (over hydrazine bis-borane, ammonia borane or dimethylamine borane). Using HB as borane fuel with the Pd/C electrocatalyst, the onset potential of BH_3OR can be as low as E = -300 mV *vs.* RHE (while its values is E = 0 V *vs.* RHE on platinum), demonstrating a superior electrocatalytic property of palladium over platinum, but also gold and nickel alloys. On carbon-supported palladium, the hydrazine "counter-borane" fragment is valorized beyond E = 200 mV *vs.* RHE *via* the HHOR; this reaction is found to be complete (no hydrogen produced) and therefore leads to n_{e^-} = 4 exchanged electrons per hydrazine moiety in addition to the n_{e^-} = 6 exchanged electrons per borane moiety. Besides, the effects of the temperature, the HB concentration and the palladium loading have been found extremely remarkable, which denotes for the competition between the direct electrooxidation of the fuel (BH_3OR) and its catalytic decomposition followed by potential valorization of H_2 (*via* HOR), and the overall effect of the time of residence of the reactants on the completion (and nature) of the reactions.

This PhD work therefore demonstrated the feasibility of DHBFC systems using low-cost, stable and electroactive materials. This PhD work however underlined the complexity to optimize the experimental

conditions to maximize the electroacatalytic performances; more studies are required but it is believed that this present contribution will attract more researchers on the way of DHBFC development.

Three years were obviously not enough to perform all the desired experiments and I would like to describe here some aspects that seem for me essential for the future developments of DHBFC systems. First of all, I think that the scientific community should get a better understanding about which materials are suitable (or not) in terms of stability/durability for alkaline fuel cell/electrolyzer systems. This present PhD work presented the stability results only for carbon-supported platinum, palladium and nickel alloy; so far, it seems that the most noble the electrocatalyst is (in other words, the most stable one would *a priori* guess), the less stable it experimentally is. This should be further investigated with a screening of many nanocatalysts different in metallic composition but ideally rather similar in terms of particle size distribution and dispersion on their (identical) carbon support. Then, for the most stable electrocatalysts, the electrocatalytic activity should be investigated for ammonia borane, hydrazine and finally hydrazine borane electrooxidation reactions, to separate them in 4 categories: 1- the electrocatalysts only active for borane electrooxidation, 2- or only active for hydrazine electrooxidation, 3- or active for hydrazine borane electrooxidation, 4- or inactive for both hydrazine and borane electrooxidations. The most suitable materials for the DHBFC anode could be a "composite material" that is a mixture of electrocatalysts 1 and 2, or a material composed with the electrocatalysts 3. For the electroactive materials, the hydrolysis should be also investigated to anticipate the possible competition between BH_3OR, HHOR and HOR electrochemical reactions.

Otherwise, this PhD work demonstrated that noble-free electrocatalysts can be targeted for use in DLAFC fed with BBMS and I believe this direction is the best one to lower the overall technology cost. On that point, copper (and cobalt [58]) seems to be a promising material but unfortunately not really (enough) investigated during those three years; however, some rapid tests and two papers dealing with copper [180,181] have shown great properties for borane electrooxidation reaction (these two papers were not quoted in the manuscript because they were "off the radar"… no major study dealing with borane or borohydride electrooxidation has ever quoted them).

Concerning the DHBFC anode structure, it seems that the electroactivity is not dramatically impacted by the materials' purity; this can allow the next experimenters to go faster on the screening of electrocatalysts without losing time in cleaning (as it was the case during the whole PhD project). This also allows to use nanoporous electrodes, synthesized for example by selective dealloying techniques; indeed, the carbon support is maybe not necessary and a porous material could be more resistant and may ease the release of reaction products and hydrogen bubbles.

Finally, I think that the complete fuel cell experiments are now a *sine qua non* condition to understand how to manage the release of reaction products and hydrogen bubbles, the electrocatalyst's state of oxidation (passivation of the non-noble materials) and how to optimize the essential parameters such as concentrations, fluxes, and temperature. Moreover, when a large quantity of hydrogen is produced (by hydrolysis), technical strategies have to be developed to valorize that hydrogen without inducing a loss in the operating voltage (a solution could be to valorize this hydrogen in another/parallel and dedicated fuel cell with an anode electrocatalyst active for hydrogen electrooxidation reaction).

General bibliography

A. General bibliography

(1) Vielstich, W.; Lamm, A.; Gasteiger, H. A. H. *Handbook of Fuel Cells, volume 1: Fundamentals and Survey of Systems*; Vielstich, W., Lamm, A., Gasteiger, H. A., Eds.; John Wiley & Sons, Ltd: Chichester, England, 2003.

(2) Vielstich, W.; Lamm, A.; Gasteiger, H. A. *Handbook of Fuel Cells, volume 2: Fuel Cell Electrocatalysis*; Vielstich, W., Lamm, A., Gasteiger, H. A., Eds.; John Wiley & Sons, Ltd: Chichester, England, 2003.

(3) Vielstich, W.; Lamm, A.; Gasteiger, H. A. *Handbook of Fuel Cells, volumes 3 and 4: Fuel Cell Technology and Applications*; Vielstich, W., Lamm, A., Gasteiger, H. A., Eds.; John Wiley & Sons, Ltd: Chichester, England, 2003.

(4) Vielstich, W.; Lamm, A.; Gasteiger, H. A. H.; Vielstich, W.; Yokokawa, H. *Handbook of Fuel Cells, volumes 5 and 6: Advances in Electrocatalysis, Materials, Diagnostics and Durability*; Vielstich, W., Lamm, A., Gasteiger, H. A., Eds.; John Wiley & Sons, Ltd: Chichester, England, 2009.

(5) Bruce, P. G.; Hardwick, L. J.; Abraham, K. M. *MRS Bull.* **2011**, *36* (07), 506–512.

(6) Dunn, B.; Kamath, H.; Tarascon, J.-M. *Science (80-.).* **2011**, *334* (6058), 928–935.

(7) Gallagher, K. G.; Goebel, S.; Greszler, T.; Mathias, M.; Oelerich, W.; Eroglu, D.; Srinivasan, V. *Energy Environ. Sci.* **2014**, *7* (5), 1555.

(8) Sharaf, O. Z.; Orhan, M. F. *Renew. Sustain. Energy Rev.* **2014**, *32*, 810–853.

(9) Varcoe, J. R.; Slade, R. C. T. *Fuel Cells* **2005**, *5* (2), 187–200.

(10) Zhang, J.; Yang, H.; Fang, J.; Zou, S. *Nano Lett.* **2010**, *10* (2), 638–644.

(11) Koh, S.; Strasser, P. *J. Am. Chem. Soc.* **2007**, *129* (42), 12624–12625.

(12) Ruvinskiy, P. S.; Bonnefont, A.; Pham-Huu, C.; Savinova, E. R. *Langmuir* **2011**, *27* (14), 9018–9027.

(13) Ruvinskiy, P. S.; Bonnefont, A.; Houllé, M.; Pham-Huu, C.; Savinova, E. R. *Electrochim. Acta* **2010**, *55* (9), 3245–3256.

(14) Bacon, F. T.; Fry, T. M. *Proc. R. Soc. A Math. Phys. Eng. Sci.* **1973**, *334* (1599), 427–452.

(15) Durst, J.; Lamibrac, A.; Charlot, F.; Dillet, J.; Castanheira, L. F.; Maranzana, G.; Dubau, L.; Maillard, F.; Chatenet, M.; Lottin, O. *Appl. Catal. B Environ.* **2013**, *138-139*, 416–426.

(16) Guilminot, E.; Corcella, a.; Charlot, F.; Maillard, F.; Chatenet, M. *J. Electrochem. Soc.* **2007**, *154* (1), B96.

(17) Chatenet, M.; Guilminot, E.; Iojoiu, C.; Sanchez, J.-Y.; Rossinot, E.; Maillard, F. In *ECS Transactions*; ECS, 2007; Vol. 11, pp 1203–1214.

(18) Iojoiu, C.; Guilminot, E.; Maillard, F.; Chatenet, M.; Sanchez, J.-Y.; Claude, E.; Rossinot, E. *J. Electrochem. Soc.* **2007**, *154* (11), B1115.

(19) Yu, P.; Pemberton, M.; Plasse, P. *J. Power Sources* **2005**, *144* (1), 11–20.

(20) Nikkuni, F. R.; Ticianelli, E. a.; Dubau, L.; Chatenet, M. *Electrocatalysis* **2013**, *4* (2), 104–116.

(21) Dubau, L.; Maillard, F.; Chatenet, M.; Guetaz, L.; André, J.; Rossinot, E. *J. Electrochem. Soc.* **2010**, *157* (12), B1887.

(22) Durst, J.; Chatenet, M.; Maillard, F. *Phys. Chem. Chem. Phys.* **2012**, *14* (37), 13000.

(23) Castanheira, L.; Silva, W. O.; Lima, F. H. B.; Crisci, A.; Dubau, L.; Maillard, F. *ACS Catal.* **2015**, *5* (4), 2184–2194.

(24) Du, C.; Chen, M.; Cao, X.; Yin, G.; Shi, P. *Electrochem. commun.* **2009**, *11* (2), 496–498.

(25) Ioroi, T.; Senoh, H.; Yamazaki, S.; Siroma, Z.; Fujiwara, N.; Yasuda, K. *J. Electrochem.*

Soc. **2008**, *155* (4), B321.
(26) Sharma, S.; Pollet, B. G. *J. Power Sources* **2012**, *208*, 96–119.
(27) Amendola, S. *Int. J. Hydrogen Energy* **2000**, *25* (10), 969–975.
(28) Kojima, Y.; Suzuki, K.; Fukumoto, K.; Sasaki, M.; Yamamoto, T.; Kawai, Y.; Hayashi, H. *Int. J. Hydrogen Energy* **2002**, *27* (10), 1029–1034.
(29) YAO, C.; ZHUANG, L.; CAO, Y.; AI, X.; YANG, H. *Int. J. Hydrogen Energy* **2008**, *33* (10), 2462–2467.
(30) Liu, B. H.; Li, Z. P. *J. Power Sources* **2009**, *187* (2), 527–534.
(31) Demirci, U. B.; Miele, P. *Comptes Rendus Chim.* **2009**, *12* (9), 943–950.
(32) Olu, P. Y.; Deschamps, F.; Caldarella, G.; Chatenet, M.; Job, N. *J. Power Sources* **2015**, *297*, 492–503.
(33) Morris, J. H.; Gysling, H. J.; Reed, D. *Chem. Rev.* **1985**, *85* (1), 51–76.
(34) Elder, J. P.; Hickling, A. *Trans. Faraday Soc.* **1962**, *58* (0), 1852–1864.
(35) Rostamikia, G.; Janik, M. J. *Energy Environ. Sci.* **2010**, *3* (9), 1262–1274.
(36) Olu, P.-Y.; Bonnefont, A.; Rouhet, M.; Bozdech, S.; Job, N.; Chatenet, M.; Savinova, E. *Electrochim. Acta* **2015**, *179*, 637–646.
(37) Concha, B. M.; Chatenet, M.; Coutanceau, C.; Hahn, F. *Electrochem. commun.* **2009**, *11* (1), 223–226.
(38) Concha, B. M.; Chatenet, M.; Maillard, F.; Ticianelli, E. A.; Lima, F. H. B.; de Lima, R. B. *Phys. Chem. Chem. Phys.* **2010**, *12* (37), 11507.
(39) Molina Concha, B.; Chatenet, M.; Ticianelli, E. A.; Lima, F. H. B. *J. Phys. Chem. C* **2011**, *115* (25), 12439–12447.
(40) Finkelstein, D. A.; Letcher, C. D.; Jones, D. J.; Sandberg, L. M.; Watts, D. J.; Abruña, H. D. *J. Phys. Chem. C* **2013**, *117* (4), 1571–1581.
(41) Olu, P.-Y.; Barros, C. R.; Job, N.; Chatenet, M. *Electrocatalysis* **2014**, *5* (3), 288–300.
(42) Pasqualeti, A. M.; Olu, P.-Y.; Chatenet, M.; Lima, F. H. B. *ACS Catal.* **2015**, *5* (5), 2778–2787.
(43) Okinaka, Y. *J. Electrochem. Soc.* **1973**, *120* (6), 739.
(44) Nagle, L. C.; Rohan, J. F. *J. Electrochem. Soc.* **2011**, *158* (7), B772.
(45) Nagle, L. C.; Rohan, J. F. *J. Electrochem. Soc.* **2006**, *153* (11), C773.
(46) Zhang, X.; Han, S.; Yan, J.; Shioyama, H.; Kuriyama, N.; Kobayashi, T.; Xu, Q. *Int. J. Hydrogen Energy* **2009**, *34* (1), 174–179.
(47) Belén Molina Concha, M.; Chatenet, M.; Lima, F. H. B.; Ticianelli, E. a. *Electrochim. Acta* **2013**, *89*, 607–615.
(48) Martins, J. I.; Nunes, M. C. *J. Power Sources* **2008**, *175* (1), 244–249.
(49) Kiran, V.; Kalidindi, S. B.; Jagirdar, B. R.; Sampath, S. *Electrochim. Acta* **2011**, *56* (28), 10493–10499.
(50) Nagle, L. C.; Rohan, J. F. 2010; Vol. 25, pp 13–25.
(51) Plana, D.; Dryfe, R. a. W. *Electrochim. Acta* **2011**, *56* (11), 3835–3844.
(52) Plana, D.; Rodriguez, P.; Koper, M. T. M.; Dryfe, R. a. W. *Electrochim. Acta* **2011**, *56* (22), 7637–7643.
(53) Zhang, X.-B.; Yan, J.-M.; Han, S.; Shioyama, H.; Yasuda, K.; Kuriyama, N.; Xu, Q. *J. Power Sources* **2008**, *182* (2), 515–519.
(54) Burke, L. D.; Lee, B. H. *J. Appl. Electrochem.* **1992**, *22* (1), 48–56.
(55) Plana, D.; Shul, G.; Stephenson, M. J.; Dryfe, R. A. W. *Electrochem. commun.* **2009**, *11* (1), 61–64.
(56) Sargent, A.; Sadik, O. A.; Matienzo, L. J. *J. Electrochem. Soc.* **2001**, *148* (4), C257–C265.
(57) Sadik, O. A.; Xu, H.; Sargent, A. *J. Electroanal. Chem.* **2005**, *583* (2), 167–175.
(58) Burke, L. D.; Murphy, M. M. *J. Electrochem. Soc.* **1991**, *138* (1), 88.

(59) Gardiner, J. A.; Collat, J. W. *J. Am. Chem. Soc.* **1965**, *87* (8), 1692–1700.
(60) Nagle, L. C.; Rohan, J. F. *Electrochem. Solid-State Lett.* **2005**, *8* (5), C77–C80.
(61) Chatenet, M.; Molina-Concha, M. B.; El-Kissi, N.; Parrour, G.; Diard, J.-P. *Electrochim. Acta* **2009**, *54* (18), 4426–4435.
(62) Zhang, X.-B.; Han, S.; Yan, J.-M.; Chandra, M.; Shioyama, H.; Yasuda, K.; Kuriyama, N.; Kobayashi, T.; Xu, Q. *J. Power Sources* **2007**, *168* (1), 167–171.
(63) Freitas, K. S.; Concha, B. M.; Ticianelli, E. A.; Chatenet, M. *Catal. Today* **2011**, *170* (1), 110–119.
(64) Kulyk, N.; Cherevko, S.; Chung, C. H. *Electrochim. Acta* **2012**, *59*, 179–185.
(65) Yao, C.; Yang, H.; Zhuang, L.; Ai, X.; Cao, Y.; Lu, J. *J. Power Sources* **2007**, *165* (1), 125–127.
(66) Chatenet, M.; Micoud, F.; Roche, I.; Chainet, E.; Vondrák, J. *Electrochim. Acta* **2006**, *51* (25), 5452–5458.
(67) Garcia, A. C.; Lima, F. H. B.; Ticianelli, E. A.; Chatenet, M. *J. Power Sources* **2013**, *222*, 305–312.
(68) Garcia, A. C.; Linares, J. J.; Chatenet, M.; Ticianelli, E. A. *Electrocatalysis* **2014**, *5* (1), 41–49.
(69) Rosca, V.; Koper, M. T. M. *Electrochim. Acta* **2008**, *53* (16), 5199–5205.
(70) Asazawa, K.; Yamada, K.; Tanaka, H.; Taniguchi, M.; Oguro, K. *J. Power Sources* **2009**, *191* (2), 362–365.
(71) Sakamoto, T.; Asazawa, K.; Martinez, U.; Halevi, B.; Suzuki, T.; Arai, S.; Matsumura, D.; Nishihata, Y.; Atanassov, P.; Tanaka, H. *J. Power Sources* **2013**, *234*, 252–259.
(72) Sakamoto, T.; Asazawa, K.; Sanabria-Chinchilla, J.; Martinez, U.; Halevi, B.; Atanassov, P.; Strasser, P.; Tanaka, H. *J. Power Sources* **2014**, *247*, 605–611.
(73) Moury, R.; Moussa, G.; Demirci, U. B.; Hannauer, J.; Bernard, S.; Petit, E.; van der Lee, A.; Miele, P. *Phys. Chem. Chem. Phys.* **2012**, *14* (5), 1768–1777.
(74) Mayrhofer, K. J. J.; Wiberg, G. K. H.; Arenz, M. *J. Electrochem. Soc.* **2008**, *155* (1), P1.
(75) Mayrhofer, K. J. J.; Crampton, A. S.; Wiberg, G. K. H.; Arenz, M. *J. Electrochem. Soc.* **2008**, *155* (6), P78.
(76) Garsany, Y.; Singer, I. L.; Swider-Lyons, K. E. *J. Electroanal. Chem.* **2011**, *662* (2), 396–406.
(77) Dubau, L.; Castanheira, L.; Berthomé, G.; Maillard, F. *Electrochim. Acta* **2013**, *110*, 273–281.
(78) Zhao, Z.; Castanheira, L.; Dubau, L.; Berthomé, G.; Crisci, A.; Maillard, F. *J. Power Sources* **2013**, *230*, 236–243.
(79) Castanheira, L.; Dubau, L.; Maillard, F. *Electrocatalysis* **2014**, *5* (2), 125–135.
(80) Zadick, A.; Dubau, L.; Sergent, N.; Berthomé, G.; Chatenet, M. *ACS Catal.* **2015**, *5* (8), 4819–4824.
(81) Maillard, F.; Eikerling, M.; Cherstiouk, O. V.; Schreier, S.; Savinova, E.; Stimming, U. *Faraday Discuss.* **2004**, *125*, 357.
(82) Maillard, F.; Schreier, S.; Hanzlik, M.; Savinova, E. R.; Weinkauf, S.; Stimming, U. *Phys. Chem. Chem. Phys.* **2005**, *7* (2), 385–393.
(83) Maillard, F.; Savinova, E. R.; Simonov, P. A.; Zaikovskii, V. I.; Stimming, U. *J. Phys. Chem. B* **2004**, *108* (46), 17893–17904.
(84) Urchaga, P.; Baranton, S.; Coutanceau, C.; Jerkiewicz, G. *Langmuir* **2012**, *28* (7), 3658–3663.
(85) Mayrhofer, K. J. J.; Arenz, M.; Blizanac, B. B.; Stamenkovic, V.; Ross, P. N.; Markovic, N. M. *Electrochim. Acta* **2005**, *50* (25-26), 5144–5154.
(86) Fang, L.; Tao, Q.; Li, M.; Liao, L.; Chen, D.; Chen, Y. *Chinese J. Chem. Phys.* **2010**, *23* (5), 543–548.

(87) Durst, J.; Simon, C.; Hasche, F.; Gasteiger, H. A. *J. Electrochem. Soc.* **2014**, *162* (1), F190–F203.
(88) Mittermeier, T.; Weiss, A.; Hasche, F.; Gasteiger, H. a. *ECS Trans.* **2015**, *69* (17), 303–313.
(89) Hara, M.; Linke, U.; Wandlowski, T. *Electrochim. Acta* **2007**, *52* (18), 5733–5748.
(90) Huang, X.; Tang, S.; Mu, X.; Dai, Y.; Chen, G.; Zhou, Z.; Ruan, F.; Yang, Z.; Zheng, N. *Nat. Nanotechnol.* **2011**, *6* (1), 28–32.
(91) Shao, M.; Odell, J. H.; Choi, S.-I.; Xia, Y. *Electrochem. commun.* **2013**, *31*, 46–48.
(92) Zhang, G.; Zhang, L.; Shen, L.; Chen, Y.; Zhou, Y.; Tang, Y.; Lu, T. *Chempluschem* **2012**, *77* (10), 936–940.
(93) Jukk, K.; Alexeyeva, N.; Johans, C.; Kontturi, K.; Tammeveski, K. *J. Electroanal. Chem.* **2012**, *666*, 67–75.
(94) Trasatti, S.; Petrii, O. A. *J. Electroanal. Chem.* **1992**, *327* (1-2), 353–376.
(95) Grdeń, M.; Łukaszewski, M.; Jerkiewicz, G.; Czerwiński, A. *Electrochim. Acta* **2008**, *53* (26), 7583–7598.
(96) Correia, A. N.; Mascaro, L. H.; Machado, S. A. S.; Avaca, L. A. *Electrochim. Acta* **1997**, *42* (3), 493–495.
(97) Jerkiewicz, G. *Prog. Surf. Sci.* **1998**, *57* (2), 137–186.
(98) Jerkiewicz, G. *J. Electrochem. Soc.* **1996**, *143* (4), 1240.
(99) Meier, J.; Kleine, H.; Stimming, U. *Surf. Sci.* **2005**, *597* (1-3), 127–132.
(100) Zadick, A.; Dubau, L.; Zalineeva, A.; Coutanceau, C.; Chatenet, M. *Electrochem. commun.* **2014**, *48*, 1–4.
(101) Zadick, A.; Dubau, L.; Chatenet, M.; Demirci, U.; Serov, A.; Atanassov, P. *ECS Trans.* **2015**, *69* (17), 553–558.
(102) Zadick, A.; Dubau, L.; Demirci, U. B.; Chatenet, M. *J. Electrochem. Soc.* **2016**, *163* (8), F781–F787.
(103) Mayrhofer, K. J. J.; Ashton, S. J.; Meier, J. C.; Wiberg, G. K. H.; Hanzlik, M.; Arenz, M. *J. Power Sources* **2008**, *185* (2), 734–739.
(104) Markovića, N. M.; Sarraf, S. T.; Gasteiger, H. A.; Ross, P. N. *J. Chem. Soc., Faraday Trans.* **1996**, *92* (20), 3719–3725.
(105) Kiros, Y.; Schwartz, S. *J. Power Sources* **2000**, *87* (1-2), 101–105.
(106) Sheng, W.; Gasteiger, H. a.; Shao-Horn, Y. *J. Electrochem. Soc.* **2010**, *157* (11), B1529.
(107) Durst, J.; Siebel, A.; Simon, C.; Hasché, F.; Herranz, J.; Gasteiger, H. a. *Energy Environ. Sci.* **2014**, *7* (7), 2255.
(108) Cabot, P. L.; Guezala, E.; Calpe, J. C.; García, M. T.; Casado, J. *J. Electrochem. Soc.* **2000**, *147* (1), 43.
(109) Henning, S.; Herranz, J.; Gasteiger, H. A. *J. Electrochem. Soc.* **2014**, *162* (1), F178–F189.
(110) Alia, S. M.; Yan, Y. *J. Electrochem. Soc.* **2015**, *162* (8), F849–F853.
(111) Zheng, J.; Zhou, S.; Gu, S.; Xu, B.; Yan, Y. *J. Electrochem. Soc.* **2016**, *163* (6), F499–F506.
(112) Jager, R.; Hark, E.; Kasatkin, P. E.; Lust, E. *J. Electrochem. Soc.* **2014**, *161* (9), F861–F867.
(113) Härk, E.; Jäger, R.; Lust, E. *Electrocatalysis* **2015**, *6* (3), 242–254.
(114) Ge, X.; Sumboja, A.; Wuu, D.; An, T.; Li, B.; Goh, F. W. T.; Hor, T. S. A.; Zong, Y.; Liu, Z. *ACS Catal.* **2015**, *5* (8), 4643–4667.
(115) Meng, H.; Jaouen, F.; Proietti, E.; Lefèvre, M.; Dodelet, J.-P. *Electrochem. commun.* **2009**, *11* (10), 1986–1989.
(116) Jiang, L.; Hsu, A.; Chu, D.; Chen, R. *J. Electrochem. Soc.* **2009**, *156* (5), B643.
(117) Erikson, H.; Sarapuu, A.; Alexeyeva, N.; Tammeveski, K.; Solla-Gullón, J.; Feliu, J. M.

Electrochim. Acta **2012**, *59*, 329–335.
(118) Srejic, I.; Rakocevic, Z.; Nenadovic, M.; Strbac, S. *Electrochim. Acta* **2015**, *169*, 22–31.
(119) Finkelstein, D. A.; Mota, N. Da; Cohen, J. L.; Abruña, H. D. *J. Phys. Chem. C* **2009**, *113* (45), 19700–19712.
(120) Olu, P.-Y.; Gilles, B.; Job, N.; Chatenet, M. *Electrochem. commun.* **2014**, *43*, 47–50.
(121) Spendelow, J. S.; Wieckowski, A. *Phys. Chem. Chem. Phys.* **2007**, *9* (21), 2654.
(122) Liu, Z.; Zhao, B.; Guo, C.; Sun, Y.; Shi, Y.; Yang, H.; Li, Z. *J. Colloid Interface Sci.* **2010**, *351* (1), 233–238.
(123) Serov, A.; Andersen, N. I.; Kabir, S. A.; Roy, A.; Asset, T.; Chatenet, M.; Maillard, F.; Atanassov, P. *J. Electrochem. Soc.* **2015**, *162* (12), F1305–F1309.
(124) Lima, F. H. B.; Pasqualeti, A. M.; Concha, M. B. M.; Chatenet, M.; Ticianelli, E. A. *Electrochim. Acta* **2012**, *84* (SI), 202–212.
(125) Pylypko, S.; Zadick, A.; Chatenet, M.; Miele, P.; Cretin, M.; Demirci, U. B. *J. Power Sources* **2015**, *286*, 10–17.
(126) Garland, N.; Benjamin, T.; Kopasz, J. In *ECS Transactions*; ECS, 2007; Vol. 11, pp 923–931.
(127) Ohma, A.; Shinohara, K.; Iiyama, A.; Yoshida, T.; Daimaru, A. In *ECS Transactions*; 2011; Vol. 41, pp 775–784.
(128) Cherevko, S.; Zeradjanin, A. R.; Topalov, A. A.; Kulyk, N.; Katsounaros, I.; Mayrhofer, K. J. J. *ChemCatChem* **2014**, *6* (8), 2219–2223.
(129) Maillard, F.; Dubau, L.; Durst, J.; Chatenet, M.; André, J.; Rossinot, E. *Electrochem. commun.* **2010**, *12* (9), 1161–1164.
(130) Dubau, L.; Durst, J.; Maillard, F.; Chatenet, M.; André, J.; Rossinot, E. *Fuel Cells* **2012**, *12* (2), 188–198.
(131) Dubau, L.; Durst, J.; Maillard, F.; Guétaz, L.; Chatenet, M.; André, J.; Rossinot, E. In *Electrochimica Acta*; Elsevier Ltd, 2011; Vol. 56, pp 10658–10667.
(132) Dubau, L.; Lopez-Haro, M.; Castanheira, L.; Durst, J.; Chatenet, M.; Bayle-Guillemaud, P.; Guétaz, L.; Caqué, N.; Rossinot, E.; Maillard, F. *Appl. Catal. B Environ.* **2013**, *142-143*, 801–808.
(133) Dubau, L.; Castanheira, L.; Maillard, F.; Chatenet, M.; Lottin, O.; Maranzana, G.; Dillet, J.; Lamibrac, A.; Perrin, J. C.; Moukheiber, E.; Elkaddouri, A.; De Moor, G.; Bas, C.; Flandin, L.; Caqué, N. *Wiley Interdisciplinary Reviews: Energy and Environment*. November 2014, pp 540–560.
(134) Hernández, J.; Solla-Gullón, J.; Herrero, E.; Aldaz, A.; Feliu, J. M. *J. Phys. Chem. C* **2007**, *111* (38), 14078–14083.
(135) Zalineeva, A.; Baranton, S.; Coutanceau, C. *Electrochem. commun.* **2013**, *34*, 335–338.
(136) Shao, M.; Odell, J.; Humbert, M.; Yu, T.; Xia, Y. *J. Phys. Chem. C* **2013**, *117* (8), 4172–4180.
(137) Lee, C. L.; Chiou, H. P.; Liu, C. R. *Int. J. Hydrogen Energy* **2012**, *37* (5), 3993–3997.
(138) Oliveira, V. L.; Sibert, E.; Soldo-Olivier, Y.; Ticianelli, E. A.; Chatenet, M. *Electrochim. Acta* **2016**, *209*, 360–368.
(139) Oliveira, V. L.; Sibert, E.; Soldo-Olivier, Y.; Ticianelli, E. A.; Chatenet, M. *Electrochim. Acta* **2016**, *190*, 790–796.
(140) Furuya, Y.; Mashio, T.; Ohma, A.; Tian, M.; Kaveh, F.; Beauchemin, D.; Jerkiewicz, G. *ACS Catal.* **2015**, 2605–2614.
(141) Takahashi, I.; Kocha, S. S. *J. Power Sources* **2010**, *195* (19), 6312–6322.
(142) Mukerjee, S. *J. Appl. Electrochem.* **1990**, *20* (4), 537–548.
(143) Cherevko, S.; Zeradjanin, A. R.; Keeley, G. P.; Mayrhofer, K. J. J. *J. Electrochem. Soc.* **2014**, *161* (12), H822–H830.
(144) Zhao, Z.; Dubau, L.; Maillard, F. *J. Power Sources* **2012**, *217*, 449–458.

(145) Dubau, L.; Castanheira, L.; Chatenet, M.; Maillard, F.; Dillet, J.; Maranzana, G.; Abbou, S.; Lottin, O.; De Moor, G.; El Kaddouri, A.; Bas, C.; Flandin, L.; Rossinot, E.; Caqué, N. *Int. J. Hydrogen Energy* **2014**, *39* (36), 21902–21914.
(146) Castanheira, L.; Dubau, L.; Mermoux, M.; Berthom??, G.; Caqu??, N.; Rossinot, E.; Chatenet, M.; Maillard, F. *ACS Catal.* **2014**, *4* (7), 2258–2267.
(147) Shao-Horn, Y.; Sheng, W. C.; Chen, S.; Ferreira, P. J.; Holby, E. F.; Morgan, D. *Top. Catal.* **2007**, *46* (3-4), 285–305.
(148) Rand, D. A. J.; Woods, R. *J. Electroanal. Chem. Interfacial Electrochem.* **1972**, *35* (1), 209–218.
(149) Wells, P. P.; Crabb, E. M.; King, C. R.; Wiltshire, R.; Billsborrow, B.; Thompsett, D.; Russell, A. E. *Phys. Chem. Chem. Phys.* **2009**, *11* (27), 5773.
(150) Flávio R. Nikkunia, Benoit Vion-Durya, Laetitia Dubaua, Frédéric Maillarda, Edson A. Ticianellic, M. C.; Nikkuni, F. R.; Vion-Dury, B.; Dubau, L.; Maillard, F.; Ticianelli, E. a.; Chatenet, M. *Appl. Catal. B Environ.* **2014**, *156-157*, 301–306.
(151) Nikkuni, F. R.; Dubau, L.; Ticianelli, E. A.; Chatenet, M. *Appl. Catal. B Environ.* **2015**, *176-177*, 486–499.
(152) Simões, M.; Baranton, S.; Coutanceau, C. *J. Phys. Chem. C* **2009**, *113* (30), 13369–13376.
(153) Simoes, M.; Baranton, S. S.; Coutanceau, C.; Simões, M.; Baranton, S. S.; Coutanceau, C. *Appl. Catal. B Environ.* **2010**, *93* (3-4), 354–362.
(154) Simões, M.; Baranton, S. S.; Coutanceau, C.; Sim??es, M.; Baranton, S. S.; Coutanceau, C. *Electrochim. Acta* **2010**, *56* (1), 580–591.
(155) Holby, E. F.; Shao-Horn, Y.; Sheng, W.; Morgan, D. In *ECS Transactions*; ECS, 2009; Vol. 25, pp 583–592.
(156) Metin, Ö.; Kayhan, E.; Özkar, S.; Schneider, J. J. *Int. J. Hydrogen Energy* **2012**, *37* (10), 8161–8169.
(157) Hannauer, J.; Demirci, U. B.; Geantet, C.; Herrmann, J.-M.; Miele, P. *Int. J. Hydrogen Energy* **2012**, *37* (14), 10758–10767.
(158) Pattabiraman, R. *Appl. Catal. A Gen.* **1997**, *153* (1-2), 9–20.
(159) Yamada, K.; Yasuda, K.; Tanaka, H.; Miyazaki, Y.; Kobayashi, T. *J. Power Sources* **2003**, *122* (2), 132–137.
(160) Seo, M. H.; Choi, S. M.; Kim, H. J.; Kim, W. B. *Electrochem. commun.* **2011**, *13* (2), 182–185.
(161) Shao, M. *J. Power Sources* **2011**, *196* (5), 2433–2444.
(162) Erikson, H.; Sarapuu, A.; Tammeveski, K.; Solla-Gullón, J.; Feliu, J. M. *Electrochem. commun.* **2011**, *13* (7), 734–737.
(163) Cui, C.; Gan, L.; Heggen, M.; Rudi, S.; Strasser, P. *Nat. Mater.* **2013**, *12* (8), 765–771.
(164) Arán-Ais, R. M.; Yu, Y.; Hovden, R.; Solla-Gullón, J.; Herrero, E.; Feliu, J. M.; Abruña, H. D. *J. Am. Chem. Soc.* **2015**, *137* (47), 14992–14998.
(165) Hoshi, N.; Nakamura, M.; Maki, N.; Yamaguchi, S.; Kitajima, A. *J. Electroanal. Chem.* **2008**, *624* (1-2), 134–138.
(166) Fernandez-Guillermet, A. *Mater. Res. Adv. Tech.* **1987**, *78* (9), 639–647.
(167) Perry, R. H.; Green, D. W. *Perry's Chemical Engineers' Handbook*; McGraw-Hill, Ed.; New York, 1997.
(168) Jusys, Z.; Behm, R. J. *Electrochem. commun.* **2015**, *60*, 9–12.
(169) Finkelstein, D. A.; Imbeault, R.; Garbarino, S.; Roué, L.; Guay, D. *J. Phys. Chem. C* **2016**, *120* (9), 4717–4738.
(170) Sanabria-Chinchilla, J.; Asazawa, K.; Sakamoto, T.; Yamada, K.; Tanaka, H.; Strasser, P. *J. Am. Chem. Soc.* **2011**, *133* (14), 5425–5431.
(171) Denuault, G.; Mirkin, M. V.; Bard, A. J. *J. Electroanal. Chem. Interfacial Electrochem.*

1991, *308* (1-2), 27–38.
(172) Koper, M. T. M.; Lukkien, J. J.; Lebedeva, N. P.; Feliu, J. M.; van Santen, R. A. *Surf. Sci.* **2001**, *478* (1--2), L339–L344.
(173) de Vooys, A. C. .; Koper, M. T. .; van Santen, R. .; van Veen, J. A. . *J. Electroanal. Chem.* **2001**, *506* (2), 127–137.
(174) Zhang, L.; Niu, W.; Gao, W.; Qi, L.; Zhao, J.; Xu, M.; Xu, G. *Electrochem. commun.* **2013**, *37*, 57–60.
(175) Ye, L. Q.; Li, Z. P.; Qin, H. Y.; Zhu, J. K.; Liu, B. H. *J. Power Sources* **2011**, *196* (3), 956–961.
(176) Serov, A.; Kwak, C. *Appl. Catal. B Environ.* **2010**, *98* (1-2), 1–9.
(177) Chen, L.; Hu, G.; Zou, G.; Shao, S.; Wang, X. *Electrochem. commun.* **2009**, *11* (2), 504–507.
(178) Harrison, J. a.; Khan, Z. a. *J. Electroanal. Chem. Interfacial Electrochem.* **1970**, *26* (1), 1–11.
(179) Freitas, K. S.; Concha, B. M.; Ticianelli, E. A.; Chatenet, M. In *ECS Transactions*; 2010; Vol. 33, pp 1693–1699.
(180) Filanovsky, B.; Granot, E.; Dirawi, R.; Presman, I.; Kuras, I.; Patolsky, F. *Nano Lett.* **2011**, *11* (4), 1727–1732.
(181) Auxilia, F. M.; Tanabe, T.; Ishihara, S.; Saravanan, G.; Ramesh, G. V.; Matsumoto, F.; Ya, X.; Ariga, K.; Dakshanamoorthy, A.; Abe, H. *J. Nanosci. Nanotechnol.* **2014**, *14* (6), 4443–4448.

General list of figures

B. General list of figures